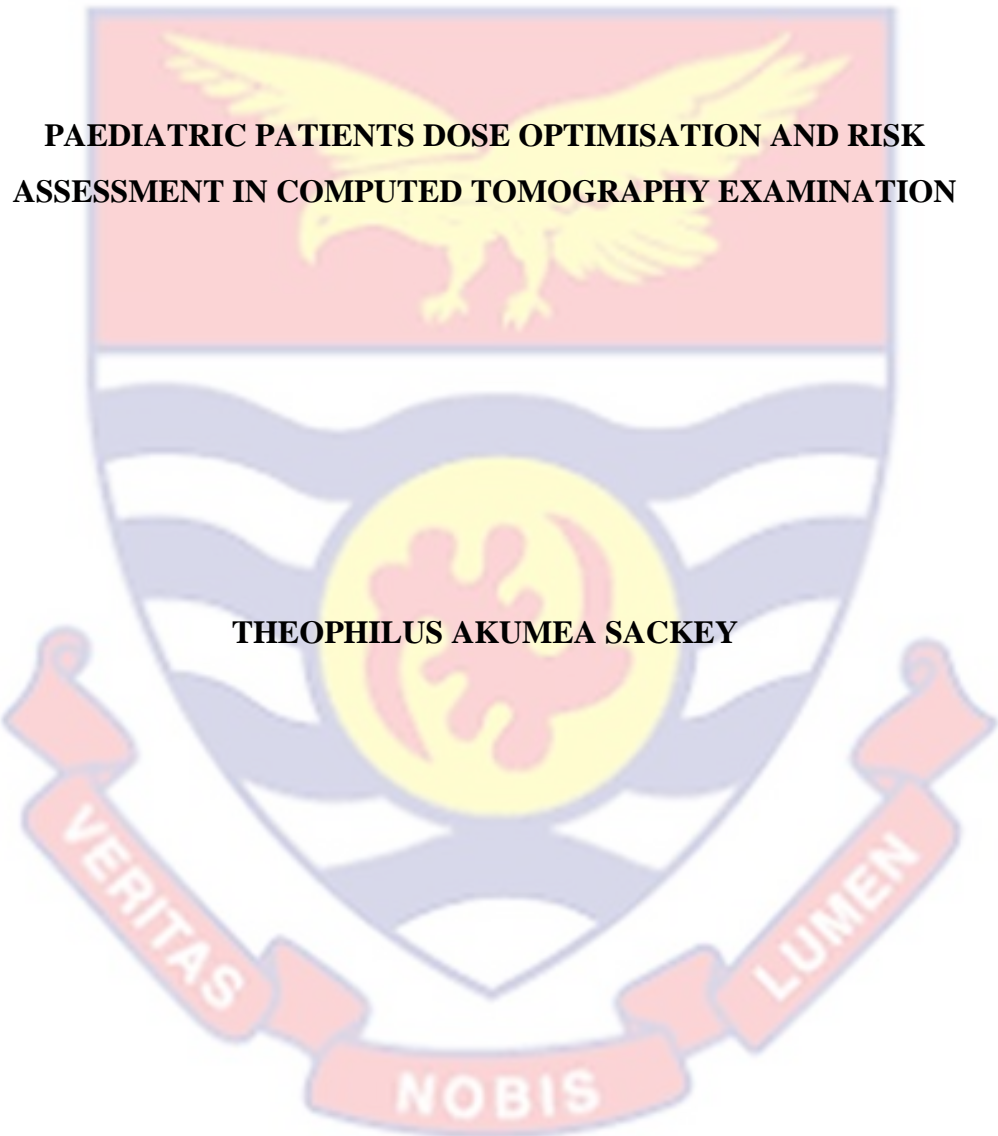**UNIVERSITY OF CAPE COAST**

**PAEDIATRIC PATIENTS DOSE OPTIMISATION AND RISK
ASSESSMENT IN COMPUTED TOMOGRAPHY EXAMINATION**

THEOPHILUS AKUMEA SACKEY

2022

© Theophilus Akumea Sackey
University of Cape Coast

UNIVERSITY OF CAPE COAST

PAEDIATRIC PATIENTS DOSE OPTIMISATION AND RISK

ASSESSMENT IN COMPUTED TOMOGRAPHY EXAMINATION

BY

THEOPHILUS AKUMEA SACKEY

Thesis Submitted to the Department of Physics of the School of Physical

Sciences, College of Agriculture and Natural Sciences, University of

Cape Coast, in Partial Fulfillment of the Requirements for the

Award of Doctor of Philosophy Degree in Physics

APRIL 2022

DECLARATION

Candidate's Declaration

I hereby declare that this thesis is the result of my own original research and that no part of it has been presented for another degree in this university or elsewhere.

Candidate's Signature ………….………………..… Date: …………..…

Name: Theophilus Akumea Sackey

Supervisors' Declaration

We hereby declare that the preparation and presentation of the thesis were supervised in accordance with the guidelines on supervision of thesis laid down by the University of Cape Coast.

Principal Supervisor's Signature ………….…………… Date: ……………

Name: Prof. Cyril Schandorf

Co-Supervisor's Signature …………………………… Date: ……………

Name: Prof. Raymond Edziah

ABSTRACT

The aim of the study was to establish and utilize national diagnostic reference levels (DRLs) of dose length product (DLP) and computed tomography dose index (CTDI) for routine computed tomography (CT) paediatric examinations. Additionally, the study estimated signal-to-noise ratio and lifetime attributable radiation risk. Materials used included multi-detector computed tomography machine, CT water phantom, electron density phantom, Head and Body phantoms and MeVisLab workstation. The methodology involved estimation of CTDI, DLP, cancer risk incidence (CRI) and signal-to-noise ratio (SNR) using a minimum of 20 patients dose parameters of head, chest, and abdomen-pelvis CT examinations. In all 300 images of randomly selected paediatric patients undergoing CT scans of head, chest, and abdomen-pelvis from these centres were collected of which 200 met the selection criterion and were analysed. The measured median and upper quartile $CTDI_{vol}$ for head CT were 6.86 and 7.33 mGy, chest CT 6.98 and 6.70 mGy, abdomen-pelvis CT 4.71 and 5.28 mGy. While DLP for head CT were 1103.00 and 1249.58 mGy-cm, chest CT were 978.86 and 1250.42 mGy-cm, abdomen-pelvis CT were 565.85 and 787.05 mGy-cm. The mean CRI was in the range of 1 in 10,000 to 4 in 1,000 for all the CT examinations. The SNR, were all above the accepted minimum of 5. The results of the CTDI, DLP, CRI and SNR were comparable to international standard values. This study recommends dose optimization of CT examination protocols to ensure that paediatric patient doses are as low as reasonably achievable by using the established CTDI and DLP as reference values for future intercomparison of data from similar studies.

KEY WORDS

Attenuation

Dosimetry

Effective Dose

MeVisLab

Optimization

Paediatric

ACKNOWLEDGEMENTS

I owe a debt of gratitude to my project supervisors, Prof. Cyril Schandorf and Prof. Raymond Edziah of the School of Nuclear and Allied Sciences (SNAS), Atomic Campus and the University of Cape Coast, Ghana respectively. For the guidance, useful suggestions and advice on literature and for painstakingly reading the script all of which enabled me to complete the project on schedule.

I would also like to express my profound gratitude to my wife, Andriana and my children, Nigel, Veronica, Brian and Shadrack for enduring my absence from the home to either go for studies, travel for data collection or to attend lectures at the University of Cape Coast and for standing by me in all situations.

Also, I received a lot of encouragement from Prof. John Amuasi, Prof. Mary Boadu, Prof. Yaw Serfor–Armah, and Dr. Francis Hasford, all of School of Nuclear and Allied Sciences, Atomic Campus and Dr. Daniel Achel of RAMSRI so I would like to thank them very much for contributing to this success story.

Dr. Issahaku Shirazu of the Radiological and Medical Sciences Research Institute (RAMSRI) of Ghana Atomic Energy Commission (GAEC) deserves special mention for assisting me with the quality control tests on the CT scanners, the data collection and some of the IT works.

Finally, I thank my mother, brothers, sisters and the rest of the family for their inspiration, encouragement and prayers, I am most grateful to all of them.

DEDICATION

To my Father, the late Reverend Maurice Nii Baah Sackey, my wife,

Andriana, my children, my siblings and to all my loved ones.

TABLE OF CONTENTS

ix

x

LIST OF TABLES

xiv

LIST OF FIGURES

xvi

LIST OF ABBREVIATIONS

AAPM	American Association of Physicists in Medicine.
ACR	American College of Radiology.
AP	Anteroposterior
ASCR	Age-Standardized Cancer Ratio.
BEIR	Biological Effects of Ionizing Radiation
CNS	Central Nervous System.
CT	Computed Tomography.
CTDI	Computed Tomography Dose Index.
CTDP	Computed Tomography Dose Profiler.
CVA	Cerebrovascular Accident.
DLP	Dose Length Product.
DRL	Diagnostic Reference Level
EPA	Environmental Protection Agency.
ESAK	Entrance Surface Air Kerma
FWHM	Full Width Half Maximum
GAEC	Ghana Atomic Energy Commission.
HVL	Half Value Layer.
ICRP	International Commission on Radiation Protection.
ICRU	International Commission on Radiation Units and Measurements.
KAP	Kerma Area Product
KATH	Komfo Anokye Teaching Hospital
KBTH	Korle-Bu Teaching Hospital.

LAR	Lifetime Attributable Risk.
LET	Linear Energy Transfer.
MDCT	Multi-Detector Computed Tomography.
MPD	Multi-Purpose Detector.
NCRP	National Council on Radiation Protection And Measurements
OSL	Optically Stimulated Luminescence
PBCR	Population Based Cancer Registries.
PF	Predisposing Factors.
PMMA	Polymethyl Metha Acrylate.
QA	Quality Assurance
QC	Quality Control.
SD	Standard Deviation.
SNAS	School of Nuclear and Allied Sciences.
SNR	Signal-To-Ratio.
CRI	Cancer Risk Incidence
TLD	Thermoluminescent Dosimeter.
UNSCEAR	United Nations Scientific Committee on the Effect of Atomic Radiation.
WHO	World Health Organization.

xviii

LIST OF SYMBOLS

μ	signal mean
E	Effective dose
M	mean value of the dosimeter readings
Q_0	reference beam quality factor
r	correlation coefficient
SD	standard deviation
σ	noise standard deviation
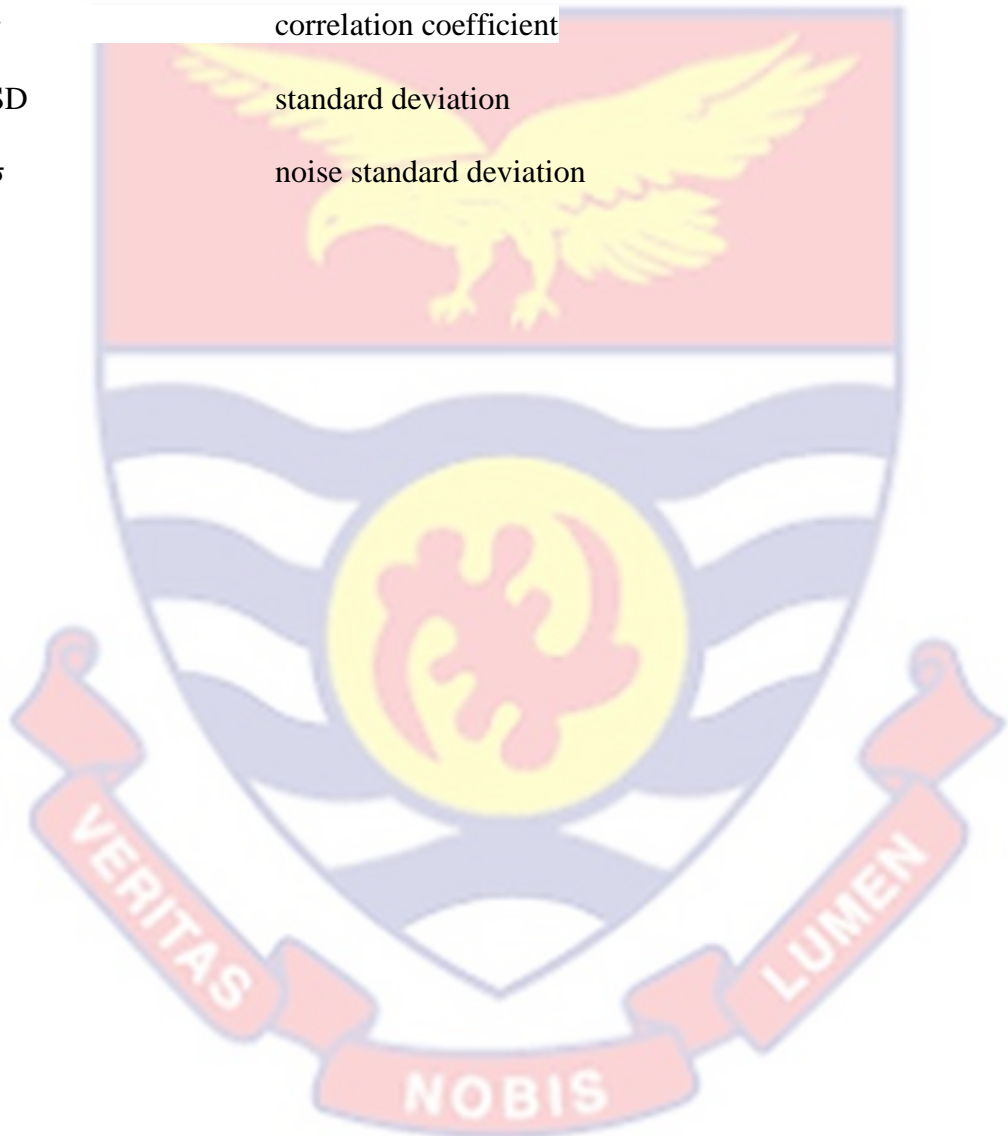
LIST OF CONSTANTS

$C_{a,100}$	CT air kerma index
CTDI	CT dose index
$CTDI_{vol}$	volume CT dose index
$CTDI_W$	Weighted-Computed Tomography dose index
C_V	coefficient of variation
K_Q	correction factor for dosimeter response at the clinical beam quality.
K_{TP}	correction factor for temperature and pressure
n	sample size
p	pitch factor

xx
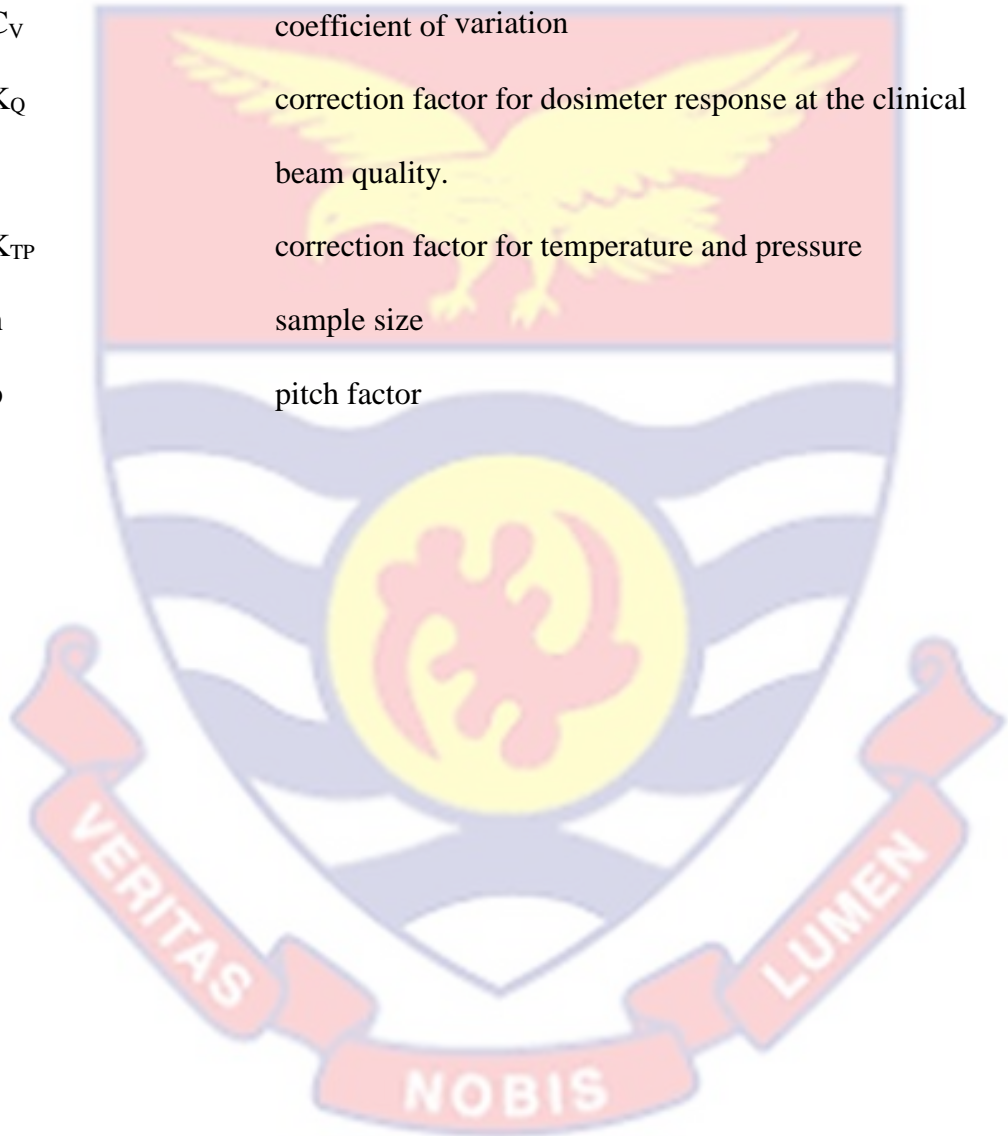
CHAPTER ONE

INTRODUCTION

Background to the Study

The study discussed Paediatric Patients Dose Optimisation and Risk Assessment in Computed Tomography (CT) Examination. It identified and answered four major challenges with the use of contiguous multidetector paediatric CT imaging in Ghana. The aim of this was to use retrospective method to obtain reliable and validated information on paediatric imaging practices, equipment performance, and paediatric patient dose parameters and to propose national DRLs for commonly used paediatric imaging procedures. This covered the determination of the relationship between organ dose and effective dose in paediatric imaging. Additionally, the study analysed approximately 200 CT images from possible sample size of 300 CT images for five different CT units in Ghana using customized DICOM software, which is a standard software for viewing any kind of medical image. an attempt to provide guidelines for imaging paediatric patients and to recommend the use of appropriate and sound clinical justification before imaging paediatric cases using high dose imaging modality like CT. Furthermore, common uses of paediatric CT procedure which include radiology, oncology, cardiology, angiography, virtual endoscopy; neurology, trauma and orthopaedics were discussed. Consequently, it further analysed why and how approximately 90% of Ghanaian CT scans for paediatric patients are for head, abdomen, and chest examinations (Inkoom et al, 2014).

In case of patient radiology, children constitute a separate group of patients. As they grow, their size, organ location, and physiology change. Additionally, they have a higher quality of life than adults, which must be considered when determining the appropriate radiation dose. In addition, paediatric imaging may require immobilization or anaesthesia to ensure image quality optimisation. Furthermore, necessary to optimize the radiation dosage protocols and maintained image quality to answer all the clinical questions without losing the essence of the procedure. It is worth noting that advances in image and detector technology, as well as dose optimization approaches, have greatly aided in dosage optimization.

Because of the higher radiosensitivity needs and the necessity for particular precautions due to the range of their body proportions, paediatric patients are a critical group of patients when it comes to medical imaging. Optimization of paediatric imaging using ionizing radiation require three important elements; applying appropriate established protocols, the use of experience imaging team and an appropriate imaging equipment. These crucial factors may result in differences in picture quality and dosage optimization techniques and protocols between departments, which must be explored and addressed. Consequently, the participatory facilities, under the framework of this study, helped to a centralized data gathering effort aimed at evaluating current techniques and facilitating the development of paediatric imaging optimization techniques. Additionally, data on dose optimization of paediatric imaging would be enhanced through the use of patient's image quality as compared to the dose during the acquisition process. Furthermore, appropriate clinical research and optimization methodologies are required to aid in the

implementation of paediatric imaging procedures to improve patient protection and safety.

Additionally, there is the need to weigh the benefits against the risk for appropriate clinical justification before imaging children using CT. However, an alternative non-ionizing imaging modalities such as Magnetic Resonance Imaging (MRI) and ultrasound, on the other hand, should be considered first in other cases (ICRP Publication 103, 2007).

Furthermore, CT is an unavoidable imaging sensory system in the diagnosis of various patients' conditions including paediatric patients. This is due to its clinical usefulness especially in situations where time restrictions would not allow other modalities like MRI or in real-time situations when large body parts need to be imaged. Consequently, International Commission on Radiation Protection (ICRP)/International Atomic Energy Agency (IAEA) has recommended that members of professional medical bodies should establish national DRLs for head, chest, spine and abdominal/pelvic paediatric inspection (ICRP Publication 103, 2007). It is vital to remember that once the DRLs are in place, they should be widely circulated and constantly monitored. Radiation dosage is expressed in absorbed dose units, which is defined as the quantity of energy consumed per unit of mass with units in Gray (1 J/kg). However, because the radiosensitivity of various tissues varies, determining the dose rate (E) with units of the Sievert (Sv) to assess the stochastic risk from radiation is occasionally beneficial. The E (mSv) is calculated by multiplying the critical organ's dose length product (mGy.cm) by an organ-specific conversion factor (k), which is based on the organ's radiosensitivity and the patient's age (ICRP Publication 103, 2007). Given the fact that E is not

3

a good metric of dose, it allows one to contrast biological effects across various diagnostic assessments (ICRP Publication 105, 2007; UNSCEAR, 2008).

Additionally, comparison of effective dose of a CT scan to natural background dose (~3 mSv/year) can assist patients to appreciate the comparative risks associated with CT scans. The volume CT dose index (CTDI$_{vol}$) (Brenner, 2001) is used to estimate the CT rdose, which is represented in milliGray (mGy). Under typical scanning circumstances, CTDIvol is measured in one of two acrylic phantoms that depict the head (16 cm) or the body (32 cm). For each scan protocol setting specified by the technologist, the CT scanner's console reports the CTDI$_{vol}$ based on manufacturer's default measurements. As part of normal quality control performance assessment, the medical physicist confirms the scanner console values by measuring the dose in the phantoms for each CT scanner. The CTDIvol can only provide an indication of the patient's dose in terms of scanner output, and its precision is determined by how near the patient's size is to the simulated size. In their work, Seibert et al, 2006 highlights on the importance of the selection of phantom sizes in relation to dose estimation (Wiest, 2002).

Based on these recommendations this study provides fundamental basic data on CT imaging of paediatric patients in Ghana. These would contribute to advance health care delivery in Ghana. By and large, comparison to adults, medical radiological examinations in new born and children carry a greater risk of disease progression per unit of radiation dosage (ICRP, 2007). The heightened incidence in children is explained by their longer lifespan,

4

which allows time for any adverse effects of radiation to manifest, as well as the fact that emerging cells and tissues are more radiosensitive. Furthermore, the risk factor for the development in younger children is larger than in older children (ICRP Publication 103, 2007). In certain countries, the annual doses of radioactive substances from diagnostic radiography have exceeded those from natural background radiation, due to increased use of X-ray technology (Wiest, 2002). As a result, all radiological exams must be justified and tailored for each patient in terms of radiological protection, which is especially critical in paediatric patients. CT scans can expose patients to high levels of radiation, and approximately 7–10% of CT scans are administered on youngsters (UNSCEAR, 2010). The assimilated doses to organs and tissues from paediatric CT are relatively high, ranging between 2 and 30 mGy to susceptible organs (ICRP, 2007).

Customized phantoms and, in some situations, radiation active component, such as more delicate air kerma area product (KAP) meters, are required for paediatric dosimetry. Effectively, there is a scarcity of dosimetric information on radiation doses and dangers for frequent paediatric exams. As a result, difficult to make decisions on risk assessment, which is necessary for legitimacy of assessments and evaluation of alternative examinations (IAEA HHS No. 24, 2013). In principle, there is the need to safeguard paediatric radiography examination methods, and the use of precise and reliable dosimetric data is a necessary precondition for successful optimization.

Similarly, dose estimations are employed for issues of risk analysis utilizing DRLs, not for the detailed characterization of radiation dose to patients during image studies. The dose reference levels are primarily used by

medical equipment suppliers, radiation regulatory agencies, and other radiation-related entities, with the primary goal of ensuring the safe use of ionizing radiation through proper consultation, regulation, and the formulation of laws to accurately provide overall patient health care. The goal is to spread a three-point program to ensure that patients are protected against radiation. Also, advocate the secure use of medical imaging technologies to both doctors and patients and lastly, assistance and enlighten clinical decision-making, i.e., the benefit verse the impacts; and Increase patient understanding of exposure and its potential health repercussions. As a result, providing regulatory authorities with knowledge on organizational dose levels based on population-specific research would go a long way toward assisting their operations and ensuring that imaging Centres serving those groups are correctly regulated. As a result, determining the radiation dosage to human tissues is critical since it plays a vital role in the patient preventive measure in healthcare services.

Similarly, estimating the radiation dosage to a human body from low-dose background radiation necessitates knowledge of the exposed individual's physiological and behavioural characteristics, as well as the exposure factors. The need for this information has become even more urgent after the discovery of CT in 1972 since a persuasive case has been made for reducing radiation exposure from CT imaging, which is thought to contribute significantly to the radiation dosage to sufferers (Mattsson & Söderberg, 2011 and NCRP, 2009). Furthermore, critical to have a sustained set of historical values to describe retrospective study of various anatomical and physiological characteristics of an affected person and the commensurate exposure parameter in order to have consistent and reproducible radiation protection

6

guidelines for CT exposure. The fact that these reference dose values for tissues and organs are added together to form a reference organ is a significant feature. The use of a full reference organ helps to guarantee that the volume or functional properties of distinct organs or tissues, as well as the consequences of radiation exposure, are defined consistently throughout the organ.

Appropriate paediatric imaging with ionizing radiation is dependent not only on following specified guidelines, but also on the personnel's competence and the equipment's suitability. These parameters contribute to significant differences in picture and dosage characteristics among imaging departments, which must be examined and addressed. Data collection should be aimed to evaluate existing practice and encourage the implementation of optimization techniques for paediatric imaging, according to IAEA 2020 coordinated research project (CRP) on 'Assessment and Optimizing of paediatric Image analysis' (E.2.40.20) (IAEA CRP, 2020). Furthermore, data on paediatric imaging dosage optimization would be improved by comparing the image quality of the patient to the dose throughout the acquisition procedure. Furthermore, this study emphasized the importance of developing and implementing of research and optimization protocols in paediatric imaging to improve patient comfort and security.

Based on these international recommendations, this study seeks to collect relevant data on imaging of paediatric patients, associated with CT dose descriptors ($CTDI_{vol}$ and DLP), estimate radiation risks and proposed diagnostic reference levels (DRLs) for consideration of the approving authorities for use by CT paediatric patients imaging in Ghana.

7

Statement of the Problem

CT examination has become an important clinical diagnostic tool, and as more CT centres are built in Ghana, there is an increase in CT applications (Inkoom et. al, 2014). However, there is a significant knowledge gap in paediatric CT imaging when it comes to the availability of trustworthy and verified information on paediatric imaging techniques, paediatric dose statistics, and performance data. Furthermore, there are no National DRLs in the country for paediatric CT scan. Again, there is no effective Quality Management System guiding Paediatric Scanning techniques in Ghana to establish whether quality management, quality control, and quality improvement needs at CT facilities in Ghana fulfil national and international standards. As a result, appropriate education and training programs in the field of paediatric imaging practice in Ghana must be established in accordance with the National Strategy for Education and Training of Health Professionals (IAEA CRP, 2020).

Objectives of the Study

The objectives of this study were to use retrospect method to obtain reliable and validated information on paediatric imaging practices, equipment performance, and paediatric patient dose data and to propose nationwide clinical practice levels for the most commonly used diagnostic tests paediatric imaging modalities.

The specific objectives were as follows:

i. To collect data designed to evaluate current practice and facilitate the development of optimization protocols for paediatric imaging

8

ii. To assess the efficiency of equipment used in paediatric imaging

iii. Assess the CTDI$_{vol}$ and DLP associated with the imaging protocols and derive the associated effective doses

iv. Assess the quality of the images of patients using ImageJ software with the estimation of SNR as the image quality index

v. Perform optimisation studies to suggest optimum imaging protocols which would provide the mechanism for the optimisation of protection of the patients undergoing the various imaging procedures

vi. Estimate the delivered organ dose to specific paediatric organs during CT scan leading to organ risk assessment.

vii. Develop and propose DRLs for the most common paediatric imaging protocols for the consideration of the approving authorities.

viii. Propose reference-imaging chart to clinicians to promote highest level of the protection of patients using the DRLs as benchmarks.

Scope of Work

The study covered the determination of the association between organ dosage and effective dose in paediatric imaging using Weighted-Computed Tomography dose index (CTDI$_W$) and Dose Length Product (DLP) respectively for the five selected CT units. The study analysed approximately 200 CT images from possible sample size of 300 CT images for five different CT units in Ghana and analyzed using customized DICOM software, which is a standard software for viewing any kind of medical images. Data were collected within 12 months. The patient throughput used for this work were 150, 120, 100, 80, 50 Paediatric patients seen in the Diagnostic Radiology

Units at the Korle Bu Teaching Hospital, Komfo Anokye Teaching Hospital, Greater Accra Regional Hospital, Sunyani Regional Hospital and Techiman Holy Family Hospital annually, respectively.

There are 48 CT scanners in the country of which 35 are functional Issahaku et al, 2017). To make the work more representative of the country, the country was grouped into three zones. The southern, middle and the upper belt. 23 of the functional ones are in Accra, 8 are in the middle belt and 4 are in the upper belt. Three of the scanners were selected from the southern belt, one from the middle belt and one also from the upper belt.

Relevance and Justification

Guidelines for imaging paediatric patients recommend that the imaging team provide appropriate and clinical justification before imaging paediatric patients with CT. Again, ultrasound and MRI are two other imaging modalities that should be studied and considered, where appropriate (ICRP 103, 2007).

Furthermore, CT is an unavoidable imaging mechanism in the diagnosis of various patients' conditions including paediatric patients. This is due to its clinical usefulness especially in situations where time restrictions would not allow other modalities like MRI or in real-time situations when large body parts need to be imaged. Consequently, ICRP/IAEA has recommended that members of professional medical bodies should establish national DRLs for head, chest, spine and abdominal/pelvic paediatric CT examination (ICRP Publication 103, 2007). Additionally, ICRP/IAEA has recommended in its coordinated research project (CRP) on 'Evaluation and

Optimization of Paediatrics Imaging' (E.2.40.20) that member states should establish diagnostic reference levels for head, chest, spine and abdominal/pelvic paediatric CT (IAEA CRP, 2020). Hence, once DRLs are established, it should be disseminated and reviewed periodically. This work is therefore in line with international and national recommendations providing baseline information for quality assured paediatric imaging practice in Ghana. (H. Delis et al, 2021)

Delimitation

Initially, this study was confined to paediatric patients undergoing CT in 26 CT facilities in Ghana. Additionally, the sample procedure was proposed to be based on head, chest, abdominal-pelvis and the spine. With an average of 20 image data for various age categories from (0-16) for each procedure and 100 image data for each Centre.

Limitation

The purposive sampling procedure used in this study produced findings that decreases the generalizability. This study was not generalized to all the CT centres due to lack of paediatric data in most of the centres and hence only 5 centres took part in the study. Additionally, there was limited data on spine CT examination and hence could not be part of the study. Furthermore, limited data was available for other procedures and hence 200 paediatric data was available that met the selection criteria for analysis.

11

Organization of the Work

The thesis write-up is presented in five chapters. Chapter One provides a detailed background information setting the stage for the study, problem statement and objectives, scope and relevance and justification for clinical application in Ghana. Chapter Two reviews the relevant literature on paediatric imaging, patients dose optimization procedures, organ risk assessment and effective dose, establishment of diagnostic references levels and current EC and ICRP recommendations. Chapter Three provides relevant information about the materials and the methodology used to achieve the desired goal of the study. This chapter also describes the various measuring procedures that were used to measure and process the primary data in order to successfully design the dose optimisation modelled equations and the various tools such as Minitab application software and statistical models that were used to analyse the data.

Chapter Four provides illustrative view of an established connection between the various considerations in tables and pictorial representations. It provides a space platform by presenting the data that are necessary to facilitate the implementation process in a pictorial format. It describes the relationship between the various measurable quantities that were used to calculate the derived quantities to draw reasonable conclusions. Finally, the presented data was analysed using various practical and theoretical tools based on the study objectives in this chapter.

Chapter Five presents a comprehensive summary of the most important conclusions in relation to the measured exposure and effective dose

optimization procedures during the paediatric CT examinations. The development of mathematical and PC assisted strategy prototypes of the measured parameters for clinical application are also presented. This chapter provides the concluding summary of this work and recommendations to relevant stakeholders.

Chapter Summary

In summary, a comprehensive discussion of the background information was done in relation to the various scientific bases of the study. In addition, it also discusses the identified problem statement and a clearly set out objectives to achieve the desired goal. Furthermore, it explained the scope in relation to its relevance and justification for use clinically in Ghana and ends with the summary of the study organization.
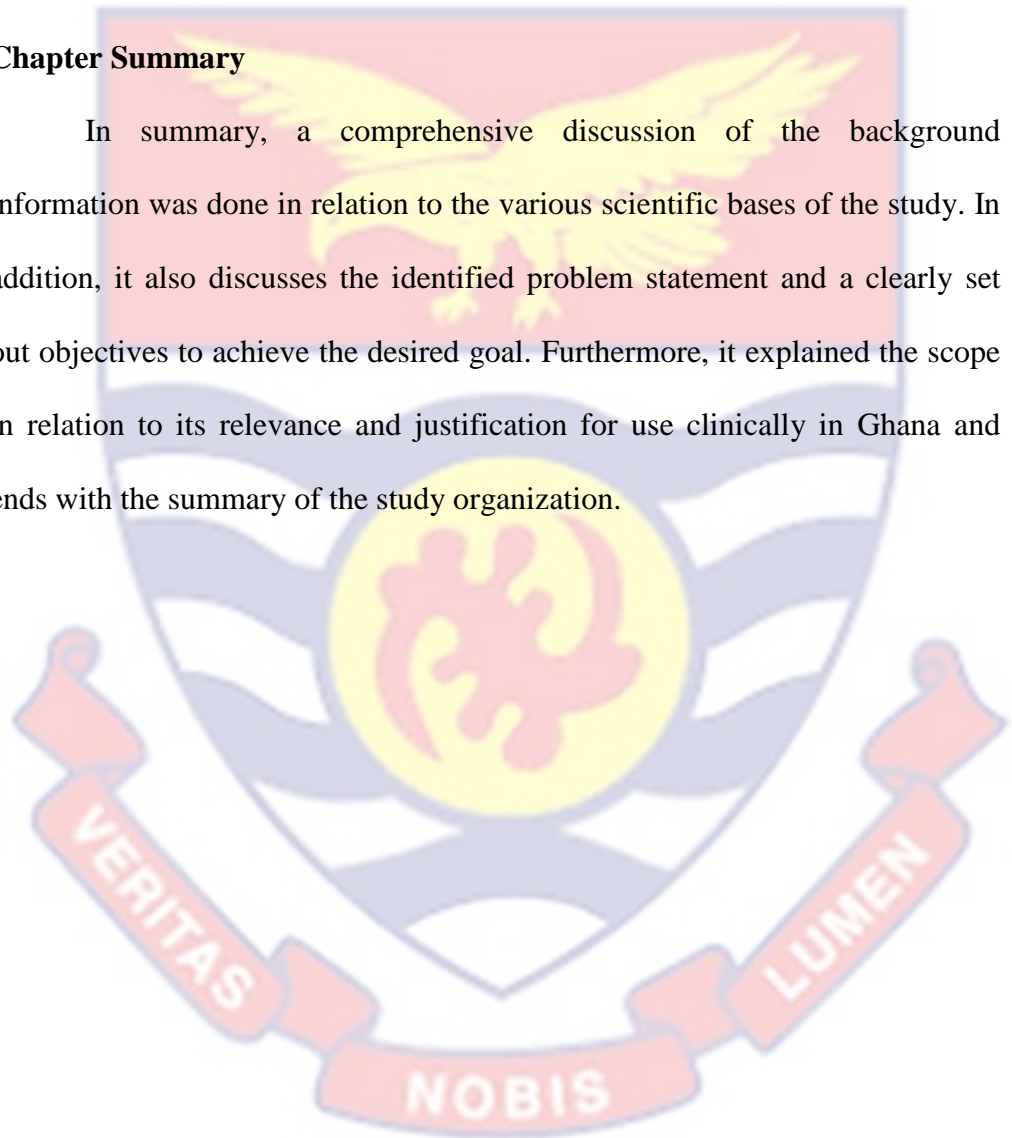
CHAPTER TWO

LITERATURE REVIEW

Introduction

A review of the literature is presented in this chapter particularly on historical development of CT scanners and their application in medical imaging; paediatric imaging dosimetry and management of patient dose; factors affecting doses and optimisation of patient protection; establishment of DLRs and patient risk assessment.

CT Scanner Developments

In 1972, the Electric and Musical Industries (EMI) scanner became the first CT scanner to be used in clinical treatment (Wiest, 2002). The scanners used a pencil beam and a sodium iodide (NaI) detector. On a moment in time basis, the detectors move the patients (i.e. translational) and produce roughly 160 data points for each projection. Another image is obtained by turning the X-ray tube and detector 1 degree; 180 projections were obtained over 180-degree revolution. A single image was created in an estimated period of 5 minutes. A first-generation system is the name given to the original EMI design, shown in Figure 1 (Weist, 2002).
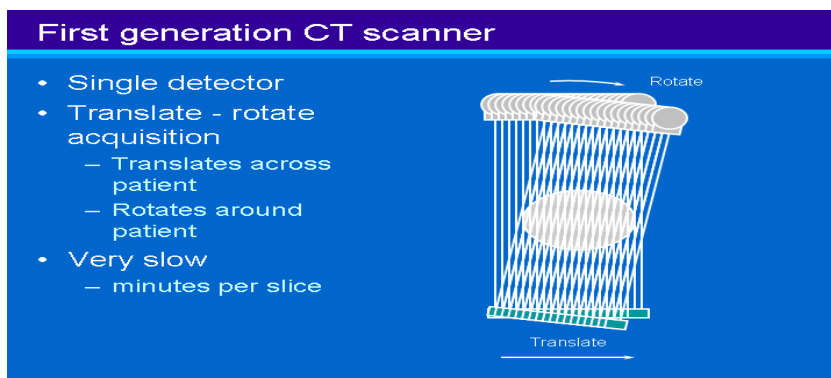
Figure 1: Schematic diagram of a first-generation CT scanner (ImPACT, 2015)

The next immediate generation scanner employs the same translational-rotation technique as the first, but with more sensors and a fan-shaped beam. These scanners offer bigger rotating intervals, resulting in speedier scans, with each section taking around a minute to generate. A revolving fan beam and detectors are used in third-generation scanners.

The fourth-generation scanners have a revolving tube and a fixed ring of detectors in the superstructure with up to 4800 detectors (rotate-fixed system). A schematic representation of a second-generation CT scanner is shown in Figure 2.
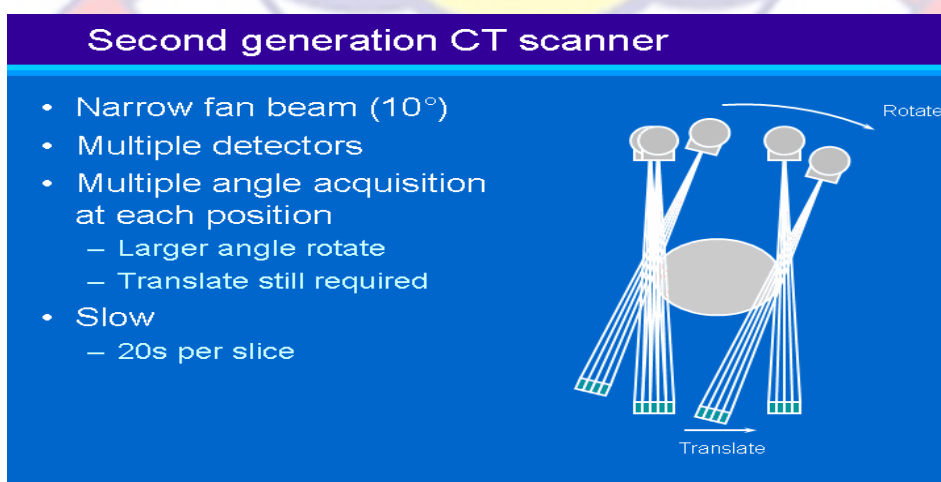
Figure 2: Schematic diagram of a second-generation CT scanner (ImPACT, 2015)

15

Scanners from the third and fourth generations included acquisition of a single image in one or two seconds. The imaging capabilities of 3rd and 4th generation CT scanners are nearly identical. Figures 3 and 4 depict schematic diagrams of third-generation and fourth-generation CT scanners, accordingly.
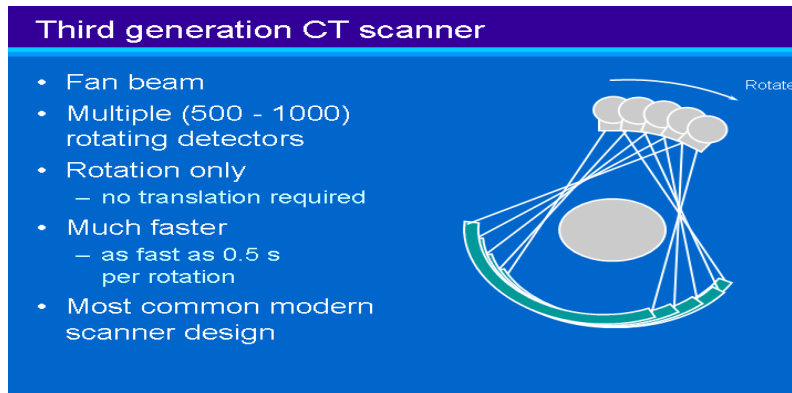
Figure 3: Schematic diagram of a third generation CT scanner. (ImPACT, 2015)
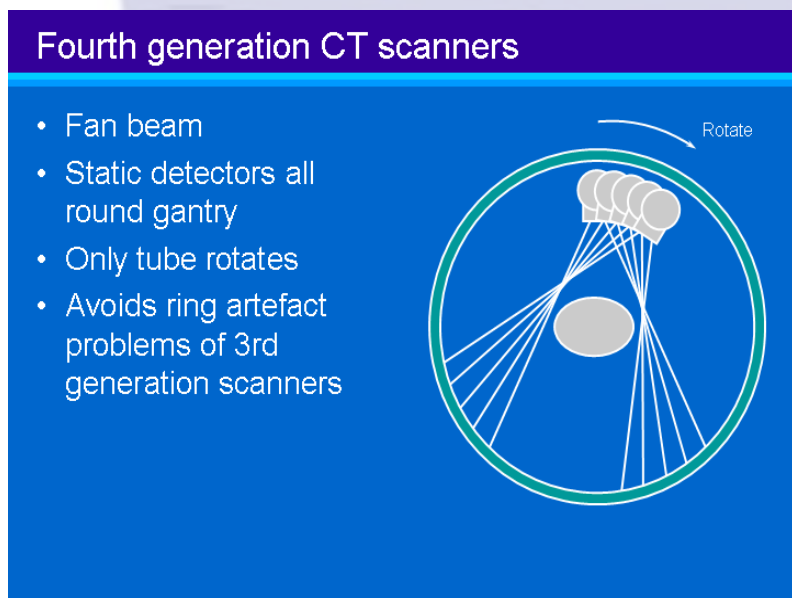
Figure 4: Schematic diagram of a fourth generation CT scanner (ImPACT, 2015)

Helical Computed Tomography

In a helical (spiral) mode, slip ring CT scanners can be employed. Unlike traditional CT scanners, which revolve the X-ray tube around the stationary patient, one part at a time, helical CT moves the patient along the

16

horizontal plane while the X-ray tube rotates around the patient at the same time, as seen in Figure 4. Throughout a CT scan, the X-ray beam enters the patient along a helical path. The pitch is the relationship between patient and tube motion, which is defined as the distance travelled by the table divided by the parallax width during each revolution of the X-ray tube (measured in millimetres).

General Computed Tomography Imaging

The basic operation is based on the background that; the structural formation of numerous perspectives of an object can be used to reconstruct it by using computer algorithms developed from mathematical equations and physics principle of attenuation based on the variation of tissue radiodensity and sensitivity (Bydder et al, 1981; Duncan et al, 2014).

This principle was initially postulated by (Radon, 1917), he was able to obtain an image of an object with an infinite number of projections through the object (Stanley, 2007). In addition, clinical applications of this principle require the physics principle of radiation attenuation, dependent on the radiation intensity, which defines how much a beam's radiant flux is lowered as it travels through a certain tissue.
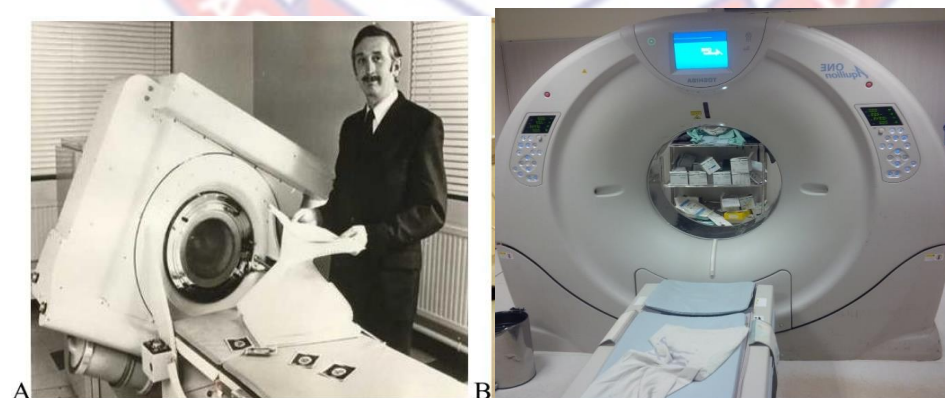
Figure 5: Old (A) and Latest (B) CT scanner systems (Emaze, 2015)

17

In clinical practice, the attenuation coefficient is represented by μ and calculated in cm^{-1} in the domain of X-rays or Gamma rays. The attenuation of X-rays through human body enables the tissue attenuation map of the human body to be estimated when photons pass through the human body, where attenuation (absorbed or scattered) of the photons by the tissues occurs (Duncan & Panahipour, 2014). The attenuation depends on photons' energy and the tissue radiodensity as it passes through human tissue. of interest to note that, the primary causes of this form of attenuation in human tissue are based on the photoelectric effect and Compton scattering (Aabha & Dixit, 2016).

This principle has been applied in the photon based imaging procedure like conventional X-ray and CT scanners, resulting in accurate and effective imaging procedures for clinical applications Table 1 shows how CT scanner technology has advanced substantially since the first scanner was released in the 1970s, as illustrated in Figure 5A.

Table 1: Old and Latest Technology of CT Scanners

Specifications	First CT Scanner (1970) (Figure 5A)	Latest CT Scanner (2014) (Figure 5B)
Acquisition Time of an image	5 minutes	0.25 seconds
Pixel size	3 mm × 3 mm	0.25 mm × 0.25 mm
Number of pixels in an image	6,400	640,000

Source: (Imagewisely, 2012)

Today's modern CT scanners (Figure 5B) can image the full abdomen and pelvis of most persons in less than 30 seconds, resulting in 640 CT images. Since 1970, the level of detail in the image has increased by a factor

of a hundred. CT imaging has grown in popularity in recent years. This is largely due to the fact that the use of CT scanners has increased tremendously, from a few hundred in the 1990s to hundreds of thousands now, even throughout Africa (Mattsson et al, 2011). Additionally, CT imaging procedures increased from a little over 2% of all radiological examinations in most developing countries a decade ago to over 15 % now (Mattsson et al, 2011). In contrast, even though CT examinations constituted only 5% of procedures worldwide in the 1990, yet it contributed 34% of the world total radiation dose in the same period and doubled in the first decade of the twenty first century and this is expected to quadruple in the next decade (NCRP, 2020). CT imaging procedures together with nuclear-powered imaging procedures (Single Photon Emission Computed Tomography-(SPECT) and Positron Emission Tomography (PET) account for more than one-third of all diagnostic imaging modality studies in the world (Mattsson & Söderberg, 2011).

Furthermore, shorter scanner time, improved temporal and spatial resolution has all been doubled, subsequently the fusion of multi-slice CT in 1977. Additionally, 64-slices spiral CT of modern, dual energy, with a gantry rotation time of 0.33s, it can scan the entire body in 25 seconds. (Mattsson & Söderberg, 2011). Multislice CTs may record up to 640 slices every rotation. Due to the significant increase in the usage of CT scans, there are worries about patient radiation exposure and the probable increased risk of cancer later in life., from single techniques to 'hybrid imaging techniques' for many applications such as SPECT-CT and PET-CT (Mullenders *et al*., 2009; Smith-Bindman et al, 2009; Einstein, et al, 2007; Berrington-Gonzalez &

Darby, 2004; Khan, 1984).

The continuous increase in CT imaging is partly due to the fact that it produces accurate, detailed visualized anatomical description of human organs. It has the best image resolution that is close to the real anatomical structure of an organ. Current CT scanners can produce 3D images of organs in 640 slices within a few seconds (Mattsson & Söderberg, 2011; NCRP, 2009). These and many more features justify the selection of CT scanner system for a study of an organ when the anatomical details and boundaries of the organ are of paramount interest.

In the geometric design of most CT scans, the rotating detectors and the X-ray tube (Figure 6), descend from the head of the patient to the feet with the axis of rotation.
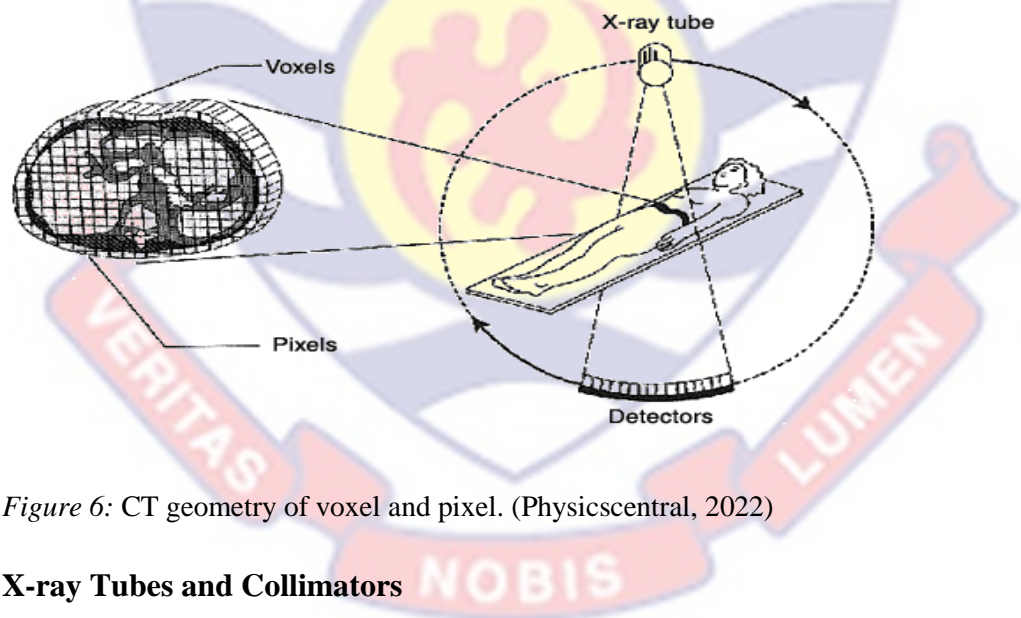
Figure 6: CT geometry of voxel and pixel. (Physicscentral, 2022)

X-ray Tubes and Collimators

The recent CT X-ray systems use high X-ray tube energies, scan times between 0.5 and 2 seconds and tube currents of hundreds of milliamperes (Mattsson et al, 2011). They are powered by a high frequency to deliver a very stable tube current and voltage. In addition, a small focal spot of about 0.6 mm

that is used to lower power rating up to 25 kW and a large focal spot in the range of 1 mm is used at great power rating up to 60 kW. Furthermore, modern CT tube systems have tube capacity of above 3 MJ and dissipation rate are quite high of about 10kW. In view of this, the heat stacking on CT X-ray pipes are mostly high which then require high terminal heating capabilities for optimal performance. (Flohr, 2013)

The standard design for X-ray tube to reduce the heel effect is to position the tube perpendicular to the imaging plane with aluminium filter which is used to reduce X-ray beam hardening effect. Additionally, aluminium half-value layer of up to 10 mm are used as heavy filtration material in most modern CT scanners to produce a beam for efficient scan energy. In addition, to diminish forceful variety of disclosures at the detector, bowtie filters are used. To reduce scatter and define section thickness, collimation are used, which are situated at the detectors as well as X-ray tubes. Finally, for efficient varied collimation, well designed adjustable section thickness between the ranges of 1mm to 10 mm are used in most modern CT scanners (Flohr, 2013).

CT Radiation Detectors

The intensity of radiation, which passes through the patient, are measured by the detector. These detectors are designed to have high fast response and good X-ray detection efficiency and operated over a wide dynamic range. The electric signal in the detectors are proportional to the incident radiation intensity, which are processed digitally and stored in the computer (Cho, 2003).

Furthermore, most detectors use Xenon gas ionization detectors, with anode and cathode terminals sustained at a potential difference. An electron-ion pair is produced when incident X-ray photons ionize the gas-filled detectors. High pressure of about 25 atmospheres are used to maintain relatively deep gas detectors in order to increase the efficiency of the X-ray detection in most third generation CT scanners. The design of these type of detectors makes them steadier than solid-state detectors with wide direct response with no delay.

Furthermore, when x-ray photons are absorbed the scintillation crystals produce light and are coupled with photodiode or photomultiplier tube. The solid-state detectors on the other hand use cadmium tungstate ($CdWO_4$), calcium fluoride, caesium iodide, and bismuth germinate for efficient X-ray detection. Because of the detection geometry in fourth generation scanners, only solid-state detectors are used with thin detectors. Additionally, CT scanners have evolved over the years and are still going through various changes to improve efficiency and dose optimisation to patients and users of these equipment. However, the overall objective is to produce images that will help diagnose diseases and help improve healthcare delivery in the world. In recent times, diagnostic equipment are used together with CT scanners to help improve diagnostic and treatment of diseases (Cho, 2003).

Overview of Paediatric Radiology

When compared to adults receiving the same dose, paediatric patients are at a higher risk of getting cancer from CT scans (ICRP 121, 2013). Besides, according to Dobbs' research, children are ten times more sensitive to

22

carcinogenesis from radiation than adults" (Dobbs, 2011). Because children have a longer life expectancy, any detrimental consequences of radiation can show during their lives, especially because developing organs and tissues are more sensitive to radiation. ICRP 121, 2013 deals with rationale and optimization principles, provides guiding principles of diagnostic radiology for referring clinicians and clinical personnel performing medical imaging and interventional procedures for paediatric patients. ICRP 121, 2013 also provides some recommendations and guidelines for radiological protection of paediatric patients using CT and other techniques.

The significance of thorough rationale for radiological operations requiring ionizing radiation is emphasized, and the use of non-ionizing imaging modalities should always be explored. The basic goal of radiological protection optimization is to adjust imaging parameters and implement protective measures such that the required image is acquired with the lowest feasible dose of radiation while maintaining sufficient quality for diagnostic evaluation. When purchasing new imaging equipment for paediatric usage, special attention should be paid to the availability of dose reduction measures (ICRP 121, 2013).

In the same vein, one distinguishing feature of paediatric imaging is the vast variation in patient size and weight, necessitating careful attention to equipment, technique, and imaging parameters for optimization and modification. Furthermore, according to the patient's weight or age, the scanned location, and the research indication, scan parameters such as mA, kVp and pitch could be adjusted to reduce radiation in computed tomography (ICRP 121, 2013).

Additionally, even with more noise, radiographs with appropriate diagnostic quality should be approved. Other dose-reduction measures include eliminating scan region overlaps, limiting multiphase testing protocols, and just scanning the required area. Furthermore, auto kV technology, tube current modulation, and iterative reconstruction, as well as organ-based dose modulation, are the most recent dose reduction technologies that should be used appropriately. As a result, the instructions in ICRP 121, 2013 will aid institutions in supporting procedural standardization, as well as increasing awareness and, eventually, improving practices for the provision of quality care.

Imaging Modalities in Paediatric Radiology

Paediatric radiology is a radiological sub-specialty that involve the imaging of young adults, adolescents, children, foetuses and infants. Although some diseases seen in adults are the same as those seen in paediatric patients, however, there are many conditions, which are seen only in infants. Teenagers are generally referred to paediatric radiologists for most clinical diagnosis because their growing bodies are more vulnerable to the harmful effects of radiation than adults of comparable size. Paediatric radiologists are typically referred to for illnesses and medical disorders affecting newborns, children, and young adults due to their specialized knowledge. They can usually detect diseases including pneumonia, appendicitis, and the effects of trauma, as well as any type of childhood cancer, quickly and efficiently. Exploratory surgery are prevented on children by using various childhood imaging techniques which are designed mainly to prevent unnecessary

radiation dose to paediatric patients. Additionally, to deal with children, paediatric radiology engages a whole range of techniques classified ionising (X-ray, CT/SPECT PET/CT) and non-ionising radiation (MRI and ultrasound) (ICRP 121, 2013).

Paediatric imaging is required to be done by trained professionals who are expected to deci.de the most suitable test for the infant, and to ensure the examination is performed properly. In Ghana, the common paediatric imaging procedures include the following: Barium Meal (Gastro); Renal Ultrasound; Abdominal Ultrasound; Hip Ultrasound for DDH; Micturating Cysto-urethrogram; X-ray Examination (General Radiography, Computed Radiography, Fluoroscopy) (ICRP 121, 2013).

Acknowledging the requirements of children in the clinical setup, rather than treating them as miniature adults, and realizing that they need to be treated on their level are critical factors for optimal treatment outcomes. Clinicians must pay attention to two primary areas of paediatric radiography in paediatric diagnoses, child communication skills and positioning techniques. Not only should the basic processes of paediatric radiography be described, but they should also be exercised (ICRP 121, 2013).

Although there are several parallels between paediatric imaging and adult radiography, such as fundamental positioning and picture quality evaluations, there are also significant variations, such as how you handle the child and dosimetry analysis. Hence, paediatric clinicians may think of an effective and innovative way to explain a particular radiographic examination to children. Raising children properly necessitates an open mind, patience,

25

inventiveness, an eagerness to adapt, and the capacity to see the world through a child's eyes (ICRP 121, 2013).

Paediatric Radiology Dosimetry

From literature, both the ICRP 103 and IAEA TRS 457 formalism are used for dosimetry evaluations in paediatric dose assessments (ICRP 103, 2007; ICRP 121, 2013; IAEA, 2014; IAEA HHR, 2013).   In general, "measured air kerma is used as the basis for directly measured application specific quantities such as entrance surface air kerma (ESAK) and air kerma area product". However, measured quantities are used to derive all other quantities by using conversion coefficients with procedures described in IAEA Human Health Series (HHS) Report No. 24, 2013.

Generally, paediatric dose measurements are to be carried out both with patients and phantoms. These phantoms are used to enable repeated calculations to be done, with a rapid evaluation of results. This is particularly useful for series of measurements on equipment and for making comparisons between different systems. Standardized phantoms are used with the same protocol and procedure to enable comparisons between centres. Because phantom dose evaluations may not provide an accurate estimate of average dosage in clinical practice for paediatric patients, phantom measures must be supplemented with measurements and dose estimation for patients using real patient data (IAEA, 2013). The outcome of this information must be made available to clinicians to enable effective and efficient evaluation of the various procedures and protocols for effective management of paediatric cases. Solid-state devices such as Thermoluminescent dosimeters (TLDs) and

26

optically stimulated luminescence (OSL) dosimeters are used in clinical measurements. For paediatric dose assessments, typical dose quantities such as incident air kerma, ESAK, air kerma area product, and air kerma length product are estimated. These measurements enable the clinical facility to compare patient dose measurements to DRLs and other benchmarks. The presence of the requisite measuring equipment as well as comparable DRL values play a role in deciding the dose quantity to test and compare (IAEA, 2013).

Phantoms for Dosimetry

Phantoms used for adults should not be used for children for purposes of dosimetry. Such phantoms are inappropriate for simulation of paediatric patients, instead phantoms of varied sizes are recommended as a basis for paediatric dosimetry. Simple phantoms can be made out of water and PMMA (Polymethyl methacrylate), both of which are quite easy to purchase or produce, and the thickness can be varied to imitate patients of various sizes. Generally, Table 2 provides suggested phantom dimensions and corresponding size equivalents. On the contrary, these are pelvic analogous phantoms, and no special chest phantoms for paediatric dosimetry are indicated (HHR 24, 2013).

Table 2: Details of Recommended Phantoms for Paediatric Dosimetry

Phantom dosimetry		Corresponding patient demographics		
Approximate tissue thickness (cm)	Polymethyl methacrylate thickness (cm)	Approximate weight (kg)	Approximate height (cm)	Approximate age (USA)
5	5	5	6	Preterm
10	10	4.7	56	New born
15	15	31	138	10 years

Source: (HHR 24, 2013). 60 –70 kV with varying filtrations.

27

Computed Tomography

The main dosimetric measures used in CT are the weighted CT, $CTDI_w$ and CT air kerma indices $C_{a,100}$. Additionally, C_w is used to derive CT air kerma index C_{VOL} ($CTDI_{vol}$) for certain scan parameters of a patient. The CT dose length product (DLP), which is now known as the CT air kerma length product ($P_{KL,CT}$), is used to represent patient doses for a comprehensive examination. The displayed CTDI should not be used to estimate paediatric dose in paediatric dosimetry. When compared to adults, this will most likely underestimate the dose to the juvenile patient. This is because the CT scanner's console display value is normally calibrated using a 16 cm diameter phantom for the head and a 32 cm diameter phantom for the body. If appropriate paediatric procedures are available, the console-displayed value can be calibrated with a 16 cm diameter phantom, however this may still result in overestimation or underestimating for extremely little or very large children (IAEA, 2011).

CT Phantom and Free-in-Air Measurements

CT air kerma indices $C_{a,100}$, and C_w are measured using a calibrated pencil ionization chamber. The tube voltage (kV) used clinically for paediatric patients should be calibrated in the chamber. In most cases, this is 120 kV; but, in other Centres, it may be less than 120 kV. The terms $C_{a,100}$ and C_w are used to describe free-in-air measurements. However, a typical CT head phantom with a diameter of 16 cm should be utilized to imitate a paediatric body. It must be noted that even the 16 cm phantom size are significantly larger or smaller than some paediatric patients, due to the wide range of

28

paediatric patients' size. As a result, the measurement process in (IAEA TRS, 2007; IAEA, 2011) should be followed for converting measurements to values in a different size phantom.

$C_{a,100}$ is given by equation 1:

$$C_{a,100} = \frac{1}{N.T} \times \overline{M_c} \times N_{PItL} \times K_Q \times K_{TP} \tag{1}$$

and the normalized value is given by equation 2:

$$n/C_{a,100} = \frac{C_{a,100}}{P_{It}} \tag{2}$$

where

M "is the mean value of the dosimeter readings for a single rotation of the X-ray tube"; N·T "is the nominal beam width in a single rotation with N = 1 for single slice scanners"; PIt "is the tube loading (mAs) for that single rotation"; $N_{PIt,Q0}$, "is the calibration factor of the dosimeter at beam quality Q_0"; K_Q "is the correction factor for dosimeter response at the clinical beam quality Q compared to Q_0"; and K_{TP} "is the correction factor for temperature and pressure", (equation 3). The peripheral sensory values for measurements taken in the head phantom are calculated and merged as follows to yield Cw and the normalized nCw (TRS, 2007, IAEA, 2011)

$$C_{PMMA,100,c} = \frac{1}{N.T} \times \overline{M_c} \times N_{PKL.Q} \times K_{PIt} \times K_{TP} \tag{3}$$

$$C_{PMMA,100,p} = \frac{1}{N.T} \times \overline{M_p} \times N_{PKL.Q} \times K_{PIt} \times K_{TP} \tag{4}$$

$$C_w = \frac{1}{3}\left(C_{PPMA,100,c} + 2C_{PMM,100,P} \right) \tag{5}$$

where subscripts c and p denote measurements in the center and periphery of the phantom, respectively. Equation 3, 4 and 5 was used to derived $CTDI_{vol}$

29

Normalized Cw (n_{C_w}) is given by equation 6:

$$n_{C_w} = \frac{C_w}{P_{It}} \qquad (6)$$

CTDI volume weighted, CTDI$_{vol}$ is given by equation 7:

$$CTDI_{vol} = n_{C_w} \times \frac{N.T}{L} \qquad (7)$$

where, L is the scan length and

N·T "is the nominal beam width

Air kerma length product is given by equation 8:

$$P_{KL,CT} = n_{C_w} \times P_{It,tot} N.T \qquad (8)$$

$P_{It,tot}$ is the total tube loading (mAs) for each series.

Patient Selection

In different nations, the protocols and procedures for routinely performed examinations on paediatric patients may differ. It is important to note that during clinically audit examinations based on methods and procedures utilized in the local radiology facility that have the maximum potential dose and/or frequency. The most common tests differ depending on the size and age of the patient. Tests using conventional protocols and processes, on the other hand, are highly recommended. The suggested examinations for paediatric patients' dose audit are listed in Table 3.

Table 3: Recommended Examinations for Patient Dose Audit

Examinations	Examination	Typical Field Size (cm x cm)		
		1 year old	5 years old	10 years old
General Radiography	Chest AP (supine)	16×13	16×18	21×31
	Chest PA erect	17×14	20×19	23×26
	Abdomen AP	15×17	21×15	26×19
	Pelvis AP	15×10	21×15	26×19
Fluoroscopy	Voiding/micturating cystourethrogram	11×11	12×12	14×14
	Contrast swallow	9×13	11×15	12×17
	Contrast meal (upper gastrointestinal tract)	8×14	13×15	-
	Contrast enema (lower gastrointestinal tract)	-	-	-
Computed Tomography	Head (brain protocol)	-	-	-
	Thorax	-	-	-
	High resolution thorax	-	-	-
	Abdomen	-	-	-
	Pelvis	-	-	-

Source: (IAEA HHS no. 24, 2013)

Effective Dose

Effective dose, E, is an important dose descriptor that provide information on the differences in biological sensitivity of various tissues in human body. Furthermore, E is a single dosage descriptor that explains the risk of a non-uniform approach in terms of a whole-body analogous exposure. Generally, E is defined as "the sum of the weighted equivalent doses in all the tissues and organs of the body". The values of DLP for an investigation using correctly normalized coefficients (EDLP) (Table 4) produced by ICRP and the European Commission provide a wide estimation of the various values of Effective dose (E). (Huda et al, 2008). The E is defined mathematically as "the product of the region-specific normalizing constant and the dose length product" (Jones et al, 1993). This is mathematically written as:

31

$$E = E_{DLP} \times DLP \qquad\qquad (9)$$

where E is the effective dose with the unit in mSv and it is important to state that E_{DLP} is the conversion factor $(mSv \cdot mGy^{-1}cm^{-1})$ that depends on patient age and scanning regions (Brandt et al., 1982). For abdomen examination, $E_{DLP} = 0.0153$.

Table 4 provides the E values in adults for various CT scans of the abdomen, pelvis and trunk regions in Europe (Tsapaki et al, 2001; Leitz et al, 1995). Table 5 provides some typical values of region specific normalized effective doses for CT examinations.

Table 4: Typical Effective Dose in Various European Countries

EU COUNTRIES	HEAD E. Dose (mSv)	TRUNK E. Dose (mSv)
Austria	14.7	4.0
Bulgaria	11.2	14.0
Croatia	11.3	10.5
Cyprus	10.4	8.0
Denmark	12.2	17.8
Estonia	10.0	15.8
Finland	6.7	8.8
France	9.4	33.0
Hungary	12.1	12.0
Ireland	8.4	8.1
Luxembourg	10.5	10.9
Macedonia	17.2	2.4
Malta	12.4	7.1
Monaco	13.5	24.4
Portugal	6.7	7.7
Russia	8.2	17.0
Slovakia	12.6	5.5
Slovenia	15.3	17.0
Ukraine	13.5	24.4
Mean	11.3	14.8
Maximum	28.7	50.5
Minimum	2.8	2.4
Max/Min	11.0	21.5

Source: (EC, 2016)

Table 5: Region Specific Normalized Effective Doses for CT Scan

CT Examination	Effective Dose	DLP mGy	CTDI$_W$ mGy	CTDI$_{VOL}$ mGy	E$_{DLP}$ (coefficients) mSv mGy cm^{-1}
Head	1-2	1050	60	73.80	0.0023
Chest	5-7	650	30	36.90	0.0170
Pelvis	3-4	570	35	43.05	0.0190
Abdomen	5-7	780	35	43.05	0.0153
Abdomen-Pelvis	8-14	780	35	43.05	0.0150

Source: (ICRP, 2018)

Factors Affecting Paediatric Radiation Dose

Although advancement in new CT technology reflect the total overall technological development in imaging procedures it provides the potential to image patients quickly using sub-second rotational rates and multislice detectors. Regrettably, an often-overlooked side effect of speedier scanning is that it encourages more frequent scanning of patients, potentially resulting in larger radiation doses. The analysis of these is dependent on a number of factors that influence the amount of radiation emitted by current CT scanners. Beam current, beam energy, pitch, detector configuration, dosage length, and the number of imaging phases in the same anatomy segment are just a few of them (Pelc NJ, 2014).

Beam Energy and Current

Tube potential (kVp) and tube current (mAs) are two key input factors in X-ray imaging. The specified tube potential when configuring the scan protocol determines the X-ray photon energy spectrum. The number of electrons propelled across the X-ray tube, and hence the quantity of X-rays produced, is determined by the tube current (X-ray fluence). When all other parameters are held constant, radiation dose changes when switching between

33

two different kVps and is roughly proportional to the square of the percentage change in tube potential, resulting in a significant increase in radiation exposure to patients (Pelc, 2014). Decreasing kVp in children can reduce the radiation dose and may improve soft tissue contrast. Firstly, when the tube current per second (mAs) is increased to keep noise levels constant; secondly, the size or weight based kVp technique chart are used to determine when a lower kVp is appropriate; third, a lower kVp may require longer scan times because of mAs limits that can increase motion artifacts; and fourth, a lower kVp may increase iodine conspicuity but not necessarily improve other soft tissue contrast in examinations where contrast are used". Dose is exactly proportional to the average of the mA and the slice scan time (s) or milliAmpere second in terms of tube current, which is provided in mA. This takes into account the patient's body size and allows for large dose reductions by lowering the mAs. (Pelc, 2014).

Multiple Detector CT Systems

Multiple detector systems, which were developed and made available for clinical usage in the mid-1990s, are used in today's CT scanners. These CT scanners with several detectors provide similar resolution in the X, Y, and Z directions while cutting scan times in half. The number of data channels times the detector width for each data channel determines the beam width, or aperture, collimation. Also, "as the aperture increases, the relative CTDI$_{vol}$ decreases, with the result that possible to achieve significant dose savings by using the widest possible aperture subject to considerations related to pitch" (Pelc NJ, 2014).

34

Pitch

The table moves via the gantry in one of two ways during scanning: continuously for helical scanning or step-and-shoot for axial scanning. The scan pitch is calculated by dividing the table feed per table gantry rotation by the beam width. However, when the table moves the same distance as the beam width, the pitch is equal to one. The dose to patients is approximately equal to the pitch, therefore if the pitch is less than one, the beam will overlap previously radiated tissue with each turn, increasing the radiation. When the pitch is greater than one, the dose is reduced, but some tissue is not radiographed completely, potentially lowering image quality or introducing gaps that could overlook crucial anatomy (Pelc NJ, 2014).

Helical Over-Ranging

It is worth noting that helical over-ranging can be a problem for younger patients, who have shorter acquisition distances than adults. These parameters defined a scanning operation that did not include a full rotation at a specific slice point (Brady et. al, 2011). As a result, the dose from helical over-ranging in paediatric patients is much higher than in adults, and it often happens at the conclusion of the acquisition. In general, for young patients, a single helical scan capture is preferable to many scans.

Effective Tube Current Time Product

The functional tube current time product (mAs), which is defined as mAs divided by the pitch factor, is an essential factor. "The effective tube current time product is directly proportional to the dose." Lowering the mAs is the most direct technique to lessen the radiation dose. However, "lowering the

35

mAs too much can produce a noisy, lower quality image resulting in a misdiagnosis or requiring a repeated scan" (Pelc NJ, 2014).

Exposure Length

The scan length, also known as the exposure length, refers to the patient's scan distance of interest in the Z direction that is exposed to the X-ray beam. The scan length should always be tailored to reduce the exposure to patients by constraining the scanning to the organs of significance (Pelc NJ, 2014).

Scan Phases

The frequency of scan phases during such patient's examination refers to the number of times the same patient anatomy is radiated. In multiphase scans, the dosage to an organ increases dramatically. The majority of documented CT overdose occurrences have been the consequence of multiphase scans, according to the literature (ICRP 121, 2013). However, the portion of anatomy scanned multiple times receives a significantly higher dose, and, therefore, scan protocol optimization is essential. The use of multiphase CT scanning in children should be limited to absolute necessity (ICRP Publication 121, 2013).

Enhanced Dose-Reduction Strategies

Several enhanced dose-reduction techniques which include; using localizer images to optimize the kVp and mAs to adapt the scan to an individual patient's anatomy. However, lager patients require higher kVp and mAs and smaller patients require lower kVp and mAs. Faster computers enable more advanced image reconstruction methods, such as iterative

36

reconstruction. and can also increase image quality while allowing for lower mAs and, hence, lower-dose imaging (Peacock NE et al, 2020).

Automatic kVp Selection

The use of localizer images to determine patient attenuation and body size to select an ideal kVp to reduce radiation dose and increase soft tissue contrast is another essential dose parameter to maximize dose to paediatric patients. Generally, larger patients require higher kVp, whereas smaller patients can be imaged using reduced kVp. Studies involving contrast also can select specific kVp values to enhance contrast material visibility (Thomas Nelson, 2014).

Tube Current Modulation

One important parameter that is used to reduce patient dose is the tube current modulation using the exposure control system. "Scanner dose control with automatic tube current modulation uses localizer images to adjust the mAs based on patient anatomy" (Pages et. al, 2003; Moss et. al, 2006), However, in order for the procedure to work correctly, the patient must be perfectly positioned in the centre of the gantry. The CTDI$_{vol}$ dose will drop for smaller patients as a result of mAs modulation, but will increase for larger patients.

Patient Immobilization in Paediatric Imaging

Immobilization of paediatric patients is a crucial approach for obtaining high-quality paediatric CT scans. As a result, immobilizing new-borns and youngsters is necessary to decrease motion artifacts and avoid

37

repeated scans. Immobilization of paediatric patients can be accomplished in a variety of ways. Using alternative acquisition procedures with a faster scan acquisition technique is one such strategy. The use of immobilization devices is another option for limiting movement. (Thomas Nelson, 2014).

Overall Strategies to Minimize CT Dose in Paediatric Patients

BEIR report states that "New scanner technology offers a variety of opportunities to reduce radiation dose while obtaining improved diagnostic information" (BEIR VII Phase 2, 2006).

Iterative reconstruction, automated tube current modulation, and automated tube potential selection can all help to reduce patient exposure while still offering high-quality diagnostic examinations. It is vital to keep in mind that new scan technology introduces additional challenges by encouraging overuse and more complex research, such as dynamic studies with repeated scanning that might result in extremely high doses (ICRP Pub.60, 1991).

The diagnostic protocol should be tailored to the patient's age and size, and dose-reduction scan techniques should be used wherever possible while still obtaining high-quality diagnostic information (Thomas Nelson, 2014).

A collaborative approach combining the radiologist, technologist, and medical physicist is required to reduce paediatric CT radiation dosage and optimize CT scan protocols in a paediatric patient. Every imaging examination in paediatric patients must be intelligent, suitable, and medically indicated for that child, according to the radiologist. The radiologic technologist is in charge of adjusting protocols to employ child-size parameters and ensuring that

suitable scan method factors are specified for each paediatric scan. The medical physicist's job is to improve picture quality by advising on acceptable paediatric procedures and ensuring that young kids are photographed with the lowest radiation doses possible (ALARA).

Paediatric Dose Quantities Used in Setting DRLs

The same practical dose quantities used to monitor adult radiology procedures should be utilized to set DRLs. However, while grouping patients for setting paediatric DRLs, special care must be taken because the size of children, and therefore the dosage levels, vary dramatically not just by age but also within a specific age. Adults typically vary in size by a factor of four (40–160 kg bodyweight), whereas paediatric patients vary by a factor of more than 200, ranging from preterm babies (e.g., 300–400 g) to obese teenagers (> 80 kg body weight).

Additionally, weight should be utilized as the criteria for patient categorization in all body inspections and DRLs based on prospective patient dose surveys. The recommended age grouping of patients for paediatric DRLs is shown in Table 6. Age can be utilized as an additional criterion for patient classification and comparison of proposed new, weight-based DRLs with older values during the transition phase (trend analysis). Age is recommended as a grouping parameter for head examinations. Table 6 shows the recommended groupings (intervals) in the PiDRL report (EU, 2018).

Table 6: Recommended Age Groupings for DRLs Determination

Recommended weight groups (intervals) for *body* examinations	Recommended age groups (intervals) for *head* examinations
< 5 kg	0 - < 3 months
5 - < 15 kg	3 months - < 1 y
15 - < 30 kg	1- < 6 y
30 - < 50 kg	≥ 6 y

Source: (EU, 2018).

According to published weight-for-age charts, there is a rough link between average weight and age categories. For the purpose of comparing weight-based DRLs with age-based DRLs, Table 7 shows the approximate equivalent of weight and age categories:

Table 7: Approximate Equivalence Weight and Age Groups

Description	Weight group	Age group based on height-for-age charts	Most common age groups used for the NDRLs (or equivalent)
Neonate	< 5 kg	< 1 m	0 y
Infant, toddler and early childhood	5 - < 15 kg	1 - < 4 y	1 y
Middle childhood	15 - < 30 kg	4 - < 10 y	5 y
Early adolescence	30 - < 50 kg	10 – < 14 y	10 y
Late adolescence	50 - < 80 kg	14 - < 16 y	15 y

Source: (ICRP publication 121, 2013)

In addition, instead of using discrete patient groups, the dosimetric quantity can be presented as a function of the parameter used for patient grouping, i.e. to define a DRL-curve, to overcome the problem caused by the need for several patient groups and the general paucity of patient dose data in paediatric imaging. By placing these data points in the graph with the DRL-curve, local patient dosage data can be compared with the DRL-curve for ten consecutive patients, regardless of age, size, or weight. However, in the absence of well-established national and local support for DRLs, they are at a

disadvantage (as, for example, a paediatric radiology facility in a less-resourced country like Ghana) (ICRP 135 , 2015).

Dose Optimization in Computed Tomography Imaging

In photon based medical imaging, diagnostic decision is primarily based on the quality of images produced which are also based on the intensity of the photon energy delivered. Unfortunately, however, the higher the number of photons (mAs) and energy of a photon (kVp) intensity the higher the dose received, as a result, there is always a need to strike a balance between image quality and patient clinician radiation exposure. These are required to ensure that acceptable picture quality is obtained for clinical decision-making while also avoiding prognostic problems by keeping the radiation exposure to patients to a bare minimum. The signal to noise ratio (SNR) or the contrast to noise ratio (CNR) are used to describe the picture quality in current CT imaging. However, an American Association of Physicists in Medicine (AAPM, 2011) journal claims that CNR has incoherent limitations, owing to the fact that it does not account for background noise correlations (Lu & Nishikawa, 2012). The SNR, on the other hand, takes into consideration noise correlations since it correlates well with human observers' performance in identifying low-contrast signals against uniform circumstances (Lu & Nishikawa, 2012).

In fact, the statistical decision theory framework is utilized to assess the image quality of medical imaging equipment. Picture quality is defined in this technique in the context of the image information available for executing a certain detection or discriminating job. This method allows for the

measurement of picture quality in relation to the identification of an image detail of interest without having to refer to the actual physical mechanisms involved in image generation or separately measuring signal flow behaviour or image noise. The signal-to-noise ratio of the ideal observer at the decision point can be used to indicate the detectability of an image detail. Clinical research scientists have advocated, and physicians have approved and implemented, the use of individual observer judgment (qualitative) in addition to quantitative analysis. As a result, image quality is determined by the connection between the process signals in the noise, which is referred to as the image's SNR (AAPM, 2011).

Qualitative and Quantitative Analysis of Image Quality

Medical images can be analysed either qualitatively (appearance) or quantitatively (measured). A radiologist usually does the qualitative analysis with assessment of the appearance of images; whilst the quantitative assessment is done, using signal-to-noise measurements. Ratio of Signal to Noise In terms of picture element value, the ratio is the mean to standard deviation of a signal or measurement when background distortion is taken into account. also provided in voxel format as a ratio of the mean to the standard deviation of voxel values, as shown in equation 10:

$$\text{SNR} = \frac{\mu}{\sigma} \; \text{SNR} = \frac{\mu}{\sigma}, \tag{10}$$

where μ is the signal mean or expected value and σ is the noise standard deviation, or a close approximation. This is important for photon counts in image processing, where the SNR of an image is typically calculated as the ratio of the mean pixel value to the standard deviation of the pixel values over

42

a specific region or backdrop also known as the second power of the signal's standard deviation mean value (equation 11).

$$SNR = \sqrt{\frac{\mu^2}{\sigma^2}} = \sqrt{\frac{r}{1-r}} \tag{11}$$

where *r* is the correlation coefficient. Equation (11) is used in cases where r is known, however, Equation (11) is the standard definition for SNR (AAPM, 2011).

Equation 11 is also used to characterize the sensitivity of imaging systems. Optimization of patient protection is done by determining the tradeoffs between the minimum dose that matches with a clinically acceptable image quality for accurate diagnosis decision. For instance, the tradeoffs between dose reduction and image quality include; reducing mAs where radiation dose is reduced in proportion to the reduction in mAs; this may however increase image noise in proportion to $\sqrt{\frac{(mAs_{original})}{(mAs_{reduced})}}$.

As a result, if the mAs is reduced to 50 percent of the original, the noise is projected to increase by 1.41 (41%) percent (Lu & Nishikawa, 2012). In conclusion, increasing the table speed or pitch may lower radiation dosage according to the increase in pitch. Even yet, this may enhance slice sensitivity, resulting in higher effective slice thickness and decreasi z-axis resolution. Reduced kVp may also lower radiation dosage, increase signal contrast for particular tissues due to increased photoelectric effect, and considerably increase beam hardening artifact if the beam energy is too low (e.g., kVp = 80) (AAPM , 2011).

Computed Tomography Examination Risk Assessment

Paediatric radiology patient risk assessment is reviewed for relevant CT imaging. CT is a useful imaging method for assisting in the diagnosis and treatment of a variety of medical disorders. Nonetheless, its growing popularity has raised public awareness of the dangers of contracting cancer, because CT produces effective doses 5–20 times higher than conventional radiology (Boone et al, 2003; Kleinman et al, 2010), resulting in organ doses of tens of milliGrays (mGy) from each scan (Boone et al, 2003; Kleinman et al, 2010).

To permit physicians to make informed decisions concerning CT examinations and to give patients and families with relevant information, a reliable quantitative assessment of potential dangers generated by radiation exposure is essential. The use of robust epidemiological evidence gained at higher doses to forecast the cancer risks associated with these low-dose exposures is one beginning approach to such an assessment. Although this method allows for the estimation of the amount of prospective dangers (Huda et. al, 2011; Christner et. al, 2010). Its veracity has been questioned in light of the premises that underpin those extrapolations, including the existence of a no-threshold relationship between cancer risk and exposure to radiation (Tsapani et. al, 2011). New studies are being done (Tzedakis et al, 2005, Velten, 2009, Leitz et al, 2005; Christner et al 2010) to provide direct risk estimates from huge populations exposed to CT scans. After an estimate of 7–10 years of follow-up, the UK study found a threefold increased incidence of brain tumors and leukemia in children and young adults who got mean organ doses of 50 and 60 mGy, respectively, compared to patients who received

44

doses of 5 mGy (Tzedakis et al, 2005). With a mean follow-up of 9.5 years, the Australian study found increased cancer risks at various sites, as well as a 20 percent increase in the risk of all cancers, as compared to people who were not subjected to CT scans (Velten, 2009). Finally, after 8 years of follow-up, the Taiwan study found that children and adolescents who received head CT scans had a 2.6 times higher risk of brain tumors than those who were not exposed (Leitz et. al, 2005). Extrapolating from prior epidemiological data at higher doses, the Leukemia results were similar with those expected (Huda et. al, 2011). The relative risks for central nervous system (CNS) tumors, on the other hand, were much greater than those anticipated per unit of dosage in moderate and high-dose investigations. Despite this, the absence of information about the causes for scans limits the interpretation of these current data (Lerner et. al, 1999). If these tests were done because of a suspicion of cancer (reverse causation) or for the diagnosis or monitoring of illnesses linked to an elevated cancer risk, overestimations could easily have occurred (confounding bias). Postponing the calculation of cancer incidence beyond various times of exclusion is one technique to assess the consistency of the results when the potential of reverse causation is minimized in the absence of knowledge about the reason for the investigation. However, collecting data on predisposing factors (PFs) to cancer, such as genetic disorders and immunological deficiencies, is the only approach to address the confounding bias.

In radiotherapy practice, CT imaging has shown to be a diagnostic tool as well as a tool for cancer staging and treatment planning. Ionizing radiation risk assessment has evolved in a very different way than chemical risk

assessment. Chemical carcinogen risk assessments are more often based on projections from high dose experiments with laboratory animals or on human epidemiology with relatively uncertain exposures, whereas radiation risk assessment is largely based on long-term follow-up studies of humans exposed to relatively well-known high doses of radiation. While high exposures have resulted in a variety of consequences, cancer is the predominant impact expected at lower concentrations. Cancers induced by radiological and chemical agents have been found in almost every organ of the body, depending on the agent, species, and exposure conditions (NCRP, 1989). The onset of induced cancer is usually preceded by a long latency period, which varies depending on the type of malignancy and the age of the person at the time of exposure. In broad terms, malignancies seen in exposed people are similar to cancers seen in unaffected people (though there are exceptions such as mesothelioma, which is associated with exposure to asbestos).

While the quantity of radionuclides is well-known, the number of substances regarded as being carcinogenic grows every year, even if not all are identified in the environment. Just over 800 radionuclides are listed in (ICRP 38, 1983). About 50 of these are potentially hazardous due to their abundance in emissions or wastes, as well as their toxicity. The number of substances that can cause cancer has been estimated in a variety of ways. Currently, 69 substances or industrial processes have been linked to the development of cancer in humans (IARC, 1995). More than half of the 1300 chemicals tested in the Carcinogenic Potency Database are capable of causing cancer at high exposure levels, according to chronic long-term studies in rats and mice (Gold et al, 1997), and (Ames et al, 1990, 1990a) have predicted that about half of all

46

chemicals tested, whether synthetic or from natural sources, will lead to cancer when fed in high doses to animals over long periods of time. Risk levels are rarely observable from direct observational studies of human populations because environmental exposures are minimal for both radioactive and chemical dangers. In order to generalize from reported high-dose effects and estimate low-dose effects, a suitable dose-response model must be chosen to assess the risk at lower doses. Both radiation and chemicals employ similar analytical and numerical models. Although dose-response curves for ionizing radiation and genotoxic chemical carcinogens may be nonlinear at high doses, usually accepted that they are linear at low doses. Because no threshold doses are assumed, some risk is expected to exist even at the lowest dose levels, but unrecognized and unobservable (NCRP, 1989).

Any model should be able to provide the best assessment of the risk as well as an indicator of its uncertainty. With the limited data available from epidemiological and toxicological investigations, various models can be proposed that match the data equally well but provide risk estimates at low doses that vary among many orders of magnitude (Food and Drug Administration, 1971). By adding hazardous modes of action, biologically-based models could give a more accurate basis for risk estimations (Goddard and Krewski, 1995). This would help in evaluating model-based risk projections and extrapolating beyond the circumstances under which the primary data was collected.

The most generally used model for estimating cancer risk is the multistage model, which is based on the number of steps in the carcinogenesis process (Armitage & Doll, 1961). (Crump & Howe, 1984) proposed the

updated, stability analysis multistage model for practical applications. Another set of biologically-based carcinogenesis models (Moolgavkar & Luebeck, 1990) assumes that cells begin to form after a single mutation in a normal stem cell, and that launched cells can tolerate a second mutation and evolve to a malignant cell. Clonal expansions can also help the started cell population grow, increasing the number of cells available for cancer advancement. The fact that the parameters of this type of model may be interpreted in biological terms and, in certain situations, obtained empirically is a massive benefit.

Mechanistic modelling relies heavily on physiologically based pharmacokinetic (PBPK) models. PBPK models aim to predict the dose of reactive metabolites that reach target tissues in general. Instead of using an external measure of exposure, using an appropriate measure of tissue dosage can allow for more accurate assessments of low-dose cancer risks (Krewski et. al, 1994).

Calculations of cancer risk are imprecise due to the absence of immediately detectable effects at low dosages. Inherent variability, such as measurement error in dose and exposure estimations, contributes to some uncertainty. The effects may also be influenced by physiological factors such as body weight, respiration rate, and cardiac output, which differ from person to person. For risk estimation, often only fragmentary or subjective data is available. Exposure estimates in epidemiological research on chemicals, for example, may be shaky due to a lack of historical data on individual exposures. Determining health effects, extrapolating from animals to humans, and extrapolating between routes of exposure are all causes of uncertainty. The choice of dose-response model can also have a big impact on risk

48

estimation. These ambiguities are thought to be smaller for radiation-induced cancer risk estimations, which are generally based on human randomized trials, than for chemical-induced cancer risk estimates, which are frequently based on animal research (BEIR VII, 2006).

Quantitative Risk Assessment for Ionizing Radiation

Radiological cancer risk statistics are based on demographic studies of human populations exposed to high radiation doses. Follow-up studies on Japanese survivors of the 1945 atomic bombings of Hiroshima and Nagasaki are the primary source of information on the risk of radiation-induced cancer following whole-body exposure to external radiation (Christner et al 2010). Miners exposed to large levels of radon and its decay products in the air, early radium dial painters who mistakenly ingested significant amounts of radium, and patients subjected to high doses of medical X-rays or administered radium-224, radium-226, or Thorotrast are among the other populations investigated (thorium oxide).

Extensive experiments on animals and other species have yielded additional insights. Because no significant increase in inherited disorders has been seen in the children of Japanese bomb survivors, estimates of this chance are based on research on animals. The United Nations Scientific Committee on the Effects of Atomic Radiation (UNSCEAR) reviews information of this sort on a regular basis, and produces authoritative reports to the United Nations General Assembly every five years; the most recent UNSCEAR report was published in the 2010 report (BEIR-VII, ICRP, 2007, UNSCEAR, 2010).

49

The ICRP evaluates scientific material on radiation's biological effects and provides reports with recommendations on various elements of radiological protection. The Committees on the Biological Effects of Ionizing Radiation (BEIR) in the United States also examine the data and publish reports. The BEIR reports, like the UNSCEAR reports, are solely concerned with the evaluation of impacts and provide no advice for radiation protection. These panels' risk assessments are remarkably similar (BEIR-VI 1998, BEIR-V 1990, ICRP 1991, UNSCEAR 1993, NCRP 1993, BEIR-VII, ICRP, 2007, UNSCEAR, 2010). In BEIR, UNSCEAR, and ICRP studies, issues with using data on excess malignancies in Japanese bomb survivors to forecast outcomes at lower doses and exposure rates have been thoroughly debated. One issue is determining how to extrapolate statistics on the increased number of cancer cases experienced by bomb survivors in the first 40 years after exposure to forecast the increase that would occur over the population's lifetime. To calculate lifetime risk estimates, various models associating the growth in cancer with age following exposure were utilized. Another issue is determining how to extrapolate the lifetime risk of certain malignancies in a Japanese population to other populations. Extrapolation to other populations is challenging due to differences in cancer incidence patterns between Japan and other countries. The 1991 ICRP estimates were calculated by combining the results of two extrapolation models and applying them to the populations of five countries (BEIR-VII, 2006; ICRP, 2007; UNSCEAR, 2010).

Extrapolation of data from populations exposed to varying whole-body doses of external radiation at high dose rates to projected effects of radiation at low dose rates is a third issue. ICRP Publication 60 (1991) adopted the

50

convention of dividing the cancer risks observed at high doses and high dose rates of X- and gamma-rays by a dose and dose rate effectiveness factor of two in order to obtain cancer risk estimates for low doses of ionizing radiation at low dose rates, based on theoretical considerations, experimental animal studies, and some limited human data. To put it another way, a low radiation dose administered at low dose rates is about half as effective as the same dose supplied at a high dose rate for creating long-term consequences. Low doses are now defined as fewer than 200 mSv, and low dose rates are defined as less than 0.1 mSv per minute or 6 mSv per hour, according to UNSCEAR (1993); it should be emphasized that these doses and dose rates are extremely high when compared to common public dosages.

Lastly, the data's application to those exposed to radiation dosage orders of magnitude lower than those received by atomic bomb survivors is a concern. Any increase in radiation exposure, the international radiation protection community has conservatively assumed, will result in a corresponding rise in cancer risk and the danger of genetic abnormalities (although there is some evidence to the contrary). This assumption has been investigated in the linear no-threshold model (i.e. linear dose response down to zero dose) (ACRP-18, 1996). Some research from both human and animal studies suggests that in some circumstances, such as the production of bone cancer by radium-226, there is a realistic threshold dose below which the risk of developing bone cancer within a normal lifespan is almost minimal (BEIR-IV 1988). There is also evidence of a decrease in cancer rates in humans after exposure to very low amounts of radioactivity, possibly due to the stimulation of repair mechanisms. However, the statistics currently available are

insufficient to take this into consideration in radiological protection (ACRP-18, 1996).

Regarding these issues and the inherent uncertainties, a probability estimate for radiation-induced malignancies is required for radiation protection purposes. Following a protracted whole-body exposure to low dose and low dose rate radiation, (ICRP Publication 60, 1991) recommends lifetime fatal cancer risk estimates of 0.04 per Sv for the adult population and 0.05 per Sv for the total population including all age categories. The ICRP risk estimates represent a consensus of international scientific opinion, and at low doses, they may exaggerate risk. While the linear no-threshold paradigm cannot determine the outcome of actual doses to an individual or a community, a useful tool for comparing risk mitigation and regulatory choices.

Risk parameters have been projected for total harm caused by all late effects, including victims, non-fatal cancers normalized for magnitude and ease of cure, years of life lost or seriously impaired, and the risk of serious genetic disorders constructing in subsequent generations, in addition to fatal cancers. Radiation-induced leukaemia, for example, is given a higher priority than radiation-induced skin cancer, which is treatable. The ICRP has recommended a risk coefficient for overall harm for an adult population of 0.056 per Sv, and 0.073 per Sv for the general public, based on these considerations (ICRP, 1991). Due to a lack of definitive evidence of these impacts in human populations, risk estimates for genetic disorders are derived from rodent data exposed to a wide variety of dosages and dose rates. Teratogenic effects (abnormalities in the developing embryo) have also been considered; however, they are assumed to be nil below the dose limits

suggested by the International Commission on Radiation Protection and Measurements for public exposure (ICRU, 1991).

The hypothesis of a linear no-threshold relationship between dose and risk has the critical consequence that the collective dose becomes a predictor of communal danger (aggregated risk to the whole community). The total dose to the community as a whole may be significant if a large number of people were exposed to low amounts of radiation from diverse sources, below any limit imposed for individuals. The chance of unfavourable health consequences from radiation is considered to rise linearly with dosage in the linear no-threshold model, and the population size dose would be assessing the potential societal impact. Individual doses of less than 10 microsieverts per year (roughly 5% of the radiation dose everyone receives on average per year from natural sources) should be individuals from and not added to collective or total population doses, according to the AECB Advisory Committee on Radiological Protection. Even if the linear no-threshold theory is supposed to be valid, this proposal implies a lower level of worry about the health consequences of such doses, which are regarded minimal (ACRP-18, 1996).

Many reports have been written that offer data on workers who have been considered to have received a carefully quantified low-dose radiation, the most prominent of which are (IARC, 1994), (Kato et al, 1994), and (Kato et al, 1994) thorough findings on occupational exposure in the nuclear sector (Kendall et. al, 1992). The IARC study, which included nearly 90,000 nuclear workers from Canada, the United States, and the United Kingdom, was the largest evaluation of potential side effects associated with workplace radiation exposures. Because this study was unable to establish a clear cancer risk at

low dose levels, of little use in inferring dangers linked with ambient radiation exposures. (Cardis et al, 1995; Létourneau et al, 1994; Alavanja et al, 1994; Pershagen et al, 1994; Lubin et al, 1994; ACRP-18, 1996) attempted to get supporting data of risk from individuals who had received low dose treatments, such as those arising from household radon contamination. There have not being any conclusive findings on direct estimates risk from population who have received low doses form radon exposure. Although it is difficult to clearly establish extra lung cancer risks based on the general human studies (Lubin & Buice, 1997), the BEIR-VI 1998 review found that, based on molecular and cellular concerns and studies of miners subjected to elevated doses of radon, about 10-15% of lung cancer in the general population could be due to residential radon toxicity.

Chapter Summary

In conclusion, a comprehensive and accurate review and analysis of the literature was presented, which encased the history of CT scanners and their use in diagnostic imaging devices, with a focus on paediatric imaging; paediatric radiology and associated dosimetry; factors affecting paediatric patient dose; procedure optimization and patient protection; and patient risk assessment.

CHAPTER THREE

RESEARCH METHODS

Introduction

This chapter covers the materials as well as the processes of measuring, analyzing, and calculating dosage parameters using mathematical formulae. It begins by defining the various materials and testing processes used to determine SNR and dosage optimization during CT scans. The techniques and protocols for determining effective organ dose for dose optimization using SNR is also included. It also comes with a set of Minitab statistical tools and MVL application software for modeling the various equations. It concludes with a discussion on the limitations encountered prior to, during, and after the measurements, modeling, and clinical applications.

Equipment

The assessments, layout, and modeling needs were all tailored to the desired specifications, including materials and execution methods. Weighing machines, Automatic BMI Machine, Philip Tomoscan MDCT Machine, Siemens Somatom plus MDCT Machine, GE Max 640 Machine, and Toshiba e/CT Machine, Abdominal MDCT radiographs, Input user interface, and MeVisLab (MVL) workstation and interface are all listed in Table 8.

55

Table 8: Specifications of CT Scanners

Manufacturers	Scanner Model/Scan Mode
Philips	Brilliance 64, Multislice, Axial and Helical Modes
Siemens	Emotions 16, Multislice, Axial and Helical Modes
General Electric	Lightspeed VCT 64, Multislice, Axial and Helical Modes
Toshiba	Toshiba-Aquilion ONE, Multislice, Axial and Helical Modes

Source: (Huda, 2010)

Figure 7: Aquilion CT Scanner (KBTH, 2018)

56
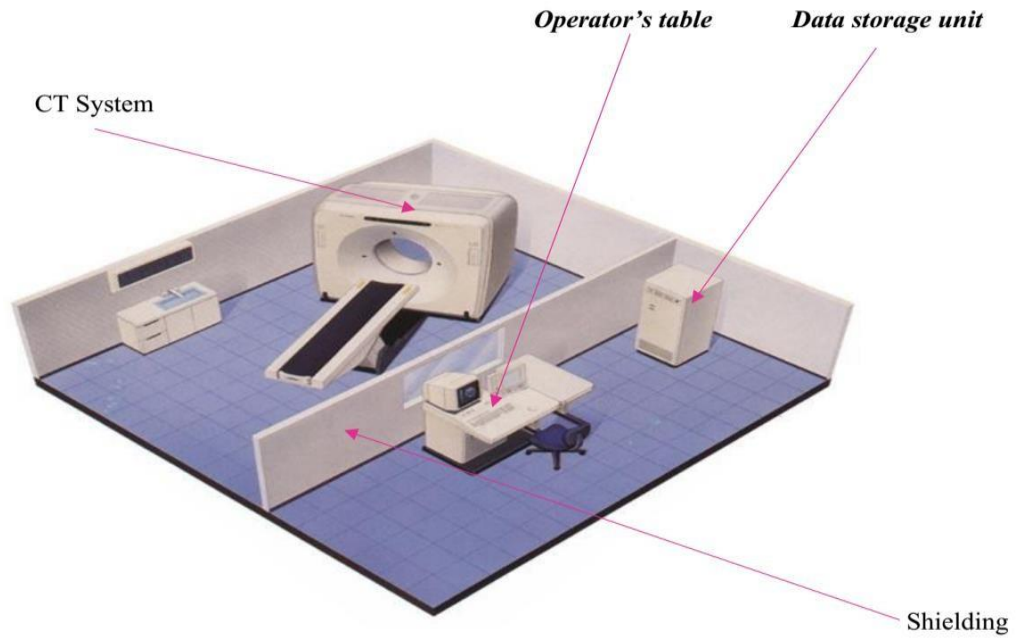
Figure 8: A CT room layout showing CT scanner, the console and data storage device
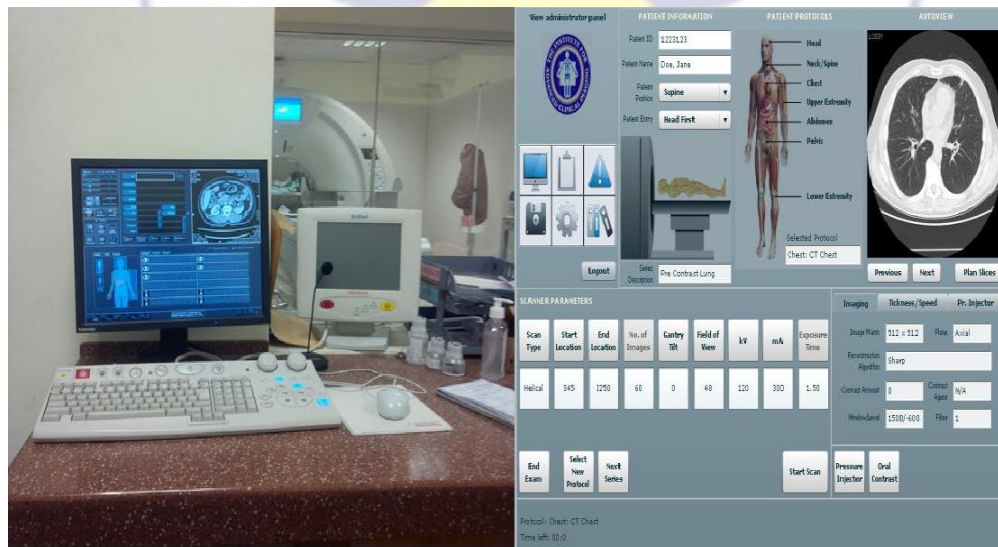
Figure 9: Input CT data user interface (KBTH, 2018)

Two instruments for measuring, together with an input user interface as shown in Figure 9 where the input data is gathered, were employed as part of the clinical management of patients prior to imaging as pre-imaging tools. Other equipment used included four distinct MDCT machine models (Figure

57

7), each with a distinct number of slices ranging from 16 to 640. (Specifications shown in Table 8). The MDCT images that met the selection criteria were copied onto DVD and transferred onto the MVL application workstation (Figure 10). The MVL operating system allows for a variety of measurements in the coronary and axial planes. It also illustrates the MVL user interface, which may be used to measure digital information as well as capture picture data.

Figure 10: MeVisLab Version 13, interface with image data

Method

Patient data collection and quality control (QC) measurements were the procedures used. Quality Control measurements carried out on the CT machine include:

1. kV accuracy

2. Half value layer

3. CTDI$_{vol}$ and DLP

58

4. CTDI free-in-air and Geometric Efficiency.

The DICOM application software specification extension for reporting dosage parameters in CT was released in 2007. (Shrimpton et al, 2013). This has now become a requirement for all makers of medical diagnostic equipment, including CT scanners. The equipment must include a software component that generates a thorough preliminary report for the whole consultation session as well as an amassed dose report. That is, the report should include both the input and output study parameters; the patient clearly defined set, health history, and general machinery information should all be gathered and saved in the structured report's general section. This technological advancement provides a comprehensive solution to the evident challenges of acquiring information about the distribution of dosage within the body during CT imaging. More useful dosimetric variables acqu   ired during the imaging procedure are included in the report and can be utilized to estimate these parameters (CTDIw, CTDI vol, DLP, E) from closely related measurements. The risk-related numbers were calculated using the relevant dose-conversion coefficients in Table 5 from the practical input dosimetric quantities CTDI and DLP, which led to an estimate of effective dose. Relevant information of the CTDIvol and DLP were accessible for capture on the MeVisLab platform as part of the dosage report of the image data. On the same system, the mean and standard deviation of each of the several zones of interest created on the radiographs were recorded (AAPM, 2011).

Effective Dose Using CTDIw and DLP

The weighted CTDI (CTDI$_W$) was estimated by multiplying the volume CTDI (CTDI$_{VOL}$) by the pitch factor (p) expressed mathematically as:

$$CTDI_W = pCTDI_{VOL} \qquad (12)$$

where p varies from 0.813-1.0 is the average pitch factor of the scanning protocol. Utilizing equations 1 and 2 with the required ICRP region-specific adjusted effective dose coefficient in Table 9, the CTDI$_W$ and DLP allow organ and effective dose estimation. As a result, using the suitably adjusted coefficients, broad values of effective dose (E) were generated using DLP and CTDI$_{vol}$ values for each testing.

To estimate the various effective dose, DLP and region- specific normalizing constant or DLP conversion factor (EDLP) as developed by ICRP 103 were used and defined as:

$$E = \mu DLP. \qquad (13)$$

Based on ICRP publication 103, the Abdomen, Chest, Pelvis, and Head region-specific normalization constants of 0.0153, 0.017, 0.019, and 0.0023 were used to estimate effective dose. This is due to the fact that the effective dose is a descriptive derived theoretical value for anatomical dose determined based on the organs exposed by the applied radiation combined by tissue-weighting variables, rather than a measured parameter. Because tissue-weighting factors can vary over time as new data becomes available and previous data is analyzed with more sophisticated analytical techniques, the effective dosage conversion factor estimates can also change.

60

Patient Data Collection

The Toshiba Aquilion One 640-slice CT scanner, which has been in use since December 2012, provided retrospective data. The patients for this study were chosen at random from a total of 270. Two hundred (200) of them met the selection criterion. Parameters such ask kVp, mA, DLP, CTDI$_{vol}$, pitch and scan length were gathered from the dose analysis and the programmable logic controller, (control console) with each client's serial number matched to the parameters on the dose report and the console. The MeVisLab application software was used to view and analyze the data.

Quality Control Measurement

The radiation and image quality control kit was used to evaluate image quality and CT performance as indicated by producers and by international standards. The AAPM III designed phantom for CT number evaluation was used for the CT noise measurement. For proper CT Quality Control examination, the scanner readings were validated to standard measurement. The daily necessary scanning material of known CT data, such as the AAPM (AAPM Report NO. 39, 1993) five-pin performance phantom, was used to complete a check calibration, as illustrated in Figure 11.

Processes for Data Collection and Analysis

The following procedures were undertaken to acquire data for patient dosage quantities (CTDI and DLP) in respect to current clinical research for common examinations on paediatric patients:

Displayed values of radiation dose quantity for a minimum of 20 or more typical paediatric patients undergoing CT procedures for common

61

clinical indications (head, chest and abdomen-pelvis) were recorded. These include; head examinations (e.g. in relation to hydrocephalus), chest examinations (e.g. in relation to chest pain) and abdomen examinations (e.g. in relation to acute abdominal pain). Below were the various steps taken during the process of data collection.

To begin, the correctness of the presented values of radiation dosage values on the dose report and the multimeter readings were evaluated, and if necessary, correction factors were applied.

Second, the median values of dose values for $CTDI_W$, $CTDI_{vol}$, DLP, E, SNR, and organ dose were determined for each type of examination; they indicate the typical levels of the dose that are set for typical procedures.

Thirdly, the common dose levels of the median results were compared with published DRLs for a similar practice to provide a general idea of actual performance and the immediacy of the need for imaging technique development.

Since a comparison of usual dose levels of the median values to DRLs is insufficient, for optimum protection, quality or, more broadly, the diagnostic information provided by the examination (including the effects of post-processing) were also assessed.

Unfortunately, just because the results are lower than the published DRL does not mean the performance is good. Imaging techniques were examined to see whether they might be reduced in dose without jeopardizing the clinical objective of the scan.

Ultimately, if the values exceeded the DRL, investigations were conducted to examine if simple adjustments to the imaging parameters used

for an examination might be made to lower radiation dose quantities while still giving the essential patient information, In addition, the levels of dose were reassessed following revision of imaging techniques in order to allow further comparisons.

CT Dosimetry and Effective Doses

CT dose pattern in the patient is significantly more homogeneous due to the rotational irradiation geometry in the CT, says the study (ICRP 121, 2013). To put it in another way, the dosage gradients in CT are relatively small. In most current CT scanners when they are in helical acquisition mode, they offer a dose modulation option that regulates the X-ray tube output. As the gantry rotates around the patient and the table conveys the patient via the spinning X-ray beam, the mA is varied. When the X-ray beam is positioned along a thicker X-ray path through the patient, dose modulation mode raises the dose rate or mA, and dose modification mode decreases the dose rate or mA on the thinner X-ray path through the patient.

CTDI Measurement

Dosimetry based on the CTDI is the current global standard for estimating patient dose. The CTDI is the dosage in CT determined using a Polymethyl methacrylate (PMMA) phantom with a diameter of 16 cm or 32 cm. The dosimeter is serially inserted into the center and periphery holes, and the results are added together to generate the weighted CTDI (MeVis Medical Solution, 2015).

63

A   B
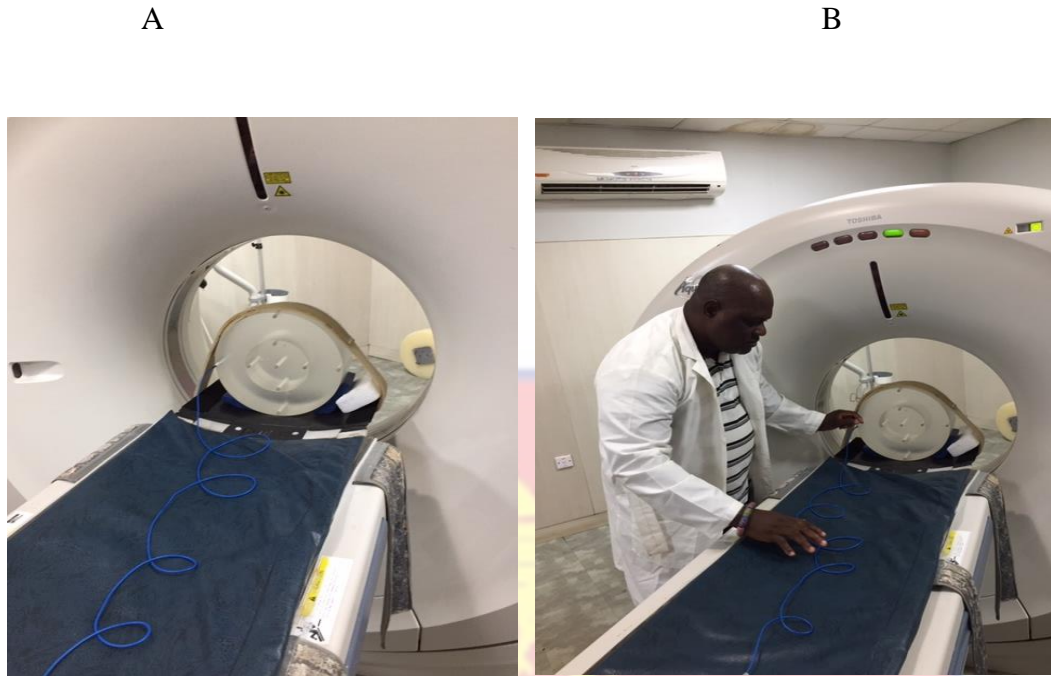
Figure 11: (A) Phantom setup (B) Demonstrating CTDI measurement

The head and body configuration is used in the experimental procedure shown in Figure 11A. A 100 mm long cylindrical ionization chamber, often known as a "pencil" chamber, with a 9 mm diameter, is put into either the centre or peripheral hole of a PMMA phantom, shown in Figure 11B, for the CTDI 100 measurement. The body phantom, which is 32 cm in diameter and 15 cm long, and the head phantom, which is 16 cm in diameter and 15 cm long, are the two standard PMMA dosimetry phantoms (Figure 8). A single axial CT scan is performed on the phantom's head phantom (the Z-direction as well as the CT gantry's center (Monson, 2006).

The $CTDI_{100}$ is defined as

$$CTDI_{100} = \frac{1}{nT}\int_{L=-50mm}^{+50mm} D(z)\,dz \qquad (14)$$

64

The $CTDI_{100}$, describes the measurement of the dose distribution along the $Z-direction$ from a single circular rotation at the scanner. nT describes the nominal beam width and n is the number of active detectors (for a 64 channel CT scanner ($n=64$)) and $T-$ is the size of each detector channel.

The $CTDI_{100}$ measurements are made for both the centre ($CTDI_{100}_{/centre}$) and periphery ($CTDI_{100}_{/periphery}$) combining the centre and peripheral measurements using $\frac{1}{3}$ and $\frac{2}{3}$ weighting scheme provides a good estimate of the average dose to the phantom (at the central CT slice along Z) giving rise to the weighted CTDI, known as $CTDI_W$.

$$CTDI_W = \frac{1}{3}CTDI_{100}_{/centre} + \frac{2}{3}CTDI_{100}_{/periphery} \tag{15}$$

In helical CT scanning, the CT dose is inversely related to the helical pitch used.

$$dose \propto \frac{1}{Pitch} \tag{16}$$

$$CTDI_{Vol} = \frac{CTDI_W}{Pitch} \tag{17}$$

where, pitch is defined as the table translation distance ($in\ mm$) during a full rotation of the gantry, divided by the nominal beam width nT (in mm). The

product of the $CTDI_{Vol}$ and the length of the CT scan along the $Z - axis$ of the patient, L is the Dose Length Product (DLP).

$$DLP = CTDI_{Vol} \times L \qquad (18)$$

Estimation of Effective Dose

In addition to the radiation dose to tissue or organ, biological effects from radiation are dependent on the biological sensitivity of the organ irradiated. The effective dose is a metric that efficiently determines and displays the difference between these biological effects based on biological sensitivity and radiation exposure. The danger of a non-uniform exposure in terms of an equivalent whole-body dosage is determined by the single dose criterion. The Effective dose considers the amount of radiation received by each tissue as well as the tissue's proportional radiation sensitivity. As a result, assessing the radiation dosage in terms of effective dose and comparing that value to published statistics better communicates to the patient the equal potential for damage from the medical test.

It has been shown that DLP is approximately proportional to E (Chung T et. al, 1998).

$$E = DLP \times K \qquad (19)$$

where, K is the slope of E versus the DLP relationship and there are K values for various CT examinations.

66

Table 9: Conversion Factors (K values) for estimation of Effective dose (mSv) from Dose-Length Product (mGy-cm) for various CT Examination

Tissue Organ	CONVERSION FACTOR K (E/DLP) $[mSv/mGy - cm]$
Head	0.0019
Neck	0.0051
Chest	0.0145
Abdomen	0.0153
Pelvis	0.0129

Source: (AAPM 96, 1993) (At tube voltage of 120V)

Sampling Procedure

The information was analysed across Ghana to ensure that the study reflects the whole Ghanaian population. Two sample approaches were used to accomplish this: stratified random sampling and simple random sampling. The five participating hospitals in Ghana were chosen using the Stratified Sampling approach. The country was divided into three sectors to do this: northern, middle and southern. As a result, one hospital was chosen from each of the three sectors, while two hospitals were chosen from Greater Accra based on two factors: a large density of CT units, which boosts patients' CT attendance in Accra, and the region's cosmopolitan nature. Furthermore, the two institutions chosen were referral hospitals with locations throughout Ghana; this strategy was deemed illustrative of the country due to the limited volume of paediatric patient imaging. Patients who came to the hospital for imaging were randomly selected using a simple random sampling technique, with the selection criterion of patients who had no history of any pathological disease in the selected area.

67

Furthermore, each patient was picked fully at random, and everyone had an equal chance of being included in the study. The post-imaging data collecting method included selecting images that fulfilled the selection criteria, then coding and transferring the selected images from the PACS to DVD, and then to the MVL platform for measuring the results. In addition, the post-imaging data collection included the recording of exposure and dosage parameters such as $CTDI_{vol}$, DLP, pixel size, pitch factor, and slice thickness Figure 12 shows the image data interface in more detail.

```
KVP: 120
DataCollectionDiameter: 500.00
DeviceSerialNumber: SERIALNO
SoftwareVersions: V4.82ER001
ProtocolName: ABDOMEN     - C     5 mm
ContrastBolusVolume: 0.0
ReconstructionDiameter: 417.968
GantryDetectorTilt: +0.0
TableHeight: +125.00
RotationDirection: CW
ExposureTime: 500
XRayTubeCurrent: 80
Exposure: 40
FilterType: LARGE
GeneratorPower: 9
FocalSpots: 1.6\1.4
ConvolutionKernel: FC08
PatientPosition: FFS
SpiralPitchFactor: 0.813
ExposureModulationType: 3D
EstimatedDoseSaving: 25.94
CTDIvol: 5.5
StudyInstanceUID: 1.2.392.200036.0116.2.5.1.37

AcquisitionTime: 132535.700
ContentTime: 132752.843
AccessionNumber: 15737
Modality: CT
Manufacturer: TOSHIBA
InstitutionName: KORLE-BU TEACHING HOSPITAL
ReferringPhysicianName:
StationName: ID_STATION
StudyDescription: ABDOMEN
SeriesDescription: Body 5.0 CE
InstitutionalDepartmentName: RADIOLOGY
ManufacturerModelName: Aquilion ONE
PatientName:
PatientID: 7646
PatientBirthDate:
PatientSex: M
PatientAge: 025Y
PatientComments: ? CALCULUS
ContrastBolusAgent: DELAYED CONTRAST
BodyPartExamined: ABDOMEN
ScanOptions: HELICAL_CT
SliceThickness: 5.0
```

Figure 12: Acquisition dose parameters as displayed in image data

Basic Data Collection Protocol

The earliest stages of the conduct of the study, referred to as pre-imaging data collection, included gathering basic information from patients as part of a routine medical examination prior to imaging. Patient ID, gender, age, patient comments, and scan type are among the information recorded

using primary data form A. In all five imaging centres, they were done as part of the basic imaging routine as normal practice.

Between November 2018 and December 2019, all of the imaging centres collected approximately 200 MDCT exams of patient data. This was assessed based on the patient's feedback as well as the advice and permission of the radiologist. Outpatients who sought CT examination for a variety of diagnostic requests other than those linked with any pathological problem related to the region of interest made up the study's sample population of 200 patients out of a total of 270 patients.

To unify the data for analysis based on the selection criteria, all of the scanning operations were carried out using a similar standard scanning protocol of the various regions, as stated in the fundamental technical protocol. Importantly, as part of the inclusion criteria, all images included in the study were images of simple X-rays MDCT examinations that contained all of the dosage parameters as suggested by the radiologist.

Since the study involved real patients' data, an application for ethical approval was submitted to the Korle Teaching Hospital's ethical review committee and approval was obtained. The inclusion criteria for the sample selection were children under 16 years.

Basic Technical Protocol

The CT scanner which was used for the data collection has specific parameters as the one in table 10 below.

Table 10: Technical Parameters Used in Performing the CT Scans

Technical Parameters	Applied Range
Collimation	0.625-7.00 mm
Table Speed	50.5-60.5 mm/rotation
Rotation Time	0.5-0.8 seconds
Voltage	120 kVp
Slice Thickness	5.0 mm
Exposure Time	500 s
X-ray Tube Current	850 mA
Exposure	25-126 mGy
Generator Power	9
Focal Spots:	0.8-1.6 mm
Estimated Dose Saving	0-55.51 mGy
Spiral Pitch Factor	0.813
Exposure Modulation Type	3D
Pixel Spacing	0.500 - 0.999
Window Center	40
Window Width	400

Source: (Canon Medical Equipment, 2020)

Post-Image Data Collection

The estimated parameters include CTDI, DLP, organ and effective dose using secondary data form D (Appendix A).

Estimate of Dose Parameters

For the monitoring of dosage parameters in CT scans, MeVisLab standard supplementary DICOM application software was released in 2007

70

(DICOM, 2007). This is required by all CT equipment makers in order for users to have access to image data and other pertinent data. A summary report for the entire patient examination and the accumulated dose applied after each CT scan must be stored and made available as part of these operations. The general section of the structured report stores the patient's bio data, study information, and basic equipment documentation. Since 2007, this advancement has allowed image data to be used to overcome the evident problems in estimating the distribution of dosage within tissues during CT scans. CTDI, DLP, and pitch factor were used to quickly estimate dosage parameters from closely related measures using picture data. Using the dose-conversion coefficients in Table 2, the risk-related variables were computed using pragmatic dosimetric quantities such as $CTDI_{VOL}$ and DLP.

Figure 12 shows how detailed information of the $CTDI_{vol}$ and DLP is recorded using the MeVisLab platform. The weighted total of the absorbed dose to each specified organ and tissue multiplied by the ICRP-defined tissue-weighting factor for that same organ or tissue is the effective dose for partial-body irradiation such as CT (Deak et al, 2010). Furthermore, as indicated by ICRP 103, the conversion factor for organs/tissues is determined using the $CTDI_W$ and mAs, the effective millimetre per second.. That is

$$eff(mAs) = mAs/0.813 \tag{20}$$

The estimated average exposure (mAs) for this study is 48.19mAs. Hence the eff(mAs) is 56.27mAs. The $CTDI_W$ was estimated expressed mathematically as:

$$CTDI_W = 0.813 * CTDI_{vol} \qquad (21)$$

where 0.813 is the average pitch factor of the scanning protocol used. Organ and effective doses were also determined using the above definitions, and a complete standard reference organ dose (organ absorbed dose per unit Computed Tomography dosage Index) was produced. The details of the measured values in form D are presented in Appendix E. With precise input factors, age and gender-specific dose estimations, the mathematical model was created to determine effective and organ doses. User input of patient and scan-specific parameters, as well as the calculation and presentation of effective and organ dosages, were all handled using a graphical user interface.

Cancer Risk Assessment and Estimation

The Lifetime Attribute Risk (LAR) theory was used to assess cancer risk. The LAR is described as "extra cancer risk over and above baseline cancer risk, which can be estimated for individual malignancies or for all cancers combined" (Jones, 1997). Table 13D–1 and Table 13D–2 of the BEIR VII report was used in the calculations of LAR (Appendix A and B). Whenever data was not available for specific age then linear interpolation to the nearest integer is made from the above information. The LAR was calculated using the following equation.

$$\text{BEIR VII LAR at an age} = \left(\frac{E(mSv)}{D} \times \frac{LAR(\text{cancer incidence})}{100,000} \right) \times 100\% \qquad (22)$$

Equation 22 was used for calculating cancer incidence

$$\text{BEIR VII LAR at an age} = \left(\frac{E(mSv)}{D} \times \frac{LAR(\text{cancer mortality})}{100,000} \right) \times 100\%. \qquad (23)$$

Equation 23 was used for calculating cancer mortality.

D = 100 mGy, the reference dose to the population considered in the BEIR VII report. Appendices C to H contains the data set for effective dosages and LAR values for all cancer occurrence and cancer mortality assessments. crucial to note that, where organ dose is obtainable, more realistic to estimate risk variables (cancer incidence and mortality) using organ dosage rather than effective dose, per the ICRP 103.

Measurement of Signal to Noise Ratio

By locating a uniform area within each image and computing the process signal (mean) and noise (standard deviation of signal), the homogeneous volume approach was utilized to estimate signal to noise ratios for all of the photos . That is, signal and noise were approximated using the MVL by using the possible variations of the process's end product. The message was represented by the process standard deviation of that output, and the measured parameters average and noise. The SNR of images is defined as the ratio of the mean of the standard deviation of the images to the signal. Equation 24 was used to compute the SNR.

$$SNR = \frac{\mu(Signal\ on\ organ) - \mu(Signal\ on\ Background)}{Noise\ or\ Standard\ Deviation\ (\sigma)} \qquad (24)$$

The coefficient of variation is the measure of how the signal is distributed around the mean value of the signals. To evaluate whether the image noise is uniform, the coefficient of variation (C_V) (reciprocal of SNR) was calculated using the equation 25.

$$C_v = \frac{Noise\ or\ Standard\ deviation\ (\sigma)}{\mu(Signal\ of\ organ) - \mu(signal\ of\ background)} \times 100\% \qquad (25)$$

73

The analyses were done using ImageJ application software, Version 1.5 SciJava whose user interface is shown in Figure 13.
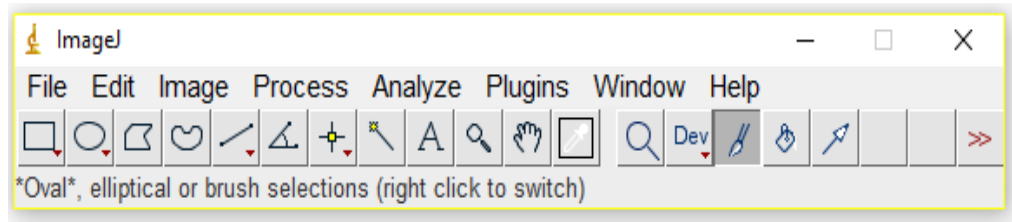
Figure 13: Image J Application Software interface

Statistical Modelling Process

This section discusses the various statistical tools that were used to perform the basic analysis of the experimental data. Decision and conclusion rules were adapted to draw reasonable conclusions. The various modelling techniques applied to achieve the desire objectives have been provided.

Basic Statistical Analysis

The data was analysed using the Minitab 16 statistical analysis software (Mazonakis et al, 2007). The tool was also used to explain the excel plot of various relational analysis of the data. This involved the use of both Multivariate techniques for the distribution of a variable, mean and variance technique for analyses of the data. The Multivariate Analysis of Variance (MANOVA) technique, suitable for large distribution of variables or sample population greater than 30 sample units or number of observations was applied, whilst the Analysis of Variance (ANOVA) which is a collection of statistical models was used to analyze the differences among the mean of the various age and gender variations and their associated procedures (Sullivan, 2010). Consequently, both ANOVA correlation and regression analyses were performed by comparing the mean and p-values. The MANOVA technique

was conducted so as to compare Paediatric Patients Dose Optimisation technique together with the Risk Assessment in CT for various age and gender variations.

The outcomes of all the compiled data were given as mean plus or minus standard deviation (± SD). The premises of the MANOVA model include multivariate normality, linearity and equality of variances of the dependent variables across the various groupings being compared.

Decision and Conclusion Principle

In order to make a decision based on the analysis of the data for the various models, the decision rule and the conclusion hypothesis were used. That is the null hypothesis to accept a model must be rejected if the p-value was less than 5% significance level ($p < 0.05$) or fail to reject if otherwise; so as to compare Paediatric Patients Dose Optimisation technique together with the Risk Assessment in CT for various age and gender variations. The output of the multiple comparison test conducted across the various age groups and gender is presented in chapter four with respect to the underlying dependent variables.

In addition, SNR to testing whether it is significantly different from zero. As a result, the hypothesis that the average value of X is significantly different from zero can be tested statistically by multiplying the SNR by $\sqrt{n}$ where n is the sample size. SNR is considered large, for example, if SNR $*\sqrt{n}$ is larger than 5, with a 99.5 percent confidence level. This suggests the

75

presence of a "signal" above and beyond the background noise. If SNR $* \sqrt{n}$

less than 5, the data could be nothing more than noise.

Statistically, various estimated parameters were presented as the average or mean values of the various parameters plus the standard deviation, written mathematically as:

$$\text{Mean, } \ddot{X} = \frac{X_i}{n-1} \tag{26}$$

$$\text{Standard Deviation, } SD = \sqrt{\frac{(\ddot{X}_i - X_a)^2}{n-1}} \tag{27}$$

$\ddot{X}$ represents an average or mean measured or estimated parameters of the sample population, with a standard deviation represented as $\pm$ SD. Hence, the standard reference renal, body and dose values will be presented as:

$$\ddot{X} = \text{mean} \pm SD = \frac{X_i}{n-1} \pm \sqrt{\frac{(X_i - \ddot{X})^2}{n-1}} \tag{28}$$

Limitations

The most important challenge with this study was the fact that, all measurements were based on individual judgment which were most likely to be affected by intra-observer and inter-observer variability and poor reproducibility. This requires expert knowledge and experience for acceptable accuracy to be achieved and stand as a serious challenge for any data to be admitted from any source for analysis.

A number of limitations are associated with MDCT scans, which militated against the reliability of the study; these include breathing and other movement artifacts during in-vivo abdominal MDCT examinations. Additionally, these introduce image artifacts which are seriously affected by

76

breathing and movement artifacts. In addition, further investigation is required to quantify inter-observer and intra-observer variation in qualitative SNR measurements using MDCT scan. Also, exposure to X-rays is one potential limitation for the use of CT for this study, due to the radiation dose involved, therefore getting enough data for the study presents a serious challenge. There is also a risk of contrast media-induced nephropathy and this made the data acquisition a serious challenge which explains why very few of such studies exist despite its importance to clinicians. Various other imaging modalities have similar risk challenges.

In conclusion, images that were from paediatric patients whose weight exceeded 80 kg and below 5 kg were not part of this study. The study only accounts for ages between 0 to 16 years. Hence, limited in scope since it does not cover every Ghanaian but only adolescents and the neonates, who are critical in the health care delivery chain in the developing world including Ghana. This study is limited in terms of establishing paediatric dose levels and comparing the estimated local values with published dose levels established in other countries since they may have potentially different CT practice and technology which may not be wholly relevant to a specific or particular circumstances, due to varied protocols that may be employed.

Finally, reported paediatric dose levels in terms of $CTDI_{vol}$ or DLP may not be represented in terms of the same standard CT dosimetry method for a given data set. Furthermore, while updating dose levels or comparing local dose levels against doses limits to dissimilar techniques, technological improvements such as reconstruction algorithms should carefully considered.

77

Chapter Summary

In summary this chapter discussed relevant information about the materials and the methodology used to achieve the study objectives. The chapter also gave a vivid information about the various measuring procedures that were used to measure and process the primary data in order to successfully design the modelled equations. It concludes with a description of the application software and statistical models that were used to analyse the data, in addition to the limitations encountered during the study.

78
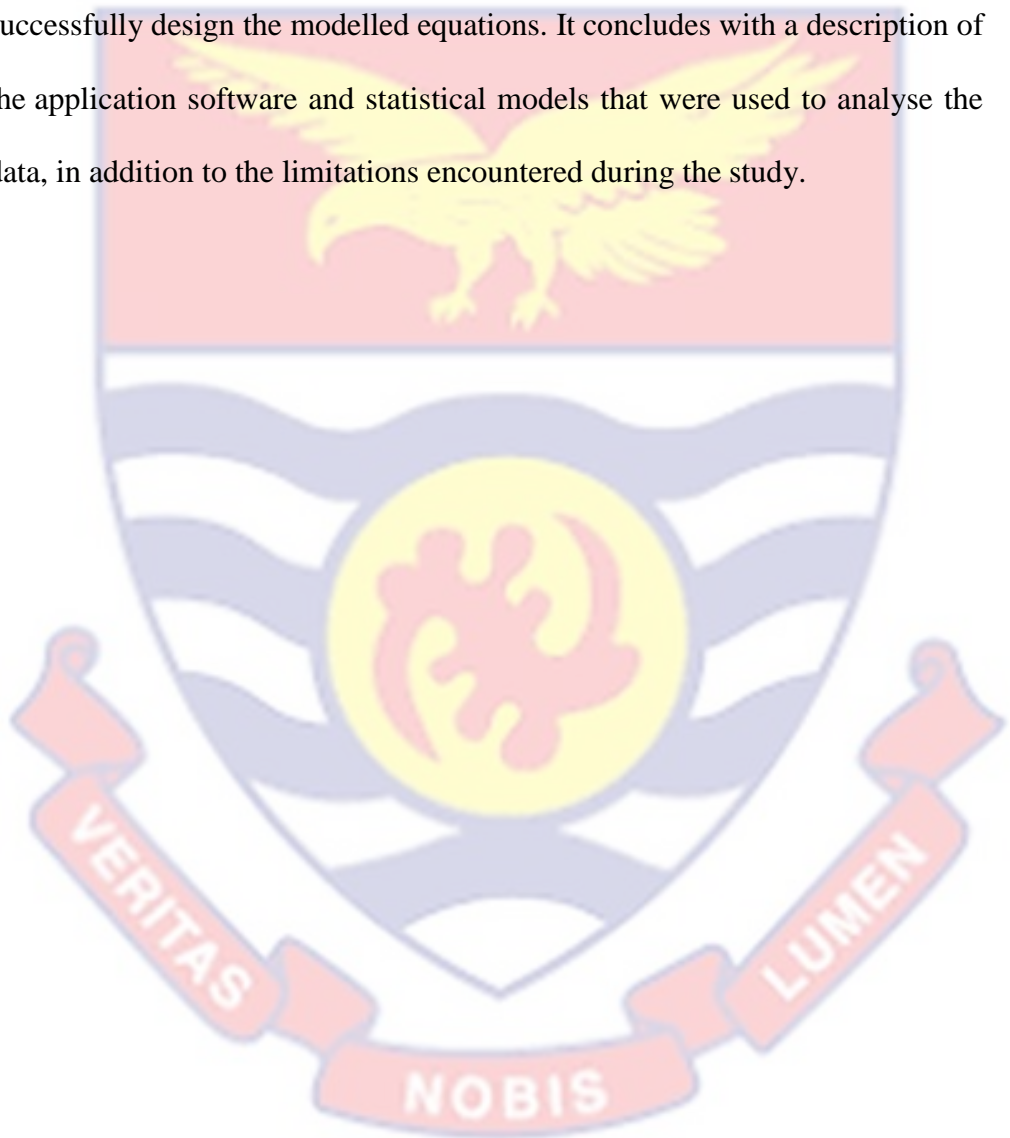
CHAPTER FOUR

RESULTS AND DISCUSSION

Introduction

This chapter discusses a comprehensive analyses of the results obtained from the quality control measurements with the phantom and real image data from the dose report. Additionally, the chapter includes readings from the CT scanner console to verify the accuracy of the patient data obtained from the dosage report. We calculated the organ dosage, effective dose, and lifetime cancer incidence and death risk of paediatric children having CT scans and presented the results.

Results

In this section, the results of the various measurements are presented based on the quality control measurement, dose parameter measurement, dose assessment and risk assessment.

Quality Control Measurements

On each of the five CT scanners, quality control tests were conducted to verify that the patient data and dosage report were correct, both on the console and in the image data. The QC test results on the five pieces of equipment utilised in the research are listed in Tables 10-16. As indicated in Table 17, all of the findings were within the permissible limits recommended by the American College of Radiology (ACR, 2012; ICRP 103, 2007).

Table 10 shows the quality control measurements of the kV accuracy, HVL accuracy and the mAs accuracy of all the machines used. This shows that all the machines were within the acceptance performance criteria.

79

Table 11: Daily QC Measurements of CT Scanner

Parameter	Five Average Deviation by all the machines	Acceptable Deviation (Value)
kV Accuracy	2.40 % ± 2%	≤ ±6.0%
HVL@120 kV	7.85 ± 2%	≥3.2%
mAs Accuracy	2.30% ± 2%	≤ 5.0%

 Source: Field Data

Table 12 represents parameters that were done as part of the CTDI measurement. These values served as reference values based on which the quality control and the patient data were estimated.

Table 12: Parameters for weighted-CTDI Measurements

Set kV (kV)	Phantom Type	Collimation (mm)	Pitch	Scan length (mm)	Tube rotation time (s)	Scan Speed (mm/s)	Measuring time (s)	Dose (mGy)
110.0	Head	10	1.000	150	1.50	6.67	16	29.51
130.0	Head	10	0.813	150	1.50	6.67	16	44.24
110.0	Body	10	0.813	150	1.50	16.67	7	10.75
130.0	Body	10	0.813	150	1.50	15.83	7	17.31

In Table 13, the summary of CTDI and DLP QC tests results for the various regions. Five statistical parameters including; the median, mean, maximum, minimum and upper quartile of the measured values are presented.

80

Table 13: Summary of Head weighted-CTDI and DLP QC tests results

HEAD	CTDI (mGy)	DLP (mGy.cm)
MEDIAN	6.60	159.1
MEAN	6.16	177.8
MAX	8.60	399.6
MIN	3.90	281.2
UPPER QUARTILE	6.75	209.7
CHEST	CTDI (mGy)	DLP (mGy.cm)
MEDIAN	2.2	141.7
MEAN	2.6	158.1
MAX	4.8	276.8
MIN	1.2	170.9
UPPER QUARTILE	3.8	176.8
Abdomen-Pelvis	CTDI (mGy)	DLP (mGy.cm)
MEDIAN	6.6	216.6
MEAN	8.7	239.9
MAX	18.0	320.0
MIN	3.6	170.9
UPPER QUARTILE	13.6	250.7

Source: Field Data

Table 14 shows factors affecting dose estimates. It shows factors that determine the strategies that can be used to minimize CT radiation dose to patients

Table 14: Factors affecting dose estimates

#	Set kV (kV)	Collimation (mm)	Pitch	Scan length (mm)	Rotation time (s)	Scan speed (mm/s)	Measuring time (s)	E. Dose (mGy)
1	80.0	10	1.0	150	1.5	6.67	15	27.59
2	110.0	10	1.0	150	1.5	6.67	15	51.87
3	130.0	10	1.0	150	1.5	6.67	15	73.47

Source: Field Data

81

Table 15 shows results for the average Geometric Efficiency and the Beam Width for the various CT equipment used. This was measured because the CTDI depends on geometry, slice width, tube performance and quality factors of the beam.

Table 15: Geometric Efficiency and the Beam Width tests results

kV	Geometric Efficiency	Beam width (FWHM)	$CTDI_{(100)}$(mGy)
80	91.6%	11.1mm	26.18

Source: Field Data

Table 16 shows $CTDI_{vol}$ and DLP Reference levels that are published by ACR, UK and Netherlands compared with those determined by this study.

Table 16: CTDIvol and DLP Reference levels

Examination	National Reference Levels				This Study	
	$CTDI_{VOL}$ (mGy)	DLP (mGy.cm)	$CTDI_{VOL}$ (mGy)	DLP (mGy.cm)	$CTDI_{VOL}$ (mGy)	DLP (mGy.cm)
Head (Paediatric)	25*	930***	65-100***	1040**	38.9	583.4
Body (Paediatric)	15*	470***	15**	700**	15.6	233.7

*ACR (IEC, 2001),   **Netherlands (Van der Molen et al, 2015, Bouwman et al, 2008),   ***UK (Shrimpton, 2004)

Demographic Statistics

This section deals with the exploratory and inferential statistical analysis of the data obtained from the total sample population. The analysis focuses on the elaborate description of the data with regard to certain demographic factors. These include age and gender variation of paediatric risk assessment in relation to exposure and dose parameters based on the various standard acquisition protocols. The measured parameters were based along the population distribution of the sample population of Ghana, as presented by Ghana Statistical Service (Ghana Statistical Service, 2020).

82

Three hundred head, chest and abdomen-pelvis CT images were collected from five selected CT centres, of which 200 images met the selection criteria. The selected images comprise 93 females (46.5%) and 107 males (53.5%). This reflected the paediatric gender population of Ghana based on Ghana Statistical Service, 2010 report (Ghana Statistical Service. 2010). The report puts the total demographic paediatric gender population of Ghana as 3.75 million for female (51%) and 3.86 million for male (49%). Furthermore, the total sample population was categorized into three age groups comprising: 0-5, 6-10 and 11-16 years, of which the study population statistics were 46, 67 and 87 people which formed: 23.0%, 33.5% and 43.5% respectively. Demographic statistics also reflected the age and the gender paediatric population distribution of Ghana (Ghana Statistical Service, 2010).

Statistical Presentation of Data

All the measured primary data were based on the body region, the age and gender variation of the patient who agreed to take part in the studies. The selection criteria of the facilities were based on the availability of paediatric images and the willingness to be part of the study by the facility. The selection of the body region was based on the common clinical examination of paediatric imaging in the selected facilities. Presentation of the summarized values of the entire experimental processes, including data analysis are made in this section, while the details of the data are presented in the Appendix. The Tables are presented as the mean, median, the upper quartile (3rd quartile), maximum and minimum values in terms of age and gender variation of the measured parameters.

In terms of frequency of requests, the head CT examination was by far the most popular, accounting for 50% of all requests, followed by the abdomen-pelvis (30%) and the chest (20%), as indicated in the table (Table 17 and Figure 14).

Table 17: Distribution of CT Examination by Body Regions

Body Regions	Examination of Body Regions	
	No. of Examinations	No. of Examinations (in %)
Head	100	50.0
Abdomen-Pelvis	60	30.0
Chest	40	20.0

Source: Field Data
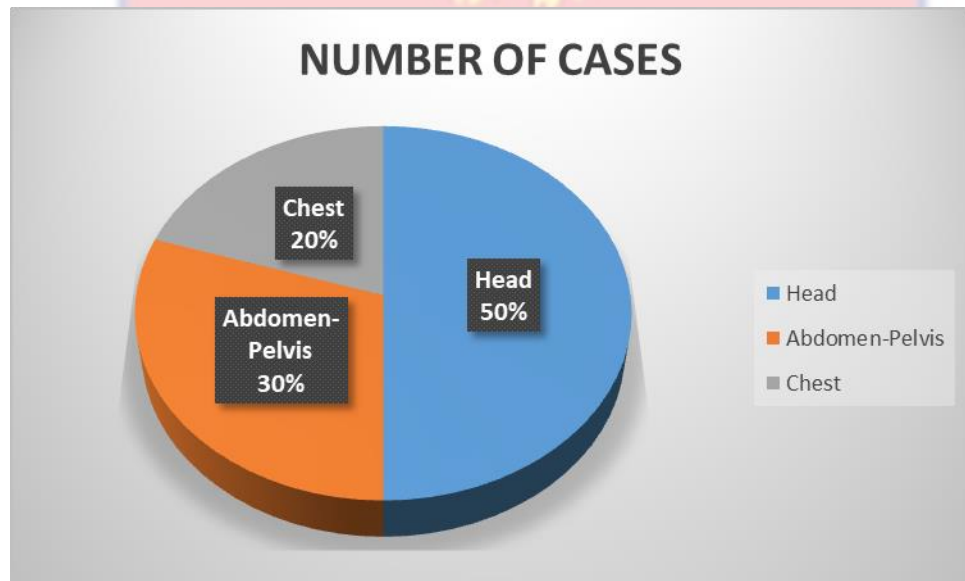
Figure 14: Distribution of examination by body regions

Head CT Examinations

Patient choice of an imaging modality depends on three main reasons. The cost of the test is the first consideration, followed by availability and, last, the purpose for the examination. However, there is an equally fourth factor when it comes to paediatric patient, which is the consequences. The head CT examination form approximately two-thirds of the most frequent requested

84

examination of all the facilities taking part in this study. This is because of two reasons, the less expensive imaging modalities like ultrasound and conventional X-ray Imaging, which are less expensive; do not provide the required quality of images for clinical application; they cannot give cross sectional images as required by most clinical request. Moreover, the CT scan of the head is critical for managing hydrocephalus, birth asphyxia, neurological disorders, developmental milestone difficulties, meningitis, motor vehicle accidents, and head traumas, as well as for staging head and neck malignancies. There were 52 men and 48 females among the 100 patients for head CT (Table 18 and Figure 15).

Table 18: Head Examinations by Age and Sex

Head Examination (with respect to age group and sex)			
Age Group (years.)	MALES	FEMALES	Total
(0 ~ 5)	13	10	23
(6 ~ 10)	19	16	35
(11 ~ 16)	20	22	42
(0 ~ 16)	52	48	100
Percentages (%)	52	48	100

Source: Field Data
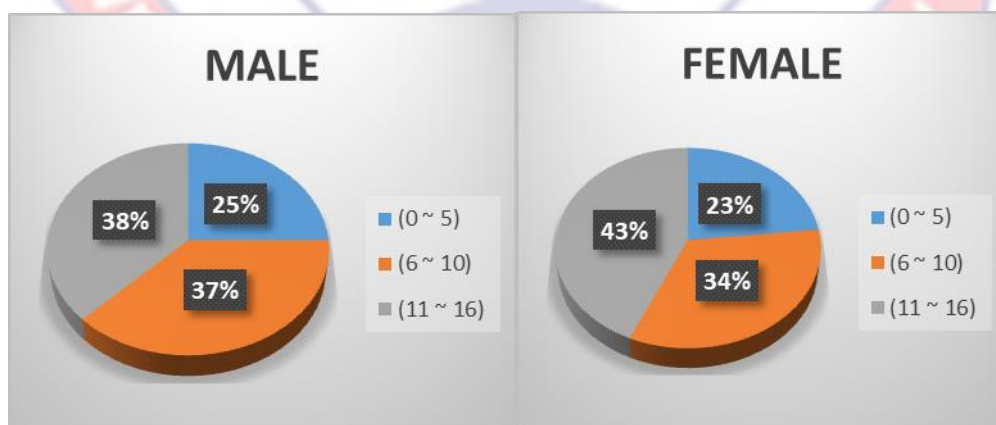
Figure 15: Distribution of male and female head examination

85

Abdominal CT Examinations

Approximately, 30% of the sample collected were abdominal cases, the reason for this was that most abdominal clinical investigations depend on the ultrasound as the core imaging modality since readily available, less expensive and more importantly non-ionizing radiation. In most abdominal cases CT scan is only a second option when the ultrasound images does not meet the needs of the clinical diagnoses or during cancer treatment planning where ultrasound cannot be used. In all, 60 cases were documented for the abdomen CT examination, 32 males and 28 females (Table 19 and Figure 16).

Table 19: Abdomen Examinations by Sex and Age

Examination of the Abdomen-Pelvis (with respect to age group and sex)			
Age Group (years.)	Males	Females	Total
(0 ~ 5)	8	7	15
(6 ~ 10)	10	9	19
(11 ~ 16)	15	11	26
(0 ~ 16)	33	27	60
Percentages	55	45	100

Source: Field Data
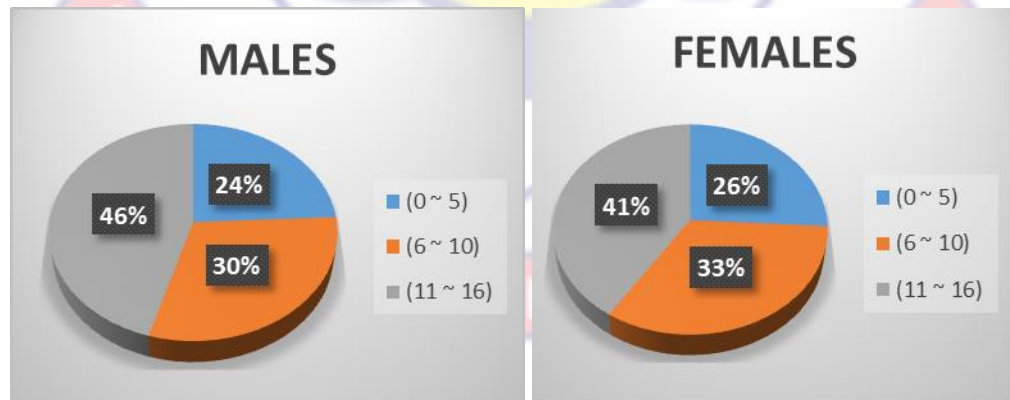
Figure 16: Distribution of male and female abdominal-pelvis examination

86

CT Examinations of the Chest

The chest examinations were 40, which denotes 20 % of the 200 examinations data collected which met the selection criteria with 22 being males and 18 females. The smaller number of the chest CT examination was mainly because; a number of alternative modalities are available. For example, a standard conventional X-ray may be utilised successfully for the majority of chest examinations, including pneumonia, cardiomegaly, and other heart-related conditions. Conventional X-rays are less expensive and more accessible to the majority of patients; many parents choose this alternative (Table 20 and Figure 17).

Table 20: Chest Examinations by Age and Sex

Examination of the Chest (with respect to age group and sex)			
Age Group (years.)	Males	Females	Total
(0 ~ 5)	5	3	8
(6 ~ 10)	7	6	13
(11 ~ 16)	10	9	19
(0-16)	22	18	40
Percentages (%)	55	45	100

Source: Field Data
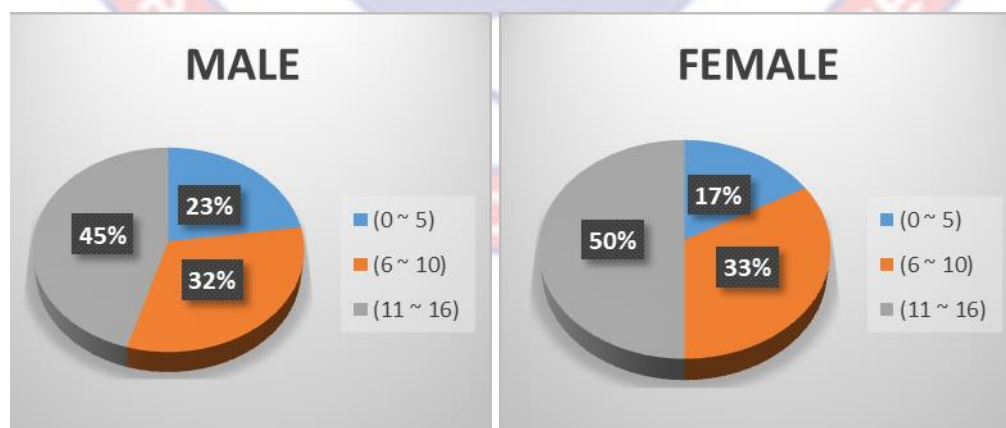
Figure 17: Distribution of male and female Chest examination

87

CT Examination Distribution by Age

The most prevalent age group was 10-16 years, followed by 0-5 years which is understandable because CT is considered very high risk modality and are hence not recommended for neonates except in extreme cases. These are represented in Table 21 and Figure 18.

Table 21: All examinations by Age and Sex

Age (Years.)	All Examination (with respect to age group)			
	Males	Females	Total	%
(0 ~ 5)	26	20	46	23.0
(6 ~ 10)	36	31	67	33.5
(11 ~ 16)	45	42	87	43.5
(0-16)	107	93	200	100.0
Percentages (%)	53.5	46.5	100	100.0

Source: Field Data
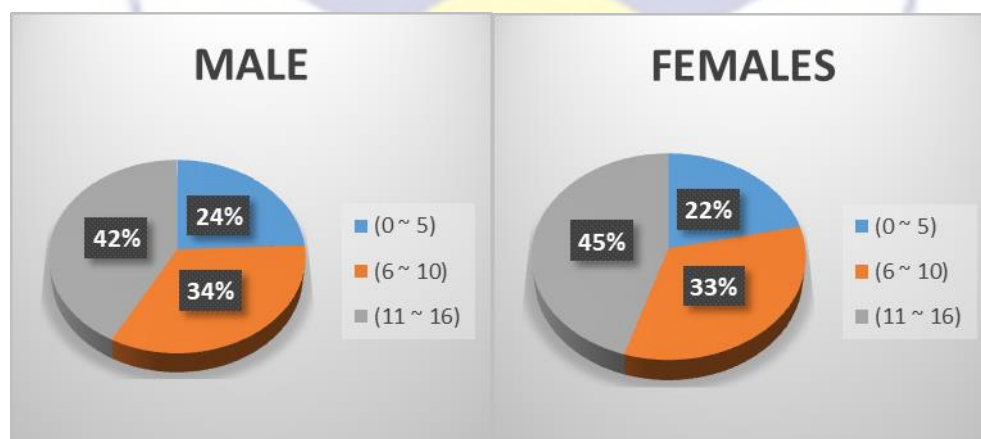
Figure 18: Distribution of male and female age variations Presentation of Dose parameter

The presentation's fundamental framework establishes a clear understanding of the link between the various variables in tables, visual representations, and model equations under risk analysis, as well as the setting of the Graphical User Interface (GUI). This provides a platform to present the data in three convenient forms. First, with tables that describe the

88

mean, median, the upper quartile (3rd quartile), maximum and minimum values of all the parameters and the spread of data sets. Second, this was followed with graphical presentations and visual description of the relationship between the various measured and the estimated parameters. Finally, the presented data was mathematically modeled using Minitab modeling tools based on the study objectives. This is followed with description, trend analysis and discussions of the results based on the scope and study objectives.

Results of Measured Dose Parameters

The summary of the image data collected from the dose report are presented in Tables 21 to 23. This figure depicts the CTDI, DLP, normalised organ, and effective dosage in terms of their mean, maximum, and lowest values as a result of age and gender variation. It also includes the three age groups (0-5, 6-10 and 11-16) for Head, Chest and Abdominal-Pelvis respectively. The detailed results are presented in Appendices C-E.

Table 22: Output Dose Parameters and Image Quality for Head Examination

ID	AGE	CTDI$_{vol}$	CTDI$_W$	DLP	Organ Dose	Effective Dose	SNR1
	Years	mGy	mGy	mGy.cm	μGy	mSv	
MEAN	8.6	6.86	5.58	1103.4	13.94	2.76	8.40
MEDIAN	8.0	5.65	4.59	911.9	11.49	2.28	8.08
MAX	16.0	16.00	13.01	3200.0	32.52	8.00	12.08
MIN	2.0	3.00	2.44	294.9	6.10	73.73	5.11
¾ Q	11.0	7.33	5.96	1249.6	14.89	3.12	9.53

Source: Field Data

Table 23: Output Dose Parameters and Image Quality for Chest Examination

ID	AGE	CTDI$_{vol}$	CTDI$_W$	DLP	Organ Dose	Effective Dose	SNR2
	Years	mGy	mGy	mGy-cm	μGy	mSv	
MEAN	9	7.0	5.68	978.86	96.51	16.64	7.85
MEDIAN	9	5.1	4.15	934.05	70.49	15.88	7.38
MAX	16	52.0	42.28	2975.60	718.69	50.59	12.77
MIN	1	4.2	3.42	195.00	58.05	3.32	5.29
¾ Q	13	6.7	5.45	1250.43	92.60	21.26	9.04

Source: Field Data

Table 24: Output Dose Parameters and Image Quality for Abdominal-Pelvis

ID	AGE	CTDI$_{vol}$	CTDI$_W$	DLP	Organ Dose	Effective Dose	SNR3
	Years	mGy	mGy	mGy-cm	μGy	mSv	
Mean	8	4.7	3.83	565.9	44.62	5.92	7.43
Median	6	4.7	3.82	549.6	57.32	3.52	6.14
Max	16	7.1	5.77	1275.9	86.58	19.14	14.25
Min	1	4.7	3.82	234.4	57.32	3.52	5.44
¾ Q	13	5.3	4.29	787.1	64.02	11.01	8.57

Source: Field Data

Tables 24 and 25 represent output dose parameters in relation to image quality based on SNR. The tables show CTDI, DLP, normalized Organ Dose and Effective Dose, with their mean, median, the upper quartile (3rd Quartile), maximum and minimum values based on age and gender variation of the measured parameters. The details of the data are presented in Appendices C-H.

90

Table 25: Risk Assessment Dose Parameters and Image Quality for Male

Examination	Age group Years	Organ Dose mGy	Effective dose mSv	Risk Incidence %	Risk Mortality %	SNR
CT brain	0-5	10.83	1.3965	0.031620	0.01396	8.19
	6–10	11.18	2.2785	0.039687	0.01877	12.08
	11-16	19.82	4.5102	0.062799	0.03113	17.42
CT chest	0-5	70.14	5.8213	0.140503	0.06110	5.11
	5–10	72.85	15.889	0.276770	0.13093	9.53
	11-16	96.14	24.059	0.335029	0.16606	16.30
CT abdomen /pelvis	0-5	0.06153	4.6980	0.113391	0.07918	8.07
	6–10	0.06319	12.334	0.214825	0.16014	9.32
	11-16	0.00783	13.965	0.187106	0.14356	15.11

Source: Field Data

Table 26: Risk Assessment of Dose Parameters and Image Quality for Female

Examination	Age group (years)	Organ Dose mGy	Effective dose mSv	Risk Incidence %	Risk Mortality %	SNR
CT brain	0-5	10.98	1.374	0.057941	0.02199	6.03
	6–10	15.65	3.190	0.102831	0.04142	6.85
	11-16	15.65	3.846	0.096211	0.04100	8.57
CT chest	0-5	64.96	3.985	0.179196	0.06714	12.99
	5–10	68.41	14.97	0.482555	0.19435	17.88
	11-16	92.60	21.16	0.529230	0.22552	24.98
CT abdomen-pelvis	0-5	57.32	3.516	0.158115	0.03690	12.70
	6–10	59.76	11.36	0.366159	0.09359	15.72
	11-16	7.52	13.74	0.328688	0.09184	25.71

Source: Field Data

Table 27: Dose Parameters in Relation to Risk Assessment and Image Quality

Examination	Age Group Years	Organ Dose mGy	Effective Dose mSv	Risk Incidence %	Risk Mortality %	SNR
CT Brain	0-5	10.83	1.3965	0.031620	0.01396	8.19
	6-10	11.18	2.2785	0.031620	0.01877	12.08
	11-16	19.82	4.5102	0.062799	0.03113	17.42
CT Chest	0-5	70.14	5.8213	0.140503	0.06110	5.11
	5-10	72.85	15.889	0.276770	0.13093	9.53
	11-16	96.14	24.059	0.335029	0.16606	16.30
CT Abdomen / Pelvis	0-5	0.06153	4.6980	0.113391	0.07918	8.07
	6-10	0.06319	12.334	0.214825	0.16014	9.32
	11-16	0.00783	13.965	0.187106	0.14356	15.11

Source: Field Data

Table 28: Dose Parameters in Relation to Risk Assessment and Image Quality

Examination	Age Group Years	Organ Dose mGy	Effective Dose mSv	Risk Incidence %	Risk Mortality %	SNR
CT Brain	0-5	10.98	1.374	0.057941	0.02199	6.03
	6-10	15.65	3.190	0.102831	0.04142	6.85
	11-16	15.65	3.846	0.096211	0.04100	8.57
CT Chest	0-5	64.96	3.985	0.179196	0.06714	12.99
	5-10	68.41	14.97	0.482555	0.19435	17.88
	11-16	92.60	21.16	0.529230	0.22552	24.98
CT Abdominal / Pelvis	0-5	57.32	3.516	0.158115	0.03690	12.70
	6-10	59.76	11.36	0.366159	0.09359	15.72
	11-16	7.52	13.74	0.328688	0.09184	25.71

Source: Field Data

Discussion of Results

Comparatively, the measured parameters show variations in males and females dose parameters. For instance, the risk factors varied from 3% to 33% in Male and 5% to 52% in female. Similarly, all the measured organ

92

doses were within the range of accepted values, as published by ICRP and certified regulatory institutions and individuals (Garland, 2014; Scholbach & Weitzel, 2012; Osafo, 2012; Ozbek *et al*., 2012; Wong *et al*., 2009; ICRP Publication 102, 2007; Lee *et al*., 1999; Ferrer, McKenna, Bauer & Miller, 1997; Ninan, *et al*., 1990; Troell, Berg, Johansson, Wikstad, 1984). Indeed, there is a positive linear correlation between the measure dose parameter parameters. Consequently, an increase in kVp or mAs (input parameter) resulted in a corresponding increase in output parameters (effective dose and risk factors).

Comparatively, the model equations can best be used to accurately predict organ volume than the Trial-and-error method which is currently in use. Unfortunately, even though CT uses ionizing radiation exposure as the source of imaging during organ studies due to; noninvasive, its ability to image bone, soft tissue, and blood vessels all at the same time, short study time (15 to 20 minutes) with high quality images and accurate anatomical study. Therefore, there is the need to assess various quantities that relate dose risk parameters together with the image quality for radiation dose optimization. The most significant dose descriptor variables that quantify the radiation dose delivered to an organ during a CT examination are tube voltage in kilovolt peaks (kVp) and tube current scanning time in milliamp-seconds (mAs). By varying the mAs and kVp values, these two parameters influence the relative image noise level. That is, there is a decrease in image noise in CT images as a result of an increase in kVp or mAs in an increase in radiation dose and vice versa. As a result, in medical imaging, there will always be a

93

trade-off between low image noise and low radiation doses to patients. (Sardinha et al, 2006).

The impacts of two exposure factors (CTDI and DLP) on the brain, chest and abdomen-pelvis was investigated in order to determine the deposition of dose into the organ, as well as the effective dose based on extrapolation using the LNT model, both of which may be associated with cancer development. Optimizing patient exposure refers to the process of reducing patient exposure to the barest minimum necessary in order to get the desired diagnostic outcome. Optimal radiation protection for patients is made possible via the use of patient dosimetry and diagnostic reference levels (DRLs). However, the country does not have DRL values, which makes it difficult to make comparisons. (Inkoom et al,2014; Botwe et al, 2010) Nevertheless, this study which established a reference data as shown in Tables 21 to 25 agreed with international/regulatory organizations such as IAEA, AAPM ICRP and the EC. Whose standards of practice, including that of the basic safety standard (BSS) by IAEA (IAEA BSS No. GSR Part 3, 2014), whose requirements and recommendations are implemented premised on the concept of optimising patient radiation protection in medical institutions utilising ionising radiation. Recommendations from these international regulatory bodies are essential practical principles that assist clinicians in clinical practice. Hence, the values of this study were compared with those from these international organizations for purposes of optimization and not exact dose values to various tissues. (IAEA,2014; AAPM, 2011; ICRP,135)

94

In general, 81 percent of the parameters in the 200 images were within the acceptable range of the guidelines, whereas 19 percent failed to satisfy these criteria. That is the measured median and upper quartile CTDI$_{vol}$ for head CT were 6.86 and 7.33 mGy, chest CT 6.98 and 6.70 mGy, abdomen-pelvis CT 4.71 and 5.28 mGy. While DLP for head CT were 1103.00 and 1249.58 mGy-cm, chest CT were 978.86 and 1250.42 mGy-cm, abdomen-pelvis CT were 565.85 and 787.05 mGy-cm. The mean CRI was in the range of 1 in 10,000 to 4 in 1,000 for all the CT examinations. CT optimization is essential because CT exams expose patients to much greater radiation exposures than other forms of conventional radiography. Radiation exposures from certain CT scanners, in particular, are in the range linked with an elevated cancer risk, according to direct epidemiological data (Feinendegen, 2005). It is also worth noting that the data from this study shows that CT radiation dose vary across institutions where the data was taken. For instance, the CTDI and the DLP varied from 3.18-6.7 mGy in hospital A and 4.7 to 8.8 mGy in hospital B. There was a wide range of values for the impacts of the measured and estimated exposures and dose parameters, despite the fact that the average values were generally more depressed than the suggested average critical levels by about 81 percent on average. This may be deceptive, since some of the individual organ dose and effective dose parameters surpassed the critical levels by up to 200 percent., that 6.3 mGy as recommended by ICRP (ICRP publication, 121, 2013). Approximately 19% of the computed values were higher than the recommended levels of 6.3 mGy for head 5.7 for Chest and 4.2 for abdomen-

95

pelvis, in terms of CTDI, which may have a negative impact on health outcomes.

The capacity to identify an abnormal structure (lesions) on a radiograph is proportional to the difference in intensity between the differential signal and the ambient noise level. This SNR was determined using abdomen CT scans with a minimum SNR value of 0.8 and a matching minimum effective dosage of 3.36 mSv. Additionally, a maximum SNR of 12.77 was calculated, corresponding to a maximum effective dose of 52.45 mSv for the patient.

In X-ray technology as in CT imaging, large numbers of photons, particles (increase mAs) and energy fluence (increase kVp) are absorbed to produce clearer images to enable clinical interpretation. However, introducing larger photons would increase the SNR of the image (improve image quality), where the signals are stronger with less noise in the image. In addition, the large photons would increase the amount of photon interaction with the body tissues hence increasing possible dose deposits. Therefore, the use of high kV and mAs would be increasing the number of photons and radiation dose to patients, hence increasing the SNR. Conversely, it was observed that measured SNR of the various CT scans of the regions studied, improved with increase in slice thickness and by decreasing the kV and mAs, this would reduce the patient dose.

The organ dose was calculated by using a conversion factor by ICRP 103 and a weighted CTDI (CTDIw) (ICRP103, 2007). The conversion factor and the weighted CTDI depend on mAs and kVp as input parameters. The value

96

of the conversion factor are chosen based on age and gender variations, since higher values increase signal strength and the dose to patients. significant to recognize that by reducing the mAs implied an increase in image noise. However, when the amount of radiation absorbed by the tissue (the dose) decreases, the image's visual noise increases. A protocol optimised for imaging is one in which the mAs is modified to provide an acceptable amount of image noise for clinical interpretation. Although increasing the pitch factor theoretically lowers the radiation organ dose, practical considerations must be made. While raising the pitch does result in a reduction in dosage when all other variables remain constant, it also has an effect on image quality. To begin, the pitch may impose a restriction on the amount of detail or spatial resolution that could be achieved in the direction of the axial slice thickness. Second, raising pitch adds noise to the radiograph. However, the majority of CT systems have a feature that automatically raises the mAs and dose to maintain a certain noise level when other parameters such as slice thickness, matrix size, field of view, and pitch are varied. When the slice thickness is reduced, that reduces the size (volume) of the individual tissue volume element (called voxels). The smaller voxels will absorb or capture less total radiation or number of X-ray photons. It is the number of photons absorbed in each voxel that affects the image noise. When the number of photons per voxel is reduced, the noise increases because of the statistical nature of the photon interactions (AAPM, 2011; ICRP 103, 2007).

The benefit of raising pitch is that it reduces scanning time, not to reduce dosage but it ends up reducing the dose. To improve the patient dose

97

description, the recommended step is to use pitch factor values that strike a balance between image quality and scan time requirements. (ICRP ,121)

This is accomplished via experience and the use of current national or international rules and relevant references, which are usually based on BSS (IAEA GSR part 3, 2014). The IAEA also offers regional and international training courses, particularly, in the field of optimization and image quality to various professionals including medical physicists, radiologists and radiographers. The goal is to provide requisite skills and knowledge to various professionals to achieve the desired ultimate objective of obtaining high quality images through best practice of imaging procedure. For instance, the physicist's duty is to establish quality control practices, provide measuring methodologies and support optimization process for patients, clinicians and general public safety. Whilst the radiologist's duty is to undertake the imaging procedure, analyse and interpret images and write report based on the requesting physicians note in order to answer all the clinical questions.

To add to that, the display information interface was designed to assess patients' general and specific information. This basic patient information is accessed using the text-based or visual indicators approach. This was developed to form part of the RIS GUI to give a comprehensive platform for all the members of the imaging team. Moreover, a more customised graphical GUI was developed using an object-oriented programming language to evaluate particular information about individual patients, such as organ and body measures in addition to the dosage optimization procedure. This interface is presented using a Visual Basic

98

application platform and integrated into the DICOM reader for usage by the radiologist and radiographers throughout the decision-making process.

In conclusion, the study, reviewed and compared measured parameters with international reference values and has been found to meet best practice all over the world as shown in Table 28, hence acceptable for adoption in Ghana for clinical application.

Furthermore, GUI model (Figures 19) was created to accurately represent the pleasant operation of all the mathematical model equations. The radiographer's input display interface has been developed to record dosage parameters in terms of mAs and kVp, as well as anticipated CTDI and DLP values. These factors were used to calculate the dosage to the organ and the effective dose. The proposed display interface allowed the prediction of organ dosage using a known effective dose, as shown in Figure 19 as the regression model's GUI). This technique was intended for use in estimating the anticipated radiation dose to patients and optimising the dose in relation to picture quality prior to imaging. Hence, the outcome of the study was expected to give appropriate technical support to the imaging team not only for quality control, but for new measurement-based assessment technologies and methods to improve on the analysis and dose optimization procedure (AAPM, 2011).

Description and Trend Analyses of Results

This section describes and analyses all the measured parameters based on stated demographic statistics. This was done based on age and gender statistics in the various health facilities in relation to measured parameters.

99

These include LAR, mAs, KVp and dose parameters (CTDI, DLP, Organ Dose and Effective Dose).

Estimates of Dose Parameters

The dosage parameter estimations were based on the ICRP categorization and usage of age categories for CT procedures (ICRP publication 121, 2013). Because conversion coefficients are typically established for a particular age group, they were matched to the study's age groups. The conversion coefficients are all expressed in terms of the 16-cm dosimetry phantom. This enables an effective and reliable estimates of dose parameters and their associated risk factors (incidence and mortality).

The dose parameters of interest were CTDI (volumetric-CTDI and weighted-CTDI), organ dose, the DLP and effective dose. The estimated organ dose in the various regions were selected based on the common procedures in the study facilities. That is grey-matter for brain scan, lungs for chest scan and kidney for abdomen scan. of interest to note that the statistical data analysis for maximum, minimum, median, mean (average) and upper quartile (¾ Q) values gradually increase in the dose estimates based on age and gender variation. For instance, the average values for head $CTDI_{VOL}$, DLP, $CTDI_W$, organ dose and effective dose were 5.30 mGy, 559 mGy.cm, 4.33 mGy, 0.0108 mGy and 1.397 mSv in the age brackets of 0-5 years respectively. On the other hand, the average values for head $CTDI_{VOL}$, $CTDI_W$, DLP, organ dose and effective dose were 5.54 mGy, 4.5 mGy, 888 mGy.cm, 0.0113 mGy and 2.22 mGy in the age brackets of 6-10 years

100

respectively. These variations were also observed in the chest and abdomen-pelvis estimates as presented in Table 13.

Moreover, critical in clinical imaging to create a connection between different input parameters (mAs and kVp) and their associated output dose estimations (organ and effective dose) in relation to the obtained image quality in order to address all clinical issues. In addition, the effect of dose parameters based on imaging as against the relationship with associated potential incidence and mortality risk are summarized in Tables 28 and 29 in chapter 5 and the detailed tables are presented in Appendices C and S, which indicates that the paediatric protocol even though not really well defined in the various facilities were within the accepted range of 3.18 to 8.78 mGy and 568 to 888 mGy.cm for CTDI and DLP values based on age and gender variations.

Tables 24 and 25 are summarized data for organ and effective dose in relation to risk factors as against image quality. The two tables indicate accepted value of 6.3 mGy and 570 mGy.cm or better results with regard to paediatric imaging in Ghana.

Measured Dose Values and International Benchmarking

The mean CTDI (CTDI$_W$ and CTDI$_{vol}$), DLP, Effective dose, and Organ dose values in all age groups obtained for brain exams were within the acceptable range of values for international Paediatric Diagnostic Reference Level (PiDRL) values, as indicated in Appendices C to S. This indicates that the brain scan procedure parameters at the five facilities are highly optimised and match current worldwide practise. However, the dosage savings seen in

101

the facilities have decreased when compared to the DLPs, implying that the measured scan lengths may be somewhat longer (<10%) on average, cancelling out the dose savings obtained via parameter selection for the procedures or protocols. Additionally, the DLP would be impacted directly by the specification of scan length for exams conducted. For example, the scan length was measured parallel to the patient's long axis on the scanner used in this research, while measuring the scan length parallel to the rotation axis would decrease the length by about 10%. As a result, the actual dose to the patient has remained constant, but the DLP has increased or decreased depending on the scan length utilised.

Furthermore, for paediatric body imaging, the measured mean values in Tables 12, 14 and 17 were significantly lower than international DRLs in terms of $CTDI_W$, $CTDI_{vol}$, organ dose, DLP, and effective dose in the under 6 years age groups compared to the international DRLs. This is most likely due to the low tube potentials used at various facilities, which vary between 80 and 120 kV and result in a significant decrease in radiation dosage. This research also discovered that almost 80 percent of centres performed chest imaging in the 6-10 and 11-16 age groups at 120 kV, whereas only around 5 percent of centres with 0-5 years performed it at 80 kV. Some of the measured values in the 5–10 years age range may be greater than other values in this group, which may also be explained by this factor. Also, 65 percent of children aged 6-10 and 11-16 had their abdomen-pelvis exams performed at 120 kV, whereas children between 0-5 had their tests performed at 100 kV, respectively. Although low-tube-potential chest imaging accounted for

102

slightly over 30 percent of all exams in the 0-5 year's age group, the research showed that in younger patients, lower tube potential chest imaging was more likely to be utilised for chest imaging than for abdomen/pelvis scanning.

In the two older age groups for chest imaging, the DLP, which was used to determine effective dosage, had lower mean values, as shown in summary of Tables 48 and 49. As a result, the measured summary DLP was found to be greater than the comprehensive mean values given in Appendices C–F. The third quartile value of the detailed data was utilised to give a realistic picture of the measured values, particularly in the age groups 6–10 years and 11–16 years, which were beyond the recommended DRL levels in ICRP report 121 (ICRP publication 121, 2013). The average scan length for children aged 5 to 10 was 28.7 cm in the research. Similarly, in this research, the DLP for chest imaging is lower in the 5–10 age group than in the 0-5 and 11-16 age groups.

Furthermore, across all age groups, the average dose values for abdomen/pelvis examinations were lower than the international DRLs of 5.7 for paediatric imaging. The dose saving obtained in the two older age groups was apparent in the CTDI$_{vol}$ values of the research, which can be seen in Appendices C to H. When evaluating the DLP values, the study was somewhat offset by a greater scan length. The average scan length was 39.6 cm in the 5–10 years age group. Similarly, the mean length for those over the age of 10 was 46.9 cm, with the upper quartile figure being 49.1 cm. Again, there is a potential for dose reduction by evaluating the scan length or scan duration for

the examination. However, the typical dose levels for abdomen/pelvis imaging are lower in comparison.

An extensive study using paediatric protocols on all scanners examined demonstrates that the majority of organ and effective dose levels are considerably lower. This is most likely the consequence of technological advancements. It may also be the consequence of protocol optimization, since part of the dose savings seem to be attributable to lower mAs values for axial CT brain scans and lower $CTDI_{vol}$ values for body imaging. For instance, none of the procedures described in this research are conducted at the lowest possible tube potential (80 kV), and the pitch for all body imaging is lower than in the present study. Only the doses for chest and abdomen/pelvis CT imaging in the youngest age group, conducted at 80 kV, are significantly lower in this research. Moreover, it has been shown that the dose estimates in term CTDI and DLP are dependent on kVp and the mAs.

Presentation of Risk Assessment Parameters

Tables 33 to 44 represent risk assessment parameters in relation to effective dose, LAR), mAs, kVp and risk incident and mortality based on age and gender variations. The tables summarise the mean, median, upper quartile (3rd Quartile), maximum, and lowest values for the measured parameters in terms of age and gender variance of the measured parameters. Appendices I – S provide information about the data.

General Statistical Models Analysis

The statistical modelling process used a linear method to simulate the relationship between scalar dependent variables and independent variables.

104

The associations between the parameters were modeled using linear predictor functions, the unknown parameters of which were determined from the data. Conversely, the linear regression model analysis was focused on the conditional probability distribution based on Normal Probability Plot (NPP) of a given variable.

The descriptive parameters of the modelled equations were obtained using the normal histogram, normal probability plot based on the statistical analysis by Chambers et al. (Chambers et al., 1983), Versus Fits and Versus Order. This section discusses four graphical methods for determining if a data collection is roughly regularly distributed. Additionally, the modelled equations 29 to 40 for all parameters were displayed against a theoretical normal distribution with the dots forming an estimated straight line.

Moreover, the plots were constructed using residual plots that created graphs for the purpose of examining the goodness-of-fit in the linear regression analysis. This enables the determination of the conventional least squares assumptions. The assumptions resulted in unbiased coefficient estimates with a minimum variance (≤ 0.05). The following four methods were identified and explained:

To begin, the histogram of residuals was utilised to determine if the data were skewed or included outliers. Second, the residuals' normal probability plot was used to validate the assumption that the residuals are normally distributed. Additionally, the residuals against fits plot were used to validate the premise that the residuals are in continuous disagreement.

Finally, the residuals were plotted against the order of the data to validate the assumption that the residuals are uncorrelated with each other. Model equations and statistical descriptive methods were used to convey the findings of these model verification platforms. Additionally, each model consists of four components: the model equation, the standard deviation, the predictor, and the p-value. A lower p-value (usually less than 0.05) shows significant evidence against the null hypothesis, which results in the rejection of the null hypothesis. The model parameters are provided in the form of risk assessment parameters, which include the predicted risk incidence and risk mortality. Finally, the input parameter that is closely related to the output dosage parameters was connected to the LAR in order to forecast risk incidence and risk mortality using a GUI. Hence, the models are presented as clinical application software for comfortable working process in dose optimisation. These were presented as dose parameter estimates software model, which has been designed for both exposures input and dose output data capturing mechanism. Both of these software models have been designed as GUI and Computer-aided design, CAD for use in clinical application. Hence it represents a graphical relationship between Modeled LAR, Input Parameters and Risk Incidence and mortality assessment. It also shows the model equations for both male and female risk assessments, in relation to incidence and mortality.

In conclusion, the modelled equations represent a linear relationship between LAR, Input Parameters and Risk Incidence, a linear method for modelling the connection between a scalar dependent variable, Risk

106

Incidence, and independent variables, LAR, and input parameters, mAs and kVp. The graphs are presented in Appendices C to S.

Risk Model Analysis

RISK Incidence (Y) Model Equation for Male Head

(NB Tube Current = X_1 and Tube Voltage = X_2)

$$Y = 0.0501 - 0.000030 \text{ LAR} + 0.000131X_1 + 0.000268X_2 \qquad (29)$$

Summary of the Model one

SD	R-sq	R-sq(adj)	R-sq(pred)	P-Value
0.0128941	94.12%	89.47%	89.60%	0.000

RISK Incidence (Y) Model Equation for Female Head

(NB Tube Current = X_1 and Tube Voltage = X_2)

$$Y = 0.1098 - 0.000033 \text{ LAR} + 0.000004 X_1 + 0.000517 X_2 \qquad (30)$$

Summary of the Model two

SD	R-sq	R-sq(adj)	R-sq(pred)	P-Value
0.0239843	89.76%	95.58%	97.01%	0.000

RISK Mortality (Y') Model Equation for Male Head

(NB Tube Current = X'_1 and Tube Voltage = X'_2)

$$Y' = 0.0548 - 0.000062 \text{ LAR} - 0.000000 X'_1 + 0.000108 X'_2 \qquad (31)$$

Summary of the Model three

SD	R-sq	R-sq(adj)	R-sq(pred)	P-Value
0.0069235	95.07%	91.32%	93.35%	0.000

RISK Mortality (Y') Model Equation for Female Head

(NB Tube Current = X'_1 and Tube Voltage = X'_2)

107

$$Y^{'} = 0.0718 - 0.000052 \text{ LAR} + 0.000001 X^{'}_1 + 0.000184 X^{'}_2 \qquad (32)$$

Summary of the Model four

SD   R-sq R-sq(adj) R-sq(pred) P-Value

0.0104686   94.29%   90.48%   92.46%   0.000

RISK Incidence (Y) Model Equation for Male Chest

(NB Tube Current = X_1 and Tube Voltage = X_2)

$$Y = 0.228 - 0.000079 \text{ LAR} - 0.00056 X_1 + 0.00137 X_2 \qquad (33)$$

Summary of the Model five

SD   R-sq R-sq(adj) R-sq(pred) P-Value

0.115049   93.27%   96.04%   90.00%   0.001

RISK Incidence (Y) Model Equation for Female Chest

(NB Tube Current = X_1 and Tube Voltage = X_2)

$$Y = 1.379 - 0.000203 \text{ LAR} - 0.00276 X_1 - 0.00209 X_2 \qquad (34)$$

Summary of the Model six

SD   R-sq R-sq(adj) R-sq(pred) P-Value

0.161600   90.67%   95.72%   93.66%   0.000

RISK Mortality ($Y^{'}$) Model Equation for Male Chest

(NB Tube Current = $X^{'}_1$ and Tube Voltage = $X^{'}_2$)

$$Y^{'} = 0.488 - 0.000344 \text{ LAR} - 0.000730 X^{'}_1 - 0.000679 X^{'}_2 \qquad (35)$$

Summary of the Model seven

SD   R-sq R-sq(adj) R-sq(pred) P-Value

0.0445271   96.83%   92.40%   91.37%   0.000

RISK Mortality ($Y^{'}$) Model Equation for Female Chest

(NB Tube Current = X'_1 and Tube Voltage = X'_2)

$$Y' = 0.689 - 0.000295 \text{ LAR} - 0.00113 \, X'_1 - 0.00095 \, X'_2 \qquad (36)$$

Summary of the Model eight

SD   R-sq R-sq(adj) R-sq(pred) P-Value

0.0689340 94.91%   90.32%   88.96%   0.000

RISK Incidence (Y) Model Equation for Male Abdominal-Pelvis

(NB Tube Current = X_1 and Tube Voltage = X_2)

$$Y = -0.239 + 0.000083 \text{ LAR} - 0.00013 \, X_1 + 0.00183 \, X_2 \qquad (37)$$

Summary of the Model nine

SD   R-sq R-sq(adj) R-sq(pred) P-Value

0.0781146 94.45%   97.32%   90.00% 0.005

RISK Incidence (Y) Model Equation for Female Abdominal-Pelvis

(NB Tube Current = X_1 and Tube Voltage = X_2)

$$Y = -0.438 + 0.000082 \text{ LAR} - 0.00018 \, X_1 + 0.00337 \, X_2 \qquad (38)$$

Summary of the Model ten

SD   R-sq R-sq(adj) R-sq(pred) P-Value

0.140431 16.33%   9.55%   0.00%   0.005

RISK Mortality (Y') Model Equation for Male Abdominal-Pelvis

(NB Tube Current = X'_1 and Tube Voltage = X'_2)

$$Y' = -0.1203 + 0.000094 \text{ LAR} + 0.000668 \, X'_1 + 0.000595 \, X'_1 \qquad (39)$$

Summary of the Model eleven

SD   R-sq R-sq(adj) R-sq(pred)   P-Value

0.0359169 96.32%   90.92%   94.53%   0.005

109

RISK Mortality (Y') Model Equation for Female Abdominal-Pelvis

(NB Tube Current = X'_1 and Tube Voltage = X'_2)

$$Y' = -0.246 + 0.000110 \text{ LAR} + 0.000719 \, X'_1 + 0.001358 \, X'_1 \qquad (40)$$

Summary of the Model twelve

SD	R-sq	R-sq(adj)	R-sq(pred)	P-Value
0.0559840	94.93%	89.44%	88.25%	0.005

Graphic User Interface (GUI) Model

Figure 19 shows the user interface for the estimate of risk incidence and mortality. It serves as a predictive model in CT imaging at diagnostic radiology.
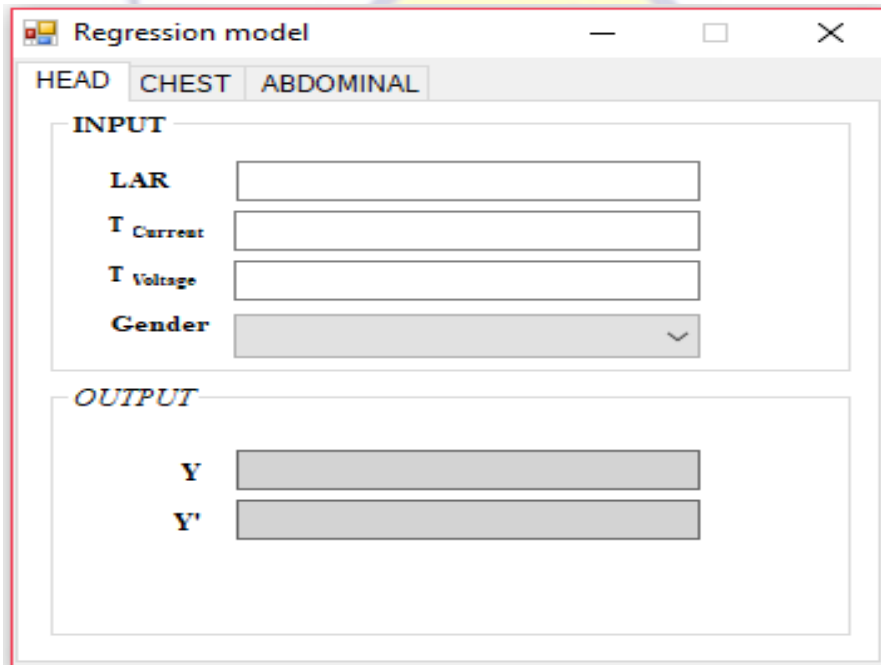
Figure 19: Graphic User Interface for the regression model

Assessment of Scan Parameters

The dose indicators would be used to draw comparisons with available research in DRLs. For the present research, this has led to the identification of chest imaging in older paediatric patients (11–16 years) as one area that may possibly be improved. However, determining the variables that need optimization is challenging using just the dosage indications. For example, the mean DLP in the oldest age group (11-16 years) was 10% greater than the mean DLP in the lowest age group (0-5 years), whereas 7% higher in the abdomen/pelvis exams. It was unclear which variables lead to this large discrepancy; therefore, a detailed analysis of the local scan parameters was required. This was accomplished by analysing the normalised $CTDI_{vol}$, average mAs values, and scan length for each kind of examination.

Dose Index for CT

CTDIvol values were highest in CT brain examinations (Figure 12). This was partially due to the smaller beam collimation utilised for body exams, which resulted in a higher dose rate due to over beaming, in which the unused penumbral area of the X-ray beam was proportionately larger with narrower collimations. Additionally, head scanning uses less filtering, resulting in a larger dosage than body scanning, which uses a more filtered beam with a better beam quality (Huda et al, 2010). Because the tube potential, beam collimation, and pitch for brain exams were consistent across age groups, the $CTDI_{vol}$ stayed constant. The small difference in normalised results seen in Figure 12, notwithstanding the use of identical protocol

111

settings, was owing to the constraints of this computation when utilising average mAs values. For a fixed tube current these values would be the same.

For the body examinations, the collimation and pitch of the beam remained constant across the three age groups, but the tube potential increased over the three age groups. This is demonstrated in Table 13 by the increasing $CTDI_{vol}$ values. Between the youngest and oldest age groups, the $CTDI_{vol}$ values for chest and abdomen-pelvis imaging both increased by 5.5 percent. For the same age groups, the chest and abdomen-pelvis values differ only by the pitch. It is interesting that the values are comparable because the two body regions exhibit markedly different characteristics of attenuation and contrast. reasonable to expect that the $CTDI_{vol}$ values, which accurately reflect the patient dose by including the mAs values, will be lower for chest imaging than for abdomen-pelvis imaging, due to decreased attenuation from the air in the lungs and the enhanced inherent contrast in this area, which allows for lower dose settings. This was not always the case, particularly among the age between 11 to 16 years (Table 13). As a result, both justification and optimization of the increased $CTDI_{vol}$ and DLP values for chest imaging in comparison to abdomen-pelvis imaging should be pursued.

Tube Current Modulation

Tube current modulation dosage reduction was utilised in all tests evaluated. This needs a user-defined reference mAs value that is adjusted to the desired image quality and represented in terms of the effective mAs value (normalized by the pitch factor). Modulation of the tube current is dependent on the size of the subject being scanned in comparison to a standard-sized

112

patient (defined at aged 5 years). Thus, it was anticipated that the range of mAs values for the examination would be smaller than the reference value for very young patients (0-5 years) and more than the reference value for older patients (11-16 years). For instance, the average value for a one-year-old infant having a CT chest examination was 49 mAs, compared to a reference value of 65 mAs. The average was 124 mAs for a 14-year-old teenager having a CT chest examination, while the reference was 80 mAs.

The average tube current for all age groups was lower than the standard value for brain exams conducted with a slanted gantry. Overall, the mAs for brain exams rose by 15% with age (Table 13), indicating that older patients (11-16 years) with a more radiodense skull needed higher reference mAs (Table 12) to obtain the same picture quality. Between the youngest (0-5 years) and oldest age (11-16 years) categories, the mean mAs values for chest exams rose by 12%. The increasing density of the bones and the bigger size of older children are anticipated to contribute to an increase in mAs. The rise in mAs for the abdomen-pelvis exams, on the other hand, was 8%.

As a result, the increase in mAs between the (0-5 years) and (11-16 years) age groups was due to the increasing reference value and/or the increasing size of the patient for chest examinations in the younger age groups (0-5 years), whereas for the older age groups (11-16 years), the increase was due solely to a larger patient size due to the fact that the reference value remained constant. As expected, patients in the oldest age group were bigger, which would have increased the examination mAs, but this was countered by a lower reference mAs, and therefore the mean examination mAs was equal across the two oldest age groups (5-10 and 11-16 years). It was thus necessary

to examine the reference mAs values for body imaging, and the relative differences between chest and abdomen-pelvis values in the same age group should be shown; otherwise, these reference values should be optimised for diagnostic image quality (SNR).

Scan Length

The average scan length for brain exams rose between the youngest age groups (0-3 years), but then remained fairly constant throughout the rest of the study. Interestingly, the fast development of the skull during the first two years of life corresponds to this (Kleinman et. al, 2010) Longer scan durations for body exams in older children indicate that their bodies have grown in size as they have progressed in their development. Compared to chest exams, the largest rise in mean scan duration occurred in the first 5 years of life, while the increase in mean scan time for abdomen/pelvis examinations were more constant across age groups.

When comparing all age groups, the duration of the scan for abdomen-pelvis exams was on average 11–13 cm longer than for chest examination. The average chest scan length was 40 percent shorter than the average abdomen-pelvis scan length for children under 5 years of age, while the average chest scan length was only 25 percent shorter for children in the higher age categories. The anatomical boundaries of the scan are seldom altered, regardless of age. Chest exams are regularly performed with the whole thorax and half of the liver being examined. Typically, the abdomen and pelvis are examined from just above the diaphragm up to the symphysis pubis in an abdominal-pelvis examination. Because of this, very probable that variations

114

in the comparative sizes of the chest and abdomen/pelvis across various age groups are caused by changes in anatomical development, which is reflected in the relative scan lengths found in the present study.

The intended length of the operator defines the mid-position of the first and last image (slice) to be rebuilt for all scans in helical mode, and the length of the table movement for a single rotation (which varies with pitch) is automatically added to this planned length (Van der Molen et. al, 2007). This additional half-rotation width at each end is computed as part of the DLP and is part of the imaged length. The DLP does not account for an additional scan length owing to over-ranging for helical data interpolation, and we have demonstrated that for the identical scanner used in this study, the over-ranging length for a CT scan with a pitch of 0.86 to 1.00 is 5 to 6 cm. As a consequence, the scan durations for body examinations calculated here reflect the photographed length and, as a result, underestimate the total length exposed and, therefore, the effective dose.

Dose Parameters Optimisation

$CTDI_{vol}$ and DLP are dose indicators that reflect the dose to cylindrical phantoms and do not account for the relative radiosensitivity of the organs and tissues exposed or the portion of the body that is directly irradiated. The organ dose and Effective dose are intended to give a measure of total radiation harm due to stochastic effects and are to be used for prospective dose assessment to aid in planning and optimization (ICRP 103, 2007). While not designed for use in estimating dosages to people in the past, used here as an optimization

115

tool that will enable comparison with comparable operations performed at various institutions.

According to ICRP 103, the breast weighing factor is higher and in the chest area, resulting in a greater effective dosage for the chest examination. The effective dosage estimates for abdomen/pelvis exams have decreased somewhat. Although the tissue weighting factor for the gonads has reduced, a rise in the weighting factor for the remainder of the tissues and organs tends to partly compensate. Furthermore, the conversion coefficients utilised in this research to calculate the effective dose used the ICRP 103 criteria based on an abdomen/pelvis examination that did not involve direct testicular irradiation. As a result, the gonad absorbed dose, which was calculated by averaging the directly irradiated ovary and testes absorbed doses, was modest in comparison to the contribution from other organs and tissues (Brady et. al, 2011).

Other studies have shown similar findings for body CT scans when examining the influence of changes in tissue-weighting factors on effective dose estimates in adults (Huda et al., 2011, Christner et al., 2010) and for children (Deak et al, 2010). However, although many of these studies (Deak et al., 2010, Huda et al., 2011) indicate an increase in the effective dose estimate for CT brain scans when compared to the ICRP 60 definition, this study, based on the authors' previous work (Brady et al., 2011), demonstrates a 4.6 to 4.1 mSv decrease. According to ICRP 60, when a single remainder organ is directly irradiated and receives an equivalent dose higher than the primary organs' maximum dose, the rest of the weighting factor is evenly split between that organ and the remainder. When the brain is directly irradiated, this splitting rule applies, and the brain should be given a tissue-weighting

116

factor of 0.025, not 0.005, when calculating the effective dose in line with ICRP 60. (Deak et al, 2010) seem to underestimate the ICRP 60 effective dose by using a tissue-weighting factor of 0.005 for the brain dosage in CT brain scans. As a consequence, Deak et al, 2010 conclude that the ICRP 103 effective dose estimate for brain examinations is higher than the ICRP 60 effective dose estimate, which contradicts the findings of the present research (Deak et al, 2010).

The work done by Huda et al., 2011 found a comparable rise in effective dose estimates for CT head exams in adults when ICRP 103 effective dose estimates are compared to ICRP 60 effective dose estimates. They used the ImPACT CT Patient Dosimetry Calculator (v. 1.0) to determine the effective dose in accordance with either ICRP 60 or ICRP 103. ImPACT uses the ICRP splitting rule for calculating the ICRP 60 effective dosage. However, ImPACT's effective dosage estimations are based on Monte Carlo simulations that use an anthropomorphic mathematical phantom. ImPACT utilised a technique of replacing known organ absorbed doses for organs and tissues not mentioned in the ICRP 103 effective dose estimate. For instance, ImPACT has assigned the brain absorbed dosage same as that of the salivary glands and oral mucosa. Because the absorbed dosage to the brain is quite large when irradiated directly in a CT brain examination, the salivary glands and oral mucosa are assigned the same absorbed dose, despite the fact that they are unlikely to be irradiated directly in this kind of scan. As a result, the ICRP 103 effective dose estimates in ImPACT are higher than the ICRP 60 effective dose estimates for a brain examination, owing to the excessively high absorbed doses allocated to these tissues, which are included in the ICRP 103

effective dose estimate but not in the ICRP 60 effective dose estimate (Deak et al, 2010).

Thomas and Wang (2008) found effective doses based on a comparable paediatric patient dosage survey for scans done on an eight-MDCT scanner without tube current modification. ICRP 60 conversion coefficients were used to determine the effective dosages in their research. Except for imaging of the chest in the older age groups, the ICRP 60 effective dose estimates provided in this research are mainly lower. Two things seem to have contributed to this. First, a higher pitch (1.35) is utilised, which reduces dosage. Second, the mAs is lower than in this research. Furthermore, the scan protocols reported in the Thomas and Wang (Thomas et al, 2008) study show that the mAs values for abdomen/pelvis examinations are consistently higher than for chest examinations in each age group, which is not the case in the current study for body examinations in the oldest age group. Again, this implies that the protocol parameters for chest examinations at the HFH should be compared to the parameters for abdomen/pelvis examinations, and that when the values for chest examinations are higher than the values for abdomen/pelvis examinations, they should be clinically justified or otherwise optimised.

Current Practice and Dose Optimization for Paediatric Imaging

Currently, in Ghana there is no dedicated paediatric imaging equipment in any of the fifty CT imaging facilities. Despite the fact that this is suggested by the ICRP,121, to help enhance paediatric patients' protection by setting up specialised imaging protocols, and still maintained acceptable

118

image quality. In ICRP 121, 2013, Radiological Protection in Paediatric Diagnostic and Interventional Radiology, a particular care and procedure depending on age is recommended to minimise children' dose and a potential future incidence and mortality risk (ICRP 121, 2013). Although most state-of-the-art equipment provides excellent picture quality in young children, excessive radiation dosage levels may arise from design flaws. This study retrospectively reviewed five imaging facilities using the dose report and found some high-level-control CT exposure dose parameters. The mean values are within the acceptable range of values and has been presented in the summary as maximum, minimum, mean, median and the upper quartile range values. However, the data in Tables 28 and 29 provides more details of current state of the paediatric imaging in Ghana based on age and gender variations.

Children are not little adults. First, their illness states vary from those of adults, which may lead to numerous diagnoses in the imaging room. To address this, a retrospective assessment of 200 CT imaging dose reports were done and that 25-34% of all the images fell outside accepted range of values as recommended by ICRP (ICRP121, 2013). Moreover, children are more susceptible to radiation than adults. Table 28 illustrates that a child's lifetime risk of radiation-induced cancer from 1 Sv of exposure during the first decade of life is about 15%, and this number decreases as the child's age rises. This emphasises the necessity of reducing the patient radiation dosage associated with each research, particularly in view of newly released

evidence on the cumulative effects of radiation damage to the skin (Wiest et al, 2002, Blackwell et al, 1996).

Furthermore, crucial to note that imaging of paediatric patients cannot presume that children are tiny adults, and therefore the paediatrics patients are imaged using adult imaging equipment protocols. As a result, imaging equipment procedure for children must be specially designed and configured, and the device must be operated to utilise these imaging capabilities at acceptable radiation dosage levels. As a result, the generator must provide a wide dynamic range of mAs values per exposure in order to minimise the required range of high voltage and scan duration as a function of patient thickness (less than 10 cm to greater than 30 cm), as well as a properly designed control AEC required to optimise paediatric image quality while exposing the child to less radiation. (ICRP 121, 2013)

Furthermore, for any operation requiring ionising radiation, the need of thorough justification of radiological techniques is stressed, and the use of non-ionising imaging modalities should always be explored. The fundamental goal of radiological protection optimization is to modify imaging settings and implement protective measures such that the necessary radiograph is produced with the lowest feasible dose of radiation and that the net benefit maximised to retain adequate quality for diagnostic interpretation. When buying new imaging equipment for paediatric usage, especially important to examine the availability of dose reduction methods. One of the distinguishing features of paediatric imaging is the broad range of patient size

(and weight), which requires particular consideration for the optimization and adjustment of equipment, method, and imaging parameters. (ICRP 121,2013)

Dose reduction protocols are not accessible in computed tomography paediatric imaging, therefore scan parameters (such as mA, kVp, and pitch) are adjusted based on patient weight or age, area scanned, and reason for the study (ICRP Publication 121, 2013). Additionally, a paediatric dosage procedure is required for images with higher noise to be approved provided they are of adequate diagnostic quality to minimise exposure to paediatric patients, as shown in the dose report. Other methods include limiting multiphase examination procedures, minimising overlapping of scan areas, and scanning just the area of interest. Modern dose reduction technologies, such as tube current modulation, organ-based dose modulation, auto kV technology, and iterative reconstruction, which are presently not part of the paediatric imaging protocol, should be used appropriately.

Analysis of Incidence and Mortality Risk Assessment

The occurrence of cancer is strongly associated with a variety of variables, including time, sex, and age, as well as environmental agents such as radiation exposure (Hall, 2002). Recognizing the precise role of radiation exposure in the development of cancer is a tough job, made much more difficult by the stochastic character of cancer incidence. Certain people exposed to carcinogens in the environment (such as ionising radiation) get cancer, whereas others do not. The same is true for people who have not been exposed (Hall, 2002). As a result, cancer is neither a required consequence of exposure, nor does exposure always result in cancer. However, the higher

121

incidence of cancer in people exposed to recognised carcinogens shows that exposure increases the chance of getting cancer (Hall, 2002). Table 29: Illustration lifetime risk of a radiation-induced cancer from 1 Sv of dose.

Table 29: Risk of fatal Cancer from CT Examination

Risk Level	Estimated increased risk of deadly cancer from a CT Examination
Negligible	Less than 1 in 1,000,000
Minimal	1 in 1,000,000 to 1 in 100,000
Very Low	1 in 100,000 to 1 in 10,000
Low	1 in 10,000 to 1 in 1,000
Moderate	1 in 1,000 to 1 in 500

(Hall, 2002)

Estimating Cancer Risk Assessment in Paediatric Imaging

Models are created and used to estimate lifetime risks of cancer incidence and death. These models take into consideration variables such as gender, age at exposure, dosage rate, and others (Lichtenstein et al, 1996). Estimates are provided for all solid malignancies, leukaemia, and cancer in a variety of different locations. The majority of these risk modelling techniques are based on data collected from survivors of the Japanese atomic bomb explosion. Due to the inherent constraints of epidemiology data, risk estimates are susceptible to many sources of uncertainty. Apart from statistical uncertainty, the populations and exposures for which risk estimates are required almost invariably vary from those for which epidemiological data exist (Lichtenstein et al, 1996).

122

Estimation of LAR of Cancer

LAR is described as extra cancer risk over and above the risk associated with baseline cancer and may be computed for individual malignancies or for all cancers combined (Jones, 1997). Data for effective dosages and LAR values for all cancer risks and fatality estimation can be found in Appendices C to S.

Dose Optimisation in Paediatric Imaging

The study was based on measurements of effective dose in relation to Paediatric Patients' Dose Optimization Procedures. The materials used include: MDCT Machine, and MVL workstation. Technical parameters were received from three randomly selected groups of patients who were undergoing CT examinations including: 100 head CT examination, 60 abdominal CT examination and 40 chest examination. A Comprehensive Clinical Decision Support Application Software was designed to provide a user-friendly platform for comfortable working process.

Finally, the trend observed demands the optimisation of CT examination protocols so as to ensure that the doses of paediatric patients are as low as reasonably achievable by using the established CTDI and DLP baseline data as reference parameters. As part of measures to enhance radiation protection and safety of patients undergoing medical exposure, the International Atomic Energy Agency (IAEA) via its Technical Cooperation initiated a project for the establishment of Diagnostic Reference Levels (DRLs) in Africa. The aim of the project was to establish and utilize national DRLs of CTDI and DLP for routine CT for paediatric examinations.

123

Additionally, the project was to estimate dose risk assessment using effective dose for clinical protocol and dose optimisation in relation to disease and patient specific CT examination in the country. The methodology involved the estimation of CTDI and DLP values from head and body phantoms together with a minimum of 20 patient images of head CT, chest CT, and abdomen/pelvis CT examinations.

Using the methods described in chapter three, the research evaluated and assessed optimization processes for paediatric imaging procedures. Optimization is a rather lengthy process, especially for less often performed procedures, due to the fact that many stages have been shown to be necessary and must be included in the process. The most significant challenges encountered were collecting dose data from the process acquired data, getting image quality data, and, in certain instances, convincing physicians to alter existing procedures recognized as poor. This last point was particularly apparent if the optimization process had not been started and carried out domestically with the participation of all key professionals (medical radiology technologists, medical physicists and radiologists). However, since many data gathering mistakes could go unnoticed internally, seeking assistance from other experts has proved beneficial.

Repeat surveys conducted in a number of countries have shown that one major process of reducing dose is by establishing Diagnostic Reference Levels in paediatric imaging (ICRP publication 121, 2013). This was because it assists in reducing radiation doses over time. The measured data in this study shows that paediatric CT imaging examinations were between 10 to

40% lower in effective and organ dose when compared with the available limited data in Ghana. The baseline data established could widely be adopted for DRL programme in the country. anticipated that at a certain point, doses to patient would not contribute to any improvement in image quality, and DRLs will be needed to protect any needless increases in dose. Hence, if national DRLs are formed, there would be substantial initial opportunities for optimization.

Chapter Summary

In summary, this chapter discusses the various results of the measured parameters using tables and graphical representation. It also describes the relationship between the various measurable quantities that were used to calculate the derived quantities in order to draw reasonable conclusions. Furthermore, it provides an account of how the research objectives were met using various practical and theoretical tools.

125
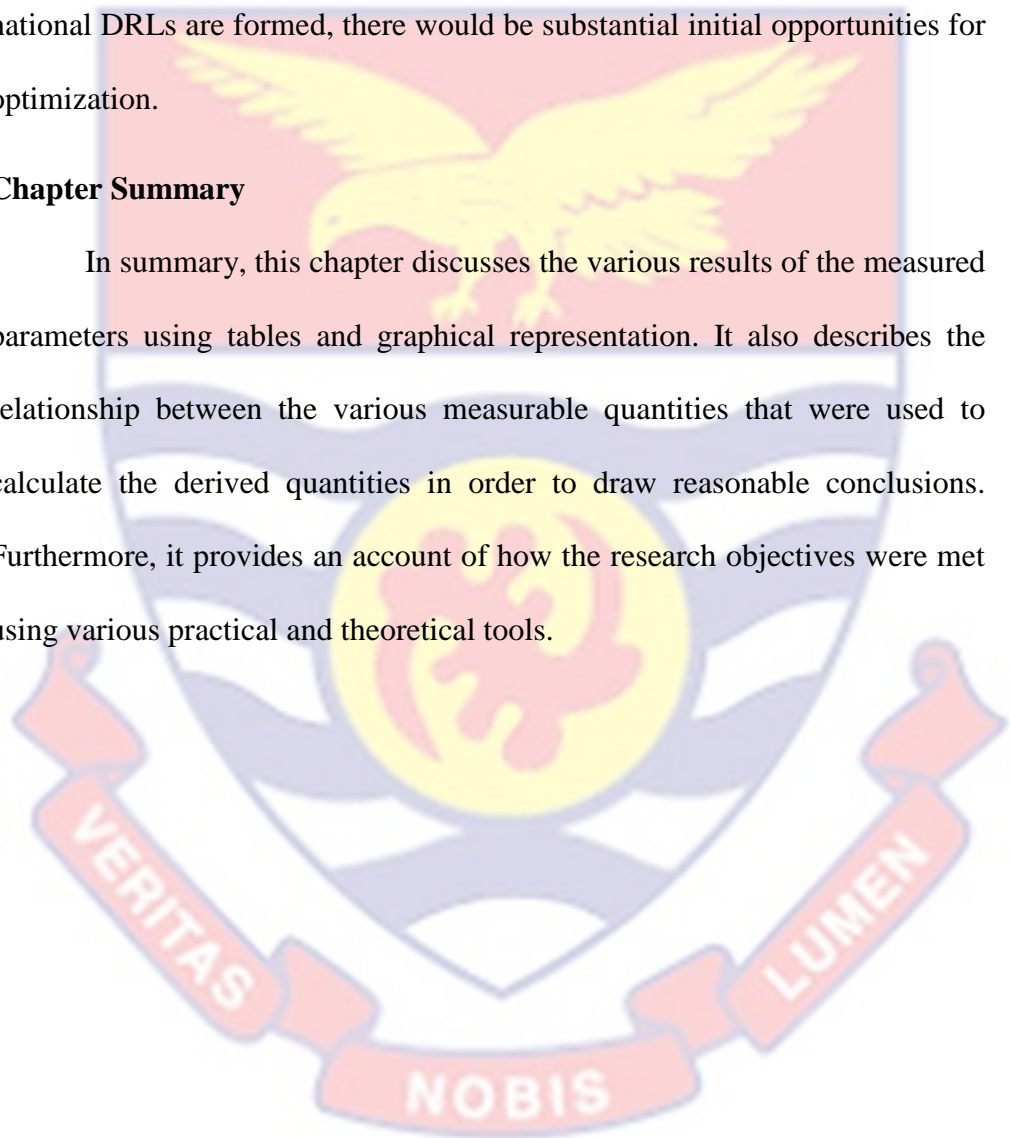
CHAPTER FIVE

SUMMARY, CONCLUSIONS AND RECOMMENDATIONS

Summary

The study sought to achieve effective interventions for optimization of chest, head, abdomen-pelvic imaging tasks in the CT facilities studied and identify key issues that have the potential to handicap the imaging process as well as risk incurred by patients undergoing examination. The study also sought to enhance the reliability and effectiveness of existing imaging protocols and to implement optimization techniques by modelling equations of parameters that affect patient and developing a Graphic User Interface to provide a tool for monitoring patient dose and dose optimisation for clinical application. The studies led to the following major findings:

In the case of head examinations; effective dose, $CTDI_{VOL}$ DLP, $CTDI_W$, and organ dose were 1.40 mGy, 5.30 mGy, 559 mGy.cm, 4.33 mGy and 10.83 μGy in the age brackets of 0-5 years respectively. Whilst, the average values for head examinations for $CTDI_{VOL}$, DLP, $CTDI_W$, effective dose and organ dose were   5.54 mGy, 888.13 mGy.cm, 4.50 mGy, 2.22 mSv and 11.26 μGy in the age brackets of 6-10 years respectively. Additionally, the average values for head examinations for $CTDI_{VOL}$, DLP, $CTDI_W$, effective dose and organ dose were   9.75 mGy, 1804 mGy.cm, 7.93 mGy, 4.51 mSv and 19.83 μGy in the age brackets of 11-16 years respectively.

In the case of Chest examinations, the $CTDI_{VOL}$, DLP, $CTDI_W$, effective dose and organ dose were 5.08 mGy, 504 mGy.cm, 4.13 mGy, 8.57 mGy and 70.14 μGy in the age brackets of 0-5 years respectively. Whilst, the

126

average values for head examinations for $CTDI_{VOL}$, DLP, $CTDI_W$, effective dose and organ dose were 5.27 mGy, 935 mGy.cm, 4.29 mGy, 15.89 mSv and 72.86 µGy in the age brackets of 6-10 years respectively. Additionally, the average values for head examinations for $CTDI_{VOL}$, DLP, $CTDI_W$, effective dose and organ dose 7.89 mGy, 1650 mGy.cm, 6.41 mGy, 29 mSv and 109.01 µGy in the age brackets of 11-16 years respectively.

In the case of abdomen-pelvis examinations the $CTDI_{VOL}$, DLP, $CTDI_W$, effective dose and organ dose were 3.85 mGy, 559 mGy.cm, 3.13 mGy, 1.40 mGy and 7.82 µGy in the age brackets of 0-5 years respectively. Whilst, the average values for abdomen-pelvis examinations for $CTDI_{VOL}$, DLP, $CTDI_W$, effective dose and organ dose were   5.2 mGy, 463 mGy.cm, 4.2 mGy, 6.94 mSv and 63.01 µGy in the age brackets of 6-10 years respectively. Additionally, the average values for head examinations for $CTDI_{VOL}$, DLP, $CTDI_W$, effective dose and organ dose were 5.18 mGy, 822 mGy.cm, 4.21 mGy, 12.33 mSv and 63.19 µGy in the age brackets of 11-16 years respectively.

The Diagnostic Reference Level and Lifetime attributable risks for incidence and mortality chart have been established. A regression model with a Graphic User interface was produced to aid in patient dose monitoring and optimisation of patient protection prior to executing the imaging protocols.

Conclusions

The CT equipment used were examined and found to be performing self-consistently within the national and international acceptance criteria and were therefore considered suitable for the research study. The methodology for

127

optimisation of paediatric patients CT imaging have been developed taking into account patients' demography, CT equipment performance, imaging protocols and modelling of the factors that influence dose and image quality.

Standard values of paediatric patient dose descriptors ($CTDI_{vol}$ and DLP) for optimization of procedures are now available to be used by clinicians during paediatric CT examinations for the head, abdomen/pelvis regions and chest. DRLs have been determined for the most common paediatric imaging for the consideration by the approving authorities.

Recommendations have been made to the relevant stakeholders. The modelled equations and their associated Graphic User Interface (GUI) developed have provided a practical tool for monitoring and optimisation of the protection of paediatric patient during paediatric imaging in Ghana when adopted by the facility management for clinical application.

Recommendations

The following recommendations are addressed to key stakeholders in order to help improve health care delivery for paediatric imaging in Ghana.

Recommendations for participating facilities

1. Facilities are encouraged to acquire dose reduction equipment/technologies and techniques to help reduce radiation dose to patients compatible with what has been done during this research work.

2. Adequate and appropriate training on optimization of patient protection be organized to meet regulatory requirements for both existing staff and those to be recruited in future.

128

3. Establish specific unified scanning protocols as established in this study. Data management units should be established and managed by qualified personnel for better Radiological Information System (RIS) in all the centres.

Recommendation to Radiographers

1. The modelled equations should be used to aid in the selection of exposure parameters.

2. Radiographers should co-work with the medical physicists and the radiologists during scanning process so that they help reduce radiation doses to patients without sacrificing image quality.

3. Various dose optimization factors should be considered during pre-set imaging procedure. These include patient size, age and gender variations to avoid unnecessary dose to patients.

Recommendation to Radiologists

The established reference values are recommended to be used as clinical guidelines values for the optimisation of protection of patients and upgrading of the clinical practice in paediatric imaging in Ghana.

Recommendation to Medical Physicists

1. The teamwork approach between the radiologists, the medical physicists as well as the radiographers should be strengthened so as to optimise radiation protection of patients.

2. Medical physicists should adopt the method used in this study to continuously monitor dose levels to advice clinicians appropriately in

their clinical practice.

3. recommended that medical physicists adopt the method used in this study to develop standard reference dosimetric values for other imaging modalities for clinical applications and research in Ghana.

Recommendations to Regulatory Authority

1. The abdominal effective dose exceeded the recommended EC and ICRP values. The Nuclear Regulatory Authority should provide regulations and guidance documents that will assist registrants and licensees to meet regulatory requirements for the control of medical exposure relevant to paediatric imaging.

Recommendations for Future Works

Further studies should be done with regard to organ model of infants and the neonates to identify root causes of the age variations of scanning protocols used in various CT centres in Ghana, in order to provide reference data for paediatric imaging for reliable baseline data.

130

REFERENCES

Alessio A, Phillips G (2010). *A pediatric CT dose and risk estimator*. Pediatr Radiol ; 40:1816–21

Blackwell D, Gorelick M, Holmes F, Bandyopadhyay S, Kuppermann N. (2007). *Pediatric head trauma: changes in use of computed tomography in emergency departments in the United States over time*. Ann Emerg Med; 49(3):320–4

Boone M, Geraghty M, Seibert A, Wootton-Gorges L. (2003). *Dose reduction in pediatric CT: a rational approach.* Radiology; 228:352–60

Brady Z, Cain T, Johnston P. (2011). *Differences in using the International Commission on Radiological Protection's publications 60 and 103 for determining effective dose in paediatric CT examinations*. Radiat Meas 2011; 46(12):2031–4

Brady Z, Cain T, Johnston P. (2011). *Paediatric CT imaging trends in Australia*. J Med Imaging Radiat Oncol ; 55(2):132–42

Brenner D, Elliston C, Hall E, Berdon W. Estimated risks of radiation-induced fatal cancer from pediatric CT. AJR Am J Roentgenol 2001;176 (2):289–96

Canon Medical Systems, (2020). Global Healthcare Market Outlook, 2019, Frost and Solution, pg 1-14.

Chapple CL, Willis S, Frame J. (2002). *Effective dose in paediatric computed tomography*. Phys Med Biol ; 47:107–15

131

Christner J, Kofler J, McCollough C. (2010). *Estimating effective dose for CT using dose-length product compared with using organ doses: consequences of adopting International Commission on Radiological Protection publication 103 or dual-energy scanning*. AJR Am J Roentgenol; 194:881–9

Chung T, Kirks D. (1998). Techniques. In: Kirks DR, Griscom NT (eds) Practical pediatric imaging. Lippincott-Raven, Philadelphia, pp 1–3

Deak D, Smal Y, Kalender A. (2010). Multisection CT protocols: sex- and age-specific conversion factors used to determine effective dose from dose-length product. Radiology ; 257:158–66.

EC, (2016). Resolution (EU) 2016/679 on the Protection of Natural Persons with Regard to the Processing Of Personal Data, EU, pp 1-10.

Emaze, (2015). Referenced from Emaze.org, Accessed 18-08-2022.

Galanski M, Nagel HD, Stamm G. (2007). *Paediatric CT exposure practice in the Federal Republic of Germany: results of a nationwide survey in 2005–2006.* Hannover, Germany: Medizinische Hochschule Hannover;

Haaga J. (2001). *Radiation dose management: weighing risk versus benefit.* AJR Am J Roentgenol; 177:289–91

Hall E. (2002). Lessons we have learned from our children: cancer risks from diagnostic radiology. Pediatr Radiol 32:700–06

132

Hart D, Wall F, Shrimpton C, Bungay D, Dance D. (2000). *Reference doses and patient size in paediatric radiology*. Report NRPB-R318 Chilton, UK: National Radiological Protection Board;

Heggie J. (2005). *Patient doses in multi-slice CT and the importance of optimisation*. Australas Phys Eng Sci Med ; 28:86–96

Huda W, Magill D, He W. (2011). *CT effective dose per dose length product using ICRP 103 weighting factors*. Med Phys ; 38:1261–5

Huda W, Sterzik A, Tipnis S. (2010). *X-ray beam filtration, dosimetry phantom size and CT patient dose conversion factors*. Phys Med Biol ; 55:551–61.

Imagewisely, (2012). Referened from Imagewisely.org, Accessed 18-08-2022.

Institute of Physics and Engineering in Medicine. (2004). Guidance on the establishment and use of diagnostic reference levels for medical X-ray examinations. IPEM Report No. 88. York, UK: IPEM;

International Commission on Radiological Protection (2007). Radiological protection in medicine. ICRP Publication 105. Ann ICRP ; 37(6):1–64.

International Commission on Radiological Protection. (1991). Recommendations of the International Commission on Radiological Protection. ICRP Publication 60. Ann ICRP ; 21(1-3):1–201.

International Commission on Radiological Protection. (1996). Radiological protection and safety in medicine. ICRP Publication 73. Ann ICRP ; 26(2):1–47.

International Commission on Radiological Protection. (2001). *Diagnostic reference levels in medical imaging: review and additional advice*. ICRP Supporting Guidance 2. Ann ICRP ; 31:33–52.

International Commission on Radiological Protection. (2007). The 2007 recommendations of the International Commission on Radiological Protection. ICRP Publication 103. Ann ICRP; 37:1–332.

ICRP, (2018). International Commission on Radiological Protection, Occupational Radiological Protection in Interventional Procedures, ICRP Publication 139, . Ann ICRP; 47 (2).

Jones K. (1997). *Smith's recognizable patterns of human malformation*, 5th edn. Saunders, Philadelphia

KBTH, (2018). Korle-Bu Teaching Hospital, Radiology Unit, Accra.

Kleinman L, Strauss J, Zurakowski D, Buckley K, Taylor G. (2010). *Patient size measured on CT images as a function of age at a tertiary care children's hospital*. AJR Am J Roentgenol ; 194:1611–19.

Leitz, W., Axelsson, B., & Szendro, G. (1995). Computed tomography dose assessment a practical approach. *Radiat. Prot. Dosimetry, 57*, 377–380.

134

Lerner, L. B., Henriquez, H. F., & Harris, R. D. (1999). Interactive 3-dimensional computerized tomography reconstruction in evaluation of the living renal donor. *Journal of Urology, 161*(2), 403-407.

Lewis MA, Edyvean S. (2005). *Patient dose reduction in CT*. Br J Radiol ; 78:880–3.

Lichtenstein DA, Klapholz L, Vardy D. (1996) Chronic radiodermatitis following cardiac catheterization. Arch Dermatol 132:663–67

Link, F., Kuhagen, S., Boskamp, T., Rexilius, J., Dachwitz, S., & Peitgen, H. O. (2004). A flexible research and development platform for medical image processing and visualization. *RSNA Publications, 453*(6), 17-32.

Löfstedt, T., Ahnlund, O., Peolsson, M., & Trygg, J. (2012). *Contrast-to-Noise ratio is not an appropriate measure of CT image quality when comparing different iterative reconstruction algorithms.* 54th Annual Meeting, University of Chicago, Chicago, IL, Charlotte, NC.

London, UK: ImPACT; © ImPACT. (2008). Referenced from http://www.impactscan.org, Accessed 18-08-2022.

Martin C. (2007). Effective dose: how should it be applied to medical exposures? Br J Radiol ; 80:639–47.

Mattsson, S., & Söderberg, M. (2011). Radiation dose management in CT, SPECT/CT and PET/CT Techniques. *Rad Prot Dosim*, *147*(1), 13–21.

Mazonakis, M., Tzedakis, A., Damilakis, J., & Gourtsoyiannis, N. (2007).

135

McAfee, J. G., Cloutier, R. J., Edwards, C. L., & Snyder, W. S. (1969). *Problems in evaluating the radiation dose for radionuclides excreted by the kidneys in medical radonuclides: Radiation dose and effects symposium.* Oak Ridge: U.S. Atomic Energy Commission.

McLean D, Malitz N, Lewis S. (2003). *Survey of effective dose levels from typical paediatric CT protocols.* Australas Radiol ; 47:135–42

MeVis Medical Solutions. (2015). *Reference guide for the MeVisLab* GUI. Bremen: Author.

Monson, R. R. (2006). *Health risks from exposure to low levels of ionising radiation.* Washington DC: The National Academies Press.

Moss M, McLean D. (2006). *Paediatric and adult computed tomography practice and patient dose in Australia.* Australas Radiol ; 50 (1) :33–40

National Research Council of the National Academies Board on Radiation Effects Research. (2006). Health risks from exposure to low levels of ionizing radiation: BEIR VII phase 2. Washington, DC: The National Academies Press;

Pages J, Buls N, Osteaux M. (2003). *CT doses in children: a multicentre study.* Br J Radiol ; 76 (911):803–11

Physicscentral, (2022). Physicscentral.com. Referened from, Accessed 18-08-2022.

Shope T. (1996). *Radiation-induced skin injuries from fluoroscopy.* Radiographics 16:1195–199

Shrimpton PC, Hillier MC, Lewis MA, Dunn M. (2003). *National survey of doses from CT in the UK*:. Br J Radiol 2006; 79(948):968–80

Shrimpton PC, Hillier MC, Lewis MA, Dunn M. (2005). *Doses from computed tomography (CT) examinations in the UK*: 2003 review. Report NRPB-W67 Chilton, UK: National Radiological Protection Board;

Shrimpton PC, Wall BF. (2000). Reference doses for paediatric computed tomography. Radiat Prot Dosimetry ; 90:249–52

Smith-Bindman R, Lipson J, Marcus R, Kim KP, Mahesh M, Gould R. (2009). *Radiation dose associated with common computed tomography examinations and the associated lifetime attributable risk of cancer*. Arch Intern Med ; 169 (22):2078–86

Theocharopoulos N, Damilakis J, Perisinakis K, Tzedakis A, Karantanas A, Gourtsoyiannis N (2006). *Estimation of effective doses to adult and pediatric patients from multislice computed tomography: a method based on energy imparted*. Med Phys ; 33:3846–56

Thomas K, Wang B. (2008). *Age-specific effective doses for pediatric MSCT examinations at a large children's hospital using DLP conversion coefficients: a simple estimation method*. Pediatr Radiol ; 38:645–56

Tsapaki, V., Kottou, S., & Papadimitriou, D. (2001). *Application of European Commission reference dose levels in CT examinations in Crete, Greece*. *British J Radiol*. *74*(885), 836-840.

137

Tzedakis A, Damilakis J, Perisinakis K, Stratakis J and Gourtsoyiannis N. (2005). *The effect of z overscanning on patient effective dose from multidetector helical computed tomography examinations*. *J. of Med Physics, 32,* 1621-1629

United Nations Scientific Committee on the Effects of Atomic Radiation Sources and effects of ionizing radiation (2010). Vol. I. UNSCEAR 2008 report to the General Assembly. Annex A: medical radiation exposures. New York, NY: United Nations;

Van der Molen AJ, Geleijns J. (2007). *Overranging in multisection CT: quantification and relative contribution to dose-comparison of four 16-section CT scanners*. Radiology ; 242:208–16

Velten, K. (2009*). Mathematical modeling and simulation: Introduction for scientists and engineers*. Weinheim: Wiley-Vch Verlag GmbH & Co.

Verdun FR, Gutierrez D, Vader JP, Aroua A, Alamo-Maestre LT, Bochud F. (2008). *CT radiation dose in children: a survey to establish age-based diagnostic reference levels in Switzerland*. Eur Radiol ; 18:1980–6

Wallace AB, Goergen SK, Schick D, Soblusky T, Jolley D. (2010). *Multidetector CT dose: clinical practice improvement strategies from a successful optimization program*. J Am Coll Radiol ; 7(8):614–24

Watson D, Coakley S. (2010). *Paediatric CT reference doses based on weight and CT dosimetry phantom size: local experience using a 64-slice CT scanner*. Pediatr Radiol ; 40:693–703

Wiest PW, Locken JA, Heintz PH, Mettler FA. (2002). *CT scanning: a major source of radiation exposure. Semin Ultrasound CT MRI* ; 23:402–10

Yakoumakis E, Karlatira M, Gialousis G, Dimitriadis A, Makri T, Georgiou E. (2009). *Effective dose variation in pediatric computed tomography: dose reference levels in Greece*. Health Phys ; 97:595–603

APPENDICES

APPENDIX A

LIFETIME ATTRIBUTABLE RISK OF CANCER INCIDENCE

TABLE 12D-1 Lifetime Attributable Risk of Cancer Incidence[a]

Cancer Site	Age at Exposure (years)										
	0	5	10	15	20	30	40	50	60	70	80
Males											
Stomach	76	65	55	46	40	28	27	25	20	14	7
Colon	336	285	241	204	173	125	122	113	94	65	30
Liver	61	50	43	36	30	22	21	19	14	8	3
Lung	314	261	216	180	149	105	104	101	89	65	34
Prostate	93	80	67	57	48	35	35	33	26	14	5
Bladder	209	177	150	127	108	79	79	76	66	47	23
Other	1123	672	503	394	312	198	172	140	98	57	23
Thyroid	115	76	50	33	21	9	3	1	0.3	0.1	0.0
All solid	2326	1667	1325	1076	881	602	564	507	407	270	126
Leukemia	237	149	120	105	96	84	84	84	82	73	48
All cancers	2563	1816	1445	1182	977	686	648	591	489	343	174
Females											
Stomach	101	85	72	61	52	36	35	32	27	19	11
Colon	220	187	158	134	114	82	79	73	62	45	23
Liver	28	23	20	16	14	10	10	9	7	5	2
Lung	733	608	504	417	346	242	240	230	201	147	77
Breast	1171	914	712	553	429	253	141	70	31	12	4
Uterus	50	42	36	30	26	18	16	13	9	5	2
Ovary	104	87	73	60	50	34	31	25	18	11	5
Bladder	212	180	152	129	109	79	78	74	64	47	24
Other	1339	719	523	409	323	207	181	148	109	68	30
Thyroid	634	419	275	178	113	41	14	4	1	0.3	0.0
All solid	4592	3265	2525	1988	1575	1002	824	678	529	358	177
Leukemia	185	112	86	76	71	63	62	62	57	51	37
All cancers	4777	3377	2611	2064	1646	1065	886	740	586	409	214

APPENDIX B

LIFETIME ATTRIBUTABLE RISK OF CANCER INCIDENCE

TABLE 12D-2 Lifetime Attributable Risk of Cancer Mortality[a]

Cancer Site	Age at Exposure (years)										
	0	5	10	15	20	30	40	50	60	70	80
Males											
Stomach	41	34	30	25	21	16	15	13	11	8	4
Colon	163	139	117	99	84	61	60	57	49	36	21
Liver	44	37	31	27	23	16	16	14	12	8	4
Lung	318	264	219	182	151	107	107	104	93	71	42
Prostate	17	15	12	10	9	7	6	7	7	7	5
Bladder	45	38	32	27	23	17	17	17	17	15	10
Other	400	255	200	162	134	94	88	77	58	36	17
All solid	1028	781	641	533	444	317	310	289	246	181	102
Leukemia	71	71	71	70	67	64	67	71	73	69	51
All cancers	1099	852	712	603	511	381	377	360	319	250	153
Females											
Stomach	57	48	41	34	29	21	20	19	16	13	8
Colon	102	86	73	62	53	38	37	35	31	25	15
Liver	24	20	17	14	12	9	8	8	7	5	3
Lung	643	534	442	367	305	213	212	204	183	140	81
Breast	274	214	167	130	101	61	35	19	9	5	2
Uterus	11	10	8	7	6	4	4	3	3	2	1
Ovary	55	47	39	34	28	20	20	18	15	10	5
Bladder	59	51	43	36	31	23	23	22	22	19	13
Other	491	287	220	179	147	103	97	86	69	47	24
All solid	1717	1295	1051	862	711	491	455	415	354	265	152
Leukemia	53	52	53	52	51	51	52	54	55	52	38
All cancers	1770	1347	1104	914	762	542	507	469	409	317	190

141

APPENDIX C

MEASURED DOSE PARAMETERS AND IMAGE QUALITY FOR HEAD CT EXAMINATION OF VARIED AGE GROUP

HEAD 0-5							
ID	Sex	AGE	CTDIvol	CTDI$_W$	DLP	Organ Dose	Effective Dose
	M/F	Y	mGy	mGy	mGy-cm	mSv	mSv
H-39	M	2	6.2	5.0406	364.8	0.0126	0.912
H-3	F	3	4.7	3.8211	468.8	0.00955	1.172
H-63	F	3	4.7	3.8211	468.8	0.00955	1.172
H-71	M	3	5.5	4.4715	294.9	0.01118	0.73725
H-4	M	5	5.5	4.4715	597.6	0.01118	1.494
H-12	F	5	5.9	4.7967	935.4	0.01199	2.3385
H-64	M	5	5.5	4.4715	597.6	0.01118	1.494
H-68	M	5	4.7	3.8211	759	0.00955	1.8975
H-35	F	5	5.3	4.3089	549.6	0.01077	1.374
H-70	F	5	5.3	4.3089	549.6	0.01077	1.374
Mean		4.1	5.33	4.33329	558.61	0.010833	1.396525
Median		5	5.4	4.3902	549.6	0.010976	1.374
Max		5	6.2	5.0406	935.4	0.012602	2.3385
Min		2	4.7	3.8211	294.9	0.009553	0.73725
¾ Q		5	5.6	4.5528	637.95	0.011382	1.594875
HEAD 6-10							
ID	Sex	AGE	CTDIvol	CTDI$_W$	DLP	Estimated Organ Dose	Effective Dose
	M/F	Y	mGy	mGy	mGy-cm	mSv	mSv
H-66	M	6	3	2.439	682.8	0.0061	1.707
H-30	M	6	5	4.065	747	0.01016	1.8675
H-51	M	6	6.2	5.0406	852.9	0.0126	2.13225
H-34	F	6	4.8	3.9024	765.88	0.00976	1.9147
H-9	M	7	4.7	3.8211	911.4	0.00955	2.2785
H-18	M	7	5.3	4.3089	942.6	0.01077	2.3565
H-59	M	7	6.2	5.0406	572.6	0.0126	1.4315
H-61	F	8	5	4.065	912.4	0.01016	2.281
H-62	M	8	5.1	4.1463	915.3	0.01037	2.28825
H-28	M	8	4.7	3.8211	794.1	0.00955	1.98525

142

ID	Sex	AGE	CTDIvol	CTDI$_W$	DLP	Organ Dose	Effective Dose
H-48	F	8	5.7	4.6341	824.9	0.01159	2.06225
H-56	F	8	5.5	4.4715	855.3	0.01118	2.13825
H-15	F	9	7.7	6.2601	987	0.01565	2.4675
H-23	M	9	5.9	4.7967	987.6	0.01199	2.469
H-65	F	9	6.7	5.4471	1128	0.01362	2.82
H-42	M	9	5.6	4.5528	942.6	0.01138	2.3565
H-67	F	10	7.1	5.7723	1275.9	0.01443	3.18975
Mean		8	5.54118	4.50498	888.134	0.01126	2.22034
Median		8	5.5	4.4715	911.4	0.01118	2.2785
Max		10	7.7	6.2601	1275.9	0.01565	3.18975
Min		6	3	2.439	572.6	0.0061	1.4315
¾ Q		9	6.2	5.0406	964.8	0.0126	2.412

HEAD 11-16

ID	Sex	AGE	CTDIvol	CTDI$_W$	DLP	Organ Dose	Effective Dose
	M/F	Y	mGy	mGy	mGy-cm	mSv	mSv
H-1	M	11	4.7	3.8211	703.2	0.00955	1.758
H-58	M	11	7.1	5.7723	1233.6	0.01443	3.084
H-75	F	11	7.7	6.2601	1538.4	0.01565	3.846
H-40	F	11	7.7	6.2601	1538.4	0.01565	3.846
H-10	M	12	4.7	3.8211	693.3	0.00955	1.73325
H-53	F	12	6	4.878	1254.9	0.0122	3.13725
H-31	F	12	7.4	6.0162	1043.57	0.01504	2.608925
H-19	M	13	15.7	12.7641	3200	0.03191	8
H-72	F	15	12.3	9.9999	2794.4	0.025	6.986
H-25	F	15	9.2	7.4796	1389	0.0187	3.4725
H-37	F	15	12.3	9.9999	2794.4	0.025	6.986
H-73	F	16	16	13.008	2634.9	0.03252	6.58725
H-38	F	16	16	13.008	2634.9	0.03252	6.58725
MEAN		13	9.753846	7.929877	1804.075	0.019825	4.510187
MEDIAN		12	7.7	6.2601	1538.4	0.01565	3.846
MAX		16	16	13.008	3200	0.03252	8
MIN		11	4.7	3.8211	693.3	0.009553	1.73325
¾ Q		15	14	11.382	2714.65	0.028455	6.786625

APPENDIX D

MEASURED DOSE PARAMETERS AND IMAGE QUALITY FOR CHEST CT EXAMINATION OF VARIED AGE GROUP

				CHEST 0-5			
ID	Sex	AGE	CTDIvol	CTDI$_W$	DLP	Organ Dose	Effective Dose
	M/F	Y	mGy	mGy	mGy-cm	mSv	mSv
CH-41	F	1	4.7	3.8211	234.4	0.06496	3.9848
CH-74	M	2	6.2	5.0406	364.8	0.08569	6.2016
CH-33	M	5	4.7	3.8211	759	0.06496	12.903
CH-29	M	5	4.7	3.8211	658.89	0.06496	11.20113
CH-71	F	2	4.7	3.8211	234.4	0.06496	3.9848
CH-23	F	4	4.5	3.6585	211.3	0.06219	3.5921
CH-33	F	3	4.2	3.4146	201.2	0.05805	3.4204
CH-34	M	2	4.3	3.4959	195	0.05943	3.315
CH22	M	4	4.2	3.4146	200.1	0.05805	3.4017
CH11	F	3	5.2	4.276	365.2	0.071869	6.2084
MEAN		3.1	4.42	7.65846	342.429	0.130194	5.821293
MEDIAN		3	4.7	3.8211	234.4	0.064959	3.9848
MAX		5	6.2	42.276	759	0.08692	12.903
MIN		1	4.2	3.4146	195	0.058048	3.315
¾ Q		4.25	4.75	4.12598	438.6225	0.070142	7.456583
				CHEST 6-10			
ID	Sex	AGE	CTDIvol	CTDI$_W$	DLP	Organ Dose	Effective Dose
	M/F	Y	mGy	mGy	mGy-cm	mSv	mSv
CH-32	M	6	5	4.065	792.6	0.06911	13.4742
CH-44	F	6	4.8	3.9024	754.8	0.06634	12.8316
CH-47	F	6	4.9	3.9837	793.8	0.06772	13.4946
CH-60	F	6	4.9	3.9837	745.2	0.06772	12.6684
CH-81	M	7	6.2	5.0406	572.6	0.08569	9.7342
CH-50	F	7	4.7	3.8211	937.6	0.06496	15.9392
CH-43	M	8	4.9	3.9837	757.2	0.06772	12.8724
CH-5	F	9	6.7	5.4471	1128	0.0926	19.176
CH-49	F	9	4.7	3.8211	1590.9	0.06496	27.0453
CH-78	M	9	5.6	4.5528	942.6	0.0774	16.0242
CH-57	M	9	4.9	3.9837	910.8	0.06772	15.4836
CH-46	M	10	5.2	4.2276	1283.2	0.07187	21.8144

144

ID	Sex	AGE	CTDIvol	CTDIW	DLP	Organ Dose	Effective Dose
CH-54	F	10	5.6	4.5528	850.2	0.0774	14.4534
CH-52	F	10	5.7	4.6341	1026.3	0.07878	17.4471
Mean		8	5.3	4.285671	934.7	0.072856	15.8899
Median		8.5	4.95	4.02435	880.5	0.068414	14.9685
Max		10	6.7	5.4471	1590.9	0.092601	27.0453
Min		6	4.7	3.8211	572.6	0.064959	9.7342
¾ Q		9.25	5.63	4.573125	1051.725	0.077743	17.87933

CHEST 11-16

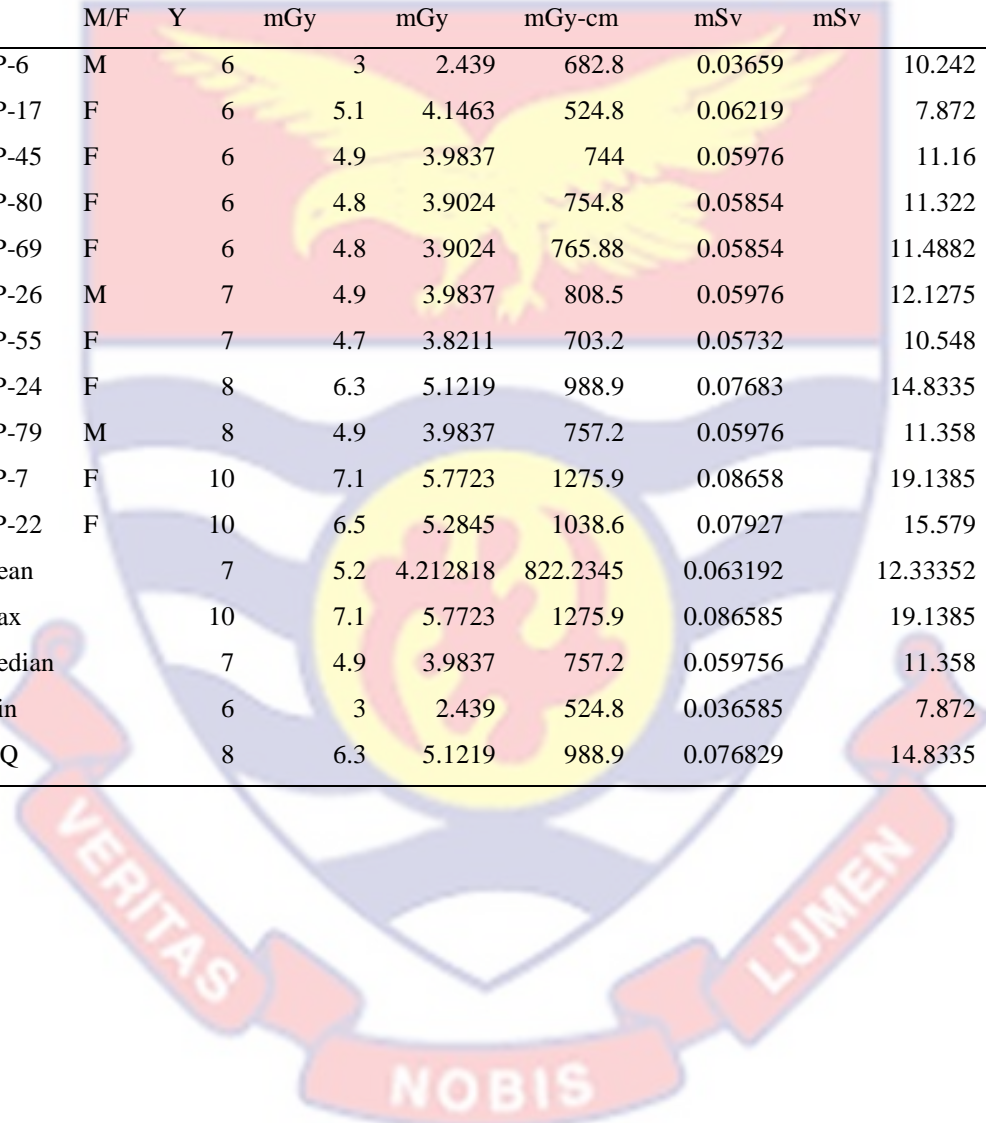| ID	Sex	AGE	CTDIvol	CTDI$_W$	DLP	Organ Dose	Effective Dose
	M/F	Y	mGy	mGy	mGy-cm	mSv	mSv
CH-27	F	11	7.1	5.7723	1065.6	0.09813	18.1152
CH-20	M	12	9.7	7.8861	2127.2	0.13406	36.1624
CH-21	F	12	8.1	6.5853	1215.9	0.11195	20.6703
CH-8	F	13	5.7	4.6341	1331.1	0.07878	22.6287
CH-11	F	13	13.5	10.9755	2975.6	0.18658	50.5852
CH-14	F	14	8.7	7.0731	1413.9	0.12024	24.0363
CH-16	F	15	5.6	4.5528	2114.89	0.0774	35.95313
CH-2	F	16	4.7	3.8211	1311.5	0.06496	22.2955
CH-12	M	16	4.7	3.8211	1256.4	0.06496	21.3588
CH-23	M	12	4.7	3.8211	930.5	0.06496	15.8185
CH-11	M	14	6.7	5.4471	1123.2	0.0926	19.0944
CH-08	M	13	6.7	5.4471	1213.4	0.0926	20.6278
CH-90	F	15	4.7	3.8211	885.6	0.06496	15.0552
CH-45	F	16	6.7	5.4471	1122.4	0.0926	19.0808
CH-44	M	11	6.9	5.6097	1232.5	0.09536	20.9525
CH-32	M	12	7.1	5.7723	1324.6	0.09813	22.5182
MEAN		13.4375	6.95625	5.655431	1415.268	0.096142	24.05956
MEDIAN		13	6.7	5.4471	1244.45	0.092601	21.15565
MAX		16	13.5	10.9755	2975.6	0.186584	50.5852
MIN		11	4.7	3.8211	885.6	0.064959	15.0552
¾ Q		15	7.85	6.38205	1393.2	0.108495	23.6844

145

APPENDIX E

MEASURED DOSE PARAMETERS AND IMAGE QUALITY FOR HEAD CT EXAMINATION OF VARIED AGE GROUP

						AP0-5	
ID	Sex	AGE	CTDIvol	CTDI$_W$	DLP	Estimated Organ Dose	Effective Dose
	M/F	Y	mGy	mGy	mGy-cm	mGy	Dose
							mSv
AP-6	M	12	4.2	3.4146	364.8	0.0085365	0.912
AP-17	F	13	3.7	3.0081	468.8	0.00752025	1.172
AP-45	F	13	3.7	3.0081	468.8	0.00752025	1.172
AP-80	M	13	3.6	2.9268	294.9	0.007317	0.73725
AP-69	M	15	5.2	4.2276	597.6	0.010569	1.494
AP-26	F	15	4.1	3.3333	935.4	0.00833325	2.3385
AP-55	M	15	3.2	2.6016	597.6	0.006504	1.494
AP-24	M	15	3.6	2.9268	759	0.007317	1.8975
AP-79	F	15	3.7	3.0081	549.6	0.00752025	1.374
AP-7	F	15	3.5	2.8455	549.6	0.00711375	1.374
Max		15	5.2	4.2276	935.4	0.010569	2.3385
Min		12	3.2	2.6016	294.9	0.006504	0.73725
Median		15	3.7	3.0081	549.6	0.00752025	1.374
Mean		14.1	3.85	3.13005	558.61	0.007825125	1.396525
¾ Q		15	4.125	3.353625	637.95	0.008384063	1.594875

						AP 6-10	
ID	Sex	AGE	CTDIvol	CTDI$_W$	DLP	Organ Dose	Effective Dose
	M/F	Y	mGy	mGy	mGy-cm	mGy	mSv
AP-76	F	1	4.7	3.8211	234.4	0.05732	3.516
AP-36	M	3	5.5	4.4715	294.9	0.06707	4.4235
AP-13	M	4	5.3	4.3089	859.2	0.06463	12.888
AP-22	M	1	4.7	3.8211	234.4	0.05732	3.516
AP-66	F	2	4.7	3.8211	234.4	0.05732	3.516
AP-55	F	2	4.7	3.8211	234.4	0.05732	3.516
AP-43	F	4	5.5	4.4715	294.9	0.06707	4.4235
AP-23	M	5	4.7	3.8211	234.4	0.05732	3.516
AP-41	F	5	4.7	3.8211	234.4	0.05732	3.516
AP-32	M	4	5.5	4.4715	294.9	0.06707	4.4235

146

ID	Sex	AGE	CTDIvol	CTDI_W	DLP	Organ Dose	Effective Dose
AP-34	M	3	5.5	4.4715	294.9	0.06707	4.4235
Mean		3	5.1	4.1020	313.2	0.061529	4.698
Median		3	4.7	3.8211	234.4	0.057317	3.516
Max		5	5.5	4.4715	859.2	0.067073	12.888
Min		1	4.7	3.8211	234.4	0.057317	3.516
¾ Q		4	5.5	4.4715	294.9	0.067073	4.4235

AP11-16

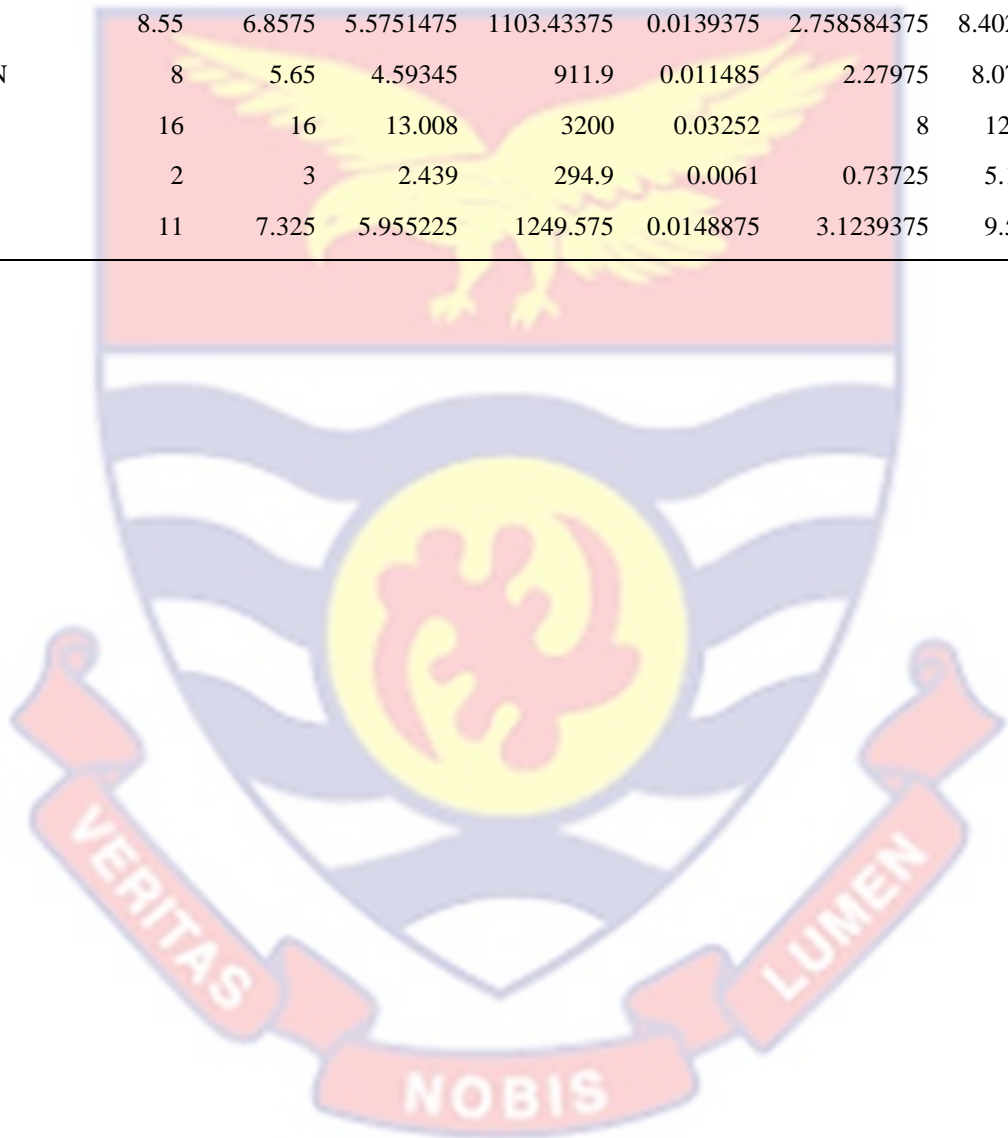| ID	Sex	AGE	CTDIvol	CTDI_W	DLP	Organ Dose	Effective Dose
	M/F	Y	mGy	mGy	mGy-cm	mSv	mSv
AP-6	M	6	3	2.439	682.8	0.03659	10.242
AP-17	F	6	5.1	4.1463	524.8	0.06219	7.872
AP-45	F	6	4.9	3.9837	744	0.05976	11.16
AP-80	F	6	4.8	3.9024	754.8	0.05854	11.322
AP-69	F	6	4.8	3.9024	765.88	0.05854	11.4882
AP-26	M	7	4.9	3.9837	808.5	0.05976	12.1275
AP-55	F	7	4.7	3.8211	703.2	0.05732	10.548
AP-24	F	8	6.3	5.1219	988.9	0.07683	14.8335
AP-79	M	8	4.9	3.9837	757.2	0.05976	11.358
AP-7	F	10	7.1	5.7723	1275.9	0.08658	19.1385
AP-22	F	10	6.5	5.2845	1038.6	0.07927	15.579
Mean		7	5.2	4.212818	822.2345	0.063192	12.33352
Max		10	7.1	5.7723	1275.9	0.086585	19.1385
Median		7	4.9	3.9837	757.2	0.059756	11.358
Min		6	3	2.439	524.8	0.036585	7.872
¾ Q		8	6.3	5.1219	988.9	0.076829	14.8335

APPENDIX F

MEASURED HEAD CT DOSE OPTIMISATION PARAMETERS

ID	Sex	AGE	CTDIvol	CTDI$_W$	DLP	Organ Dose	Effective Dose	SNR1
	M/F	Y	mGy	mGy	mGy-cm	mSv	mSv	
H-39	M	2	6.2	5.0406	364.8	0.0126	0.912	6.296296
H-3	F	3	4.7	3.8211	468.8	0.00955	1.172	8.0709
H-63	F	3	4.7	3.8211	468.8	0.00955	1.172	7.383732
H-71	M	3	5.5	4.4715	294.9	0.01118	0.73725	12.07609
H-4	M	5	5.5	4.4715	597.6	0.01118	1.494	7.421365
H-12	F	5	5.9	4.7967	935.4	0.01199	2.3385	5.112412
H-64	M	5	5.5	4.4715	597.6	0.01118	1.494	9.527273
H-68	M	5	4.7	3.8211	759	0.00955	1.8975	6.296296
H-35	F	5	5.3	4.3089	549.6	0.01077	1.374	8.0709
H-70	F	5	5.3	4.3089	549.6	0.01077	1.374	9.315789
H-66	M	6	3	2.439	682.8	0.0061	1.707	9.848866
H-30	M	6	5	4.065	747	0.01016	1.8675	7.383732
H-51	M	6	6.2	5.0406	852.9	0.0126	2.13225	8.19052
H-34	F	6	4.8	3.9024	765.88	0.00976	1.9147	12.07609
H-9	M	7	4.7	3.8211	911.4	0.00955	2.2785	7.383732
H-18	M	7	5.3	4.3089	942.6	0.01077	2.3565	8.19052
H-59	M	7	6.2	5.0406	572.6	0.0126	1.4315	12.07609
H-61	F	8	5	4.065	912.4	0.01016	2.281	7.421365
H-62	M	8	5.1	4.1463	915.3	0.01037	2.28825	5.112412
H-28	M	8	4.7	3.8211	794.1	0.00955	1.98525	9.527273
H-48	F	8	5.7	4.6341	824.9	0.01159	2.06225	6.296296
H-56	F	8	5.5	4.4715	855.3	0.01118	2.13825	8.0709
H-15	F	9	7.7	6.2601	987	0.01565	2.4675	9.315789
H-23	M	9	5.9	4.7967	987.6	0.01199	2.469	5.112412
H-65	F	9	6.7	5.4471	1128	0.01362	2.82	9.527273
H-42	M	9	5.6	4.5528	942.6	0.01138	2.3565	7.383732
H-67	F	10	7.1	5.7723	1275.9	0.01443	3.18975	8.19052
H-1	M	11	4.7	3.8211	703.2	0.00955	1.758	12.07609
H-58	M	11	7.1	5.7723	1233.6	0.01443	3.084	7.383732
H-75	F	11	7.7	6.2601	1538.4	0.01565	3.846	8.19052
H-40	F	11	7.7	6.2601	1538.4	0.01565	3.846	12.07609
H-10	M	12	4.7	3.8211	693.3	0.00955	1.73325	10.49154

148

|							
H-53	F	12	6	4.878	1254.9	0.0122	3.13725	9.803089
H-31	F	12	7.4	6.0162	1043.57	0.01504	2.608925	8.088525
H-19	M	13	15.7	12.7641	3200	0.03191	8	7.835521
H-72	F	15	12.3	9.9999	2794.4	0.025	6.986	6.780421
H-25	F	15	9.2	7.4796	1389	0.0187	3.4725	8.90806
H-37	F	15	12.3	9.9999	2794.4	0.025	6.986	11.21225
H-73	F	16	16	13.008	2634.9	0.03252	6.58725	6.798883
H-38	F	16	16	13.008	2634.9	0.03252	6.58725	5.776786
MEAN		8.55	6.8575	5.5751475	1103.43375	0.0139375	2.758584375	8.40250205
MEDIAN		8	5.65	4.59345	911.9	0.011485	2.27975	8.0797125
MAX		16	16	13.008	3200	0.03252	8	12.07609
MIN		2	3	2.439	294.9	0.0061	0.73725	5.112412
¾ Q		11	7.325	5.955225	1249.575	0.0148875	3.1239375	9.527273

APPENDIX G

MEASURED CHEST CT DOSE OPTIMISATION PARAMETERS

Chest Dose Optimisation

| ID	Sex	AGE	CTDIvol	CTDI$_W$	DLP	Organ Dose	Effective Dose	SNR2
	M/F	Y	mGy	mGy	mGy-cm	mSv	mSv	
CH-41	F	1	4.7	3.8211	234.4	0.06496	3.9848	9.041828
CH-74	M	2	6.2	5.0406	364.8	0.08569	6.2016	6.73003
CH-33	M	5	4.7	3.8211	759	0.06496	12.903	7.375546
CH-29	M	5	4.7	3.8211	658.89	0.06496	11.20113	8.869666
CH-71	F	2	4.7	3.8211	234.4	0.06496	3.9848	10.01709
CH-23	F	4	4.5	3.6585	211.3	0.06219	3.5921	7.747962
CH-33	F	3	4.2	3.4146	201.2	0.05805	3.4204	5.961563
CH-34	M	2	4.3	3.4959	195	0.05943	3.315	9.041828
CH22	M	4	4.2	3.4146	200.1	0.05805	3.4017	6.73003
CH11	F	3	52	42.276	365.2	0.71869	6.2084	7.375546
CH-32	M	6	5	4.065	792.6	0.06911	13.4742	7.190947
CH-44	F	6	4.8	3.9024	754.8	0.06634	12.8316	7.374534
CH-47	F	6	4.9	3.9837	793.8	0.06772	13.4946	8.869666
CH-60	F	6	4.9	3.9837	745.2	0.06772	12.6684	6.358374
CH-81	M	7	6.2	5.0406	572.6	0.08569	9.7342	10.01709
CH-50	F	7	4.7	3.8211	937.6	0.06496	15.9392	8.869666
CH-43	M	8	4.9	3.9837	757.2	0.06772	12.8724	6.358374
CH-5	F	9	6.7	5.4471	1128	0.0926	19.176	10.01709
CH-49	F	9	4.7	3.8211	1590.9	0.06496	27.0453	7.747962
CH-78	M	9	5.6	4.5528	942.6	0.0774	16.0242	5.961563
CH-57	M	9	4.9	3.9837	910.8	0.06772	15.4836	9.041828
CH-46	M	10	5.2	4.2276	1283.2	0.07187	21.8144	6.73003
CH-54	F	10	5.6	4.5528	850.2	0.0774	14.4534	7.375546
CH-52	F	10	5.7	4.6341	1026.3	0.07878	17.4471	7.190947
CH-27	F	11	7.1	5.7723	1065.6	0.09813	18.1152	5.961563
CH-20	M	12	9.7	7.8861	2127.2	0.13406	36.1624	9.041828
CH-21	F	12	8.1	6.5853	1215.9	0.11195	20.6703	8.869666
CH-8	F	13	5.7	4.6341	1331.1	0.07878	22.6287	6.358374
CH-11	F	13	13.5	10.9755	2975.6	0.18658	50.5852	10.01709
CH-14	F	14	8.7	7.0731	1413.9	0.12024	24.0363	8.869666
CH-16	F	15	5.6	4.5528	2114.89	0.0774	35.95313	6.358374
CH-2	F	16	4.7	3.8211	1311.5	0.06496	22.2955	10.01709

150

CH-12	M	16	4.7	3.8211	1256.4	0.06496	21.3588	9.066467
CH-23	M	12	4.7	3.8211	930.5	0.06496	15.8185	12.7731
CH-11	M	14	6.7	5.4471	1123.2	0.0926	19.0944	5.293263
CH-08	M	13	6.7	5.4471	1213.4	0.0926	20.6278	6.214432
CH-90	F	15	4.7	3.8211	885.6	0.06496	15.0552	5.880402
CH-45	F	16	6.7	5.4471	1122.4	0.0926	19.0808	4.733674
CH-44	M	11	6.9	5.6097	1232.5	0.09536	20.9525	8.971429
CH-32	M	12	7.1	5.7723	1324.6	0.09813	22.5182	9.027092
MEAN		8.95	6.9825	5.676773	978.8595	0.096505	16.64061	7.84677715
MEDIAN		9	5.1	4.1463	934.05	0.07049	15.87885	7.375546
MAX		16	52	42.276	2975.6	0.71869	50.5852	12.7731
MIN		1	4.2	3.4146	195	0.05805	3.315	5.293263
¾ Q		12.75	6.7	5.4471	1250.425	0.0926	21.25723	9.038144

151
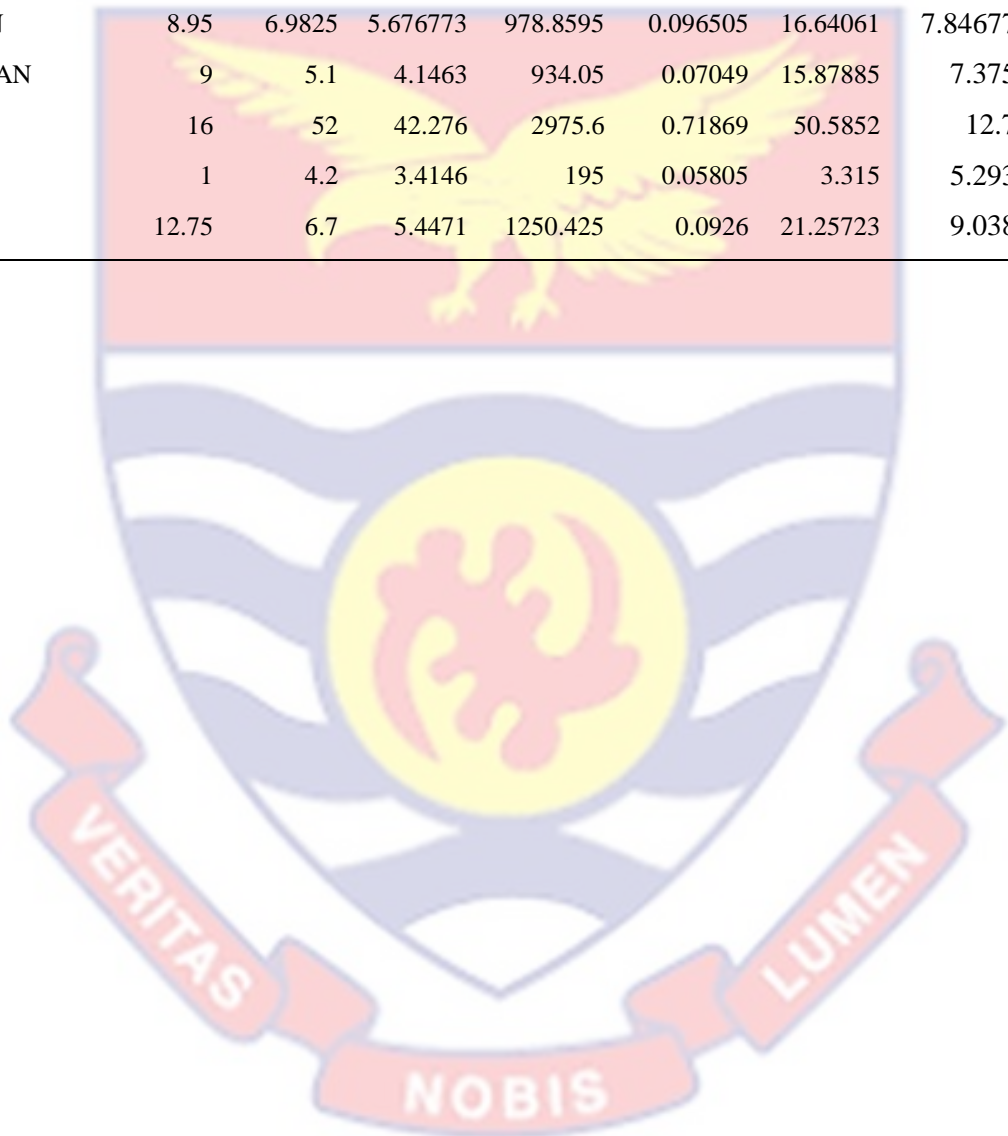
APPENDIX H

MEASURED ABDOMINAL-PELVIS CT DOSE OPTIMISATION PARAMETERS

AP Dose Optimisation

ID	Sex	AGE	CTDIvol	CTDI$_W$	DLP	Organ Dose	Effective Dose	SNR3
	M/F	Y	mGy	mGy	mGy-cm	mSv	mSv	
AP-76	F	1	4.7	3.8211	234.4	0.05732	3.516	5.693352
AP-36	M	3	5.5	4.4715	294.9	0.06707	4.4235	5.773821
AP-13	M	4	5.3	4.3089	859.2	0.06463	12.888	5.525239
AP-22	M	1	4.7	3.8211	234.4	0.05732	3.516	6.025152
AP-66	F	2	4.7	3.8211	234.4	0.05732	3.516	8.57299
AP-55	F	2	4.7	3.8211	234.4	0.05732	3.516	5.786687
AP-43	F	4	5.5	4.4715	294.9	0.06707	4.4235	9.738104
AP-23	M	5	4.7	3.8211	234.4	0.05732	3.516	6.693352
AP-41	F	5	4.7	3.8211	234.4	0.05732	3.516	5.773821
AP-32	M	4	5.5	4.4715	294.9	0.06707	4.4235	5.525239
AP-34	M	3	5.5	4.4715	294.9	0.06707	4.4235	6.253671
AP-23	F	3	5.1	4.102	313.2	0.061529	4.698	7.971443
AP-33	F	3	4.7	3.8211	234.4	0.057317	3.516	6.025152
AP-44	M	5	5.5	4.4715	859.2	0.067073	12.888	7.847047
AP-40	M	1	4.7	3.8211	234.4	0.057317	3.516	8.57299
AP-11	M	4	5.5	4.4715	294.9	0.067073	4.4235	6.025152
AP-6	M	6	3	2.439	682.8	0.03659	10.242	5.847047
AP-17	F	6	5.1	4.1463	524.8	0.06219	7.872	8.57299
AP-45	F	6	4.9	3.9837	744	0.05976	11.16	5.786687
AP-80	F	6	4.8	3.9024	754.8	0.05854	11.322	9.738104
AP-69	F	6	4.8	3.9024	765.88	0.05854	11.4882	4.693352
AP-26	M	7	4.9	3.9837	808.5	0.05976	12.1275	5.773821
AP-55	F	7	4.7	3.8211	703.2	0.05732	10.548	5.525239
AP-24	F	8	6.3	5.1219	988.9	0.07683	14.8335	14.253671
AP-79	M	8	4.9	3.9837	757.2	0.05976	11.358	9.738104
AP-7	F	10	7.1	5.7723	1275.9	0.08658	19.1385	7.693352
AP-22	F	10	6.5	5.2845	1038.6	0.07927	15.579	6.025152
AP-6	M	12	4.2	3.4146	364.8	0.00854	0.912	9.847047
AP-17	F	13	3.7	3.0081	468.8	0.00752	1.172	8.57299
AP-45	F	13	3.7	3.0081	468.8	0.00752	1.172	6.025152
AP-80	M	13	3.6	2.9268	294.9	0.00732	0.73725	6.847047

152

|							
AP-69	M	15	5.2	4.2276	597.6	0.01057	1.494	8.57299
AP-26	F	15	4.1	3.3333	935.4	0.00833	2.3385	12.993186
AP-55	M	15	3.2	2.6016	597.6	0.0065	1.494	7.877347
AP-24	M	15	3.6	2.9268	759	0.00732	1.8975	4.976665
AP-79	F	15	3.7	3.0081	549.6	0.00752	1.374	12.695535
AP-7	F	15	3.5	2.8455	549.6	0.00711	1.374	5.722905
AP-55	F	16	3.6	2.9268	912.4	0.00732	2.281	5.708105
AP-24	M	16	4.1	3.3333	915.3	0.00833	2.28825	5.442326
AP-79	M	16	4.2	3.4146	794.1	0.00854	1.98525	5.496524
Mean		7.975	4.71	3.828123	565.8445	0.044618	5.922699	7.4283373
Median		6	4.7	3.8211	549.6	0.05732	3.516	6.1394115
Max		16	7.1	5.7723	1275.9	0.08658	19.1385	14.253671
Min		1	4.7	3.8211	234.4	0.05732	3.516	5.442326
¾ Q		13	5.275	4.288575	787.045	0.06402	11.007	8.57299
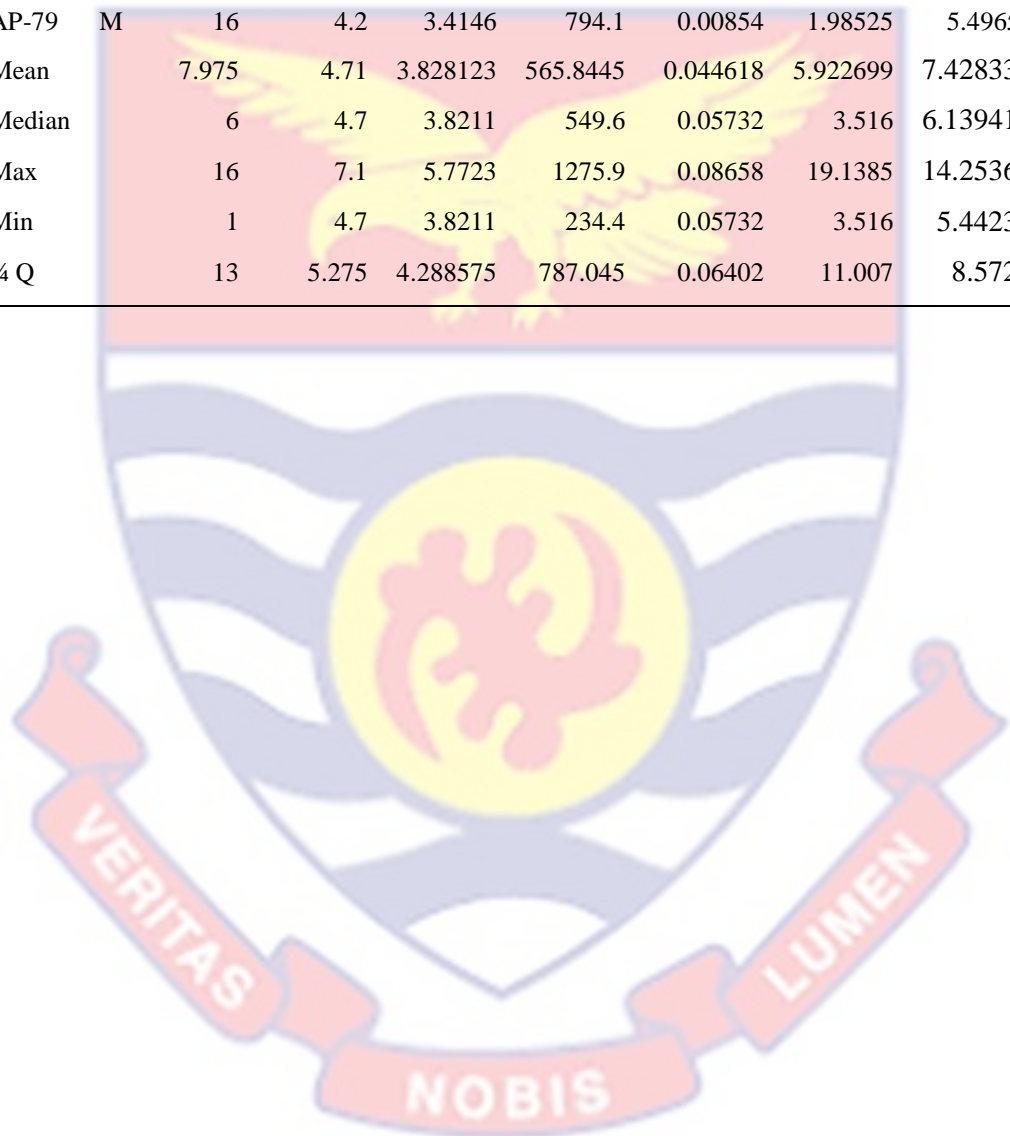
APPENDIX I

MEASURED MALE RISK INCIDENCE PARAMETERS FOR HEAD

			MALE RISK INCIDENCE			
ID	AGE	Effective Dose	LAR	Tube Current	Tube Voltage	RISK
	Y	mSv		mAs	KVP	%
H-39	2	0.912	2264.2	40	80	0.020649504
H-3	3	1.172	2114.8	40	100	0.024785456
H-63	3	1.172	2114.8	50	100	0.024785456
H-71	3	0.73725	2114.8	40	80	0.015591363
H-4	5	1.494	1816	40	100	0.02713104
H-12	5	2.3385	1816	41	120	0.04246716
H-64	5	1.494	1816	40	100	0.02713104
H-68	5	1.8975	1816	40	120	0.0344586
H-35	5	1.374	1816	40	100	0.02495184
H-70	5	1.374	1816	46	100	0.02495184
H-66	6	1.707	1741.8	40	120	0.029732526
H-30	6	1.8675	1741.8	40	120	0.032528115
H-51	6	2.13225	1741.8	40	120	0.037139531
H-34	6	1.9147	1741.8	41	120	0.033350245
H-9	7	2.2785	1667.6	56	120	0.037996266
H-18	7	2.3565	1667.6	40	120	0.039296994
H-59	7	1.4315	1667.6	40	100	0.023871694
H-61	8	2.281	1593.4	40	120	0.036345454
H-62	8	2.28825	1593.4	40	120	0.036460976
H-28	8	1.98525	1593.4	40	120	0.031632974
H-48	8	2.06225	1593.4	40	120	0.032859892
H-56	8	2.13825	1593.4	67	120	0.034070876
H-15	9	2.4675	1519.2	50	120	0.03748626
H-23	9	2.469	1519.2	40	120	0.037509048
H-65	9	2.82	1519.2	46	120	0.04284144
H-42	9	2.3565	1519.2	48	120	0.035799948
H-67	10	3.18975	1445	40	120	0.046091888

154

H-1	11	1.758	1392.4	40	100	0.024478392
H-58	11	3.084	1392.4	80	120	0.042941616
H-75	11	3.846	1392.4	47	120	0.053551704
H-40	11	3.846	1392.4	57	120	0.053551704
H-10	12	1.73325	1339.8	40	100	0.023222084
H-53	12	3.13725	1339.8	40	120	0.042032876
H-31	12	2.608925	1339.8	40	120	0.034954377
H-19	13	8	1287.2	42	120	0.102976
H-72	15	6.986	1182	46	120	0.08257452
H-25	15	3.4725	1182	40	120	0.04104495
H-37	15	6.986	1182	47	120	0.08257452
H-73	16	6.58725	1141	40	120	0.075160523
H-38	16	6.58725	1141	45	120	0.075160523
MEAN	8.55	2.758584375	1591.69	44.225	113.5	0.04015353
MEDIAN	8	2.27975	1593.4	40	120	0.036072701
MAX	16	8	2264.2	80	120	0.102976
MIN	2	0.73725	1141	40	80	0.015591363
Q. ¾	11	3.1239375	1797.45	46	120	0.04274787
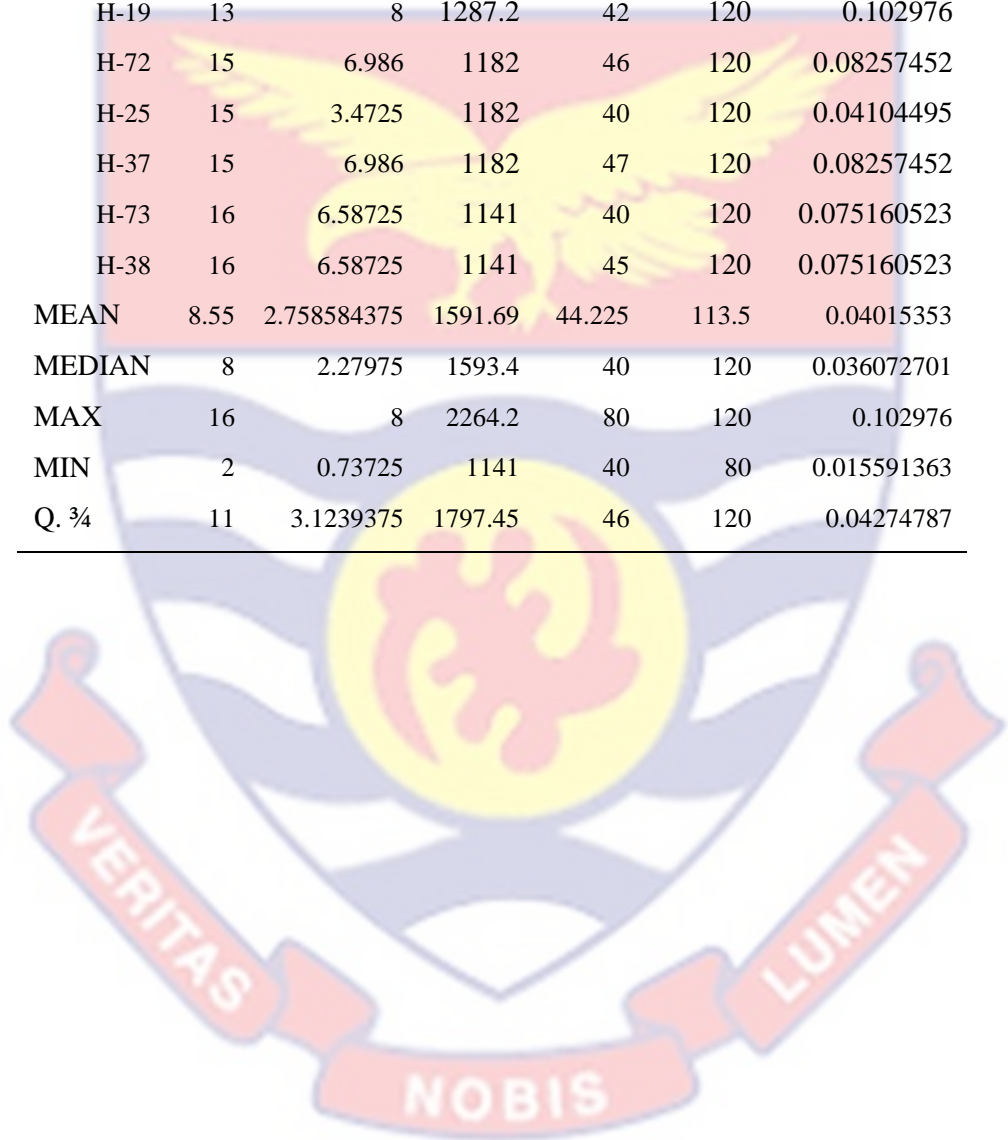
APPENDIX J

MEASURED FEMALE RISK INCIDENCE PARAMETERS FOR HEAD

ID	AGE Y	Effective Dose mSv	LAR	Tube Current Mas	Tube Voltage KVP	RISK %
			RISK INCIDENCE FEMALE			
H-39	2	0.912	4217	40	80	0.03845904
H-3	3	1.172	3937	40	100	0.04614164
H-63	3	1.172	3937	50	100	0.04614164
H-71	3	0.73725	3937	40	80	0.029025533
H-4	5	1.494	3377	40	100	0.05045238
H-12	5	2.3385	3377	41	120	0.078971145
H-64	5	1.494	3377	40	100	0.05045238
H-68	5	1.8975	3377	40	120	0.064078575
H-35	5	1.374	3377	40	100	0.04639998
H-70	5	1.374	3377	46	100	0.04639998
H-66	6	1.707	3223.8	40	120	0.055030266
H-30	6	1.8675	3223.8	40	120	0.060204465
H-51	6	2.13225	3223.8	40	120	0.068739476
H-34	6	1.9147	3223.8	41	120	0.061726099
H-9	7	2.2785	3070.6	56	120	0.069963621
H-18	7	2.3565	3070.6	40	120	0.072358689
H-59	7	1.4315	3070.6	40	100	0.043955639
H-61	8	2.281	2917.4	40	120	0.066545894
H-62	8	2.28825	2917.4	40	120	0.066757406
H-28	8	1.98525	2917.4	40	120	0.057917684
H-48	8	2.06225	2917.4	40	120	0.060164082
H-56	8	2.13825	2917.4	67	120	0.062381306
H-15	9	2.4675	2764.2	50	120	0.068206635
H-23	9	2.469	2764.2	40	120	0.068248098
H-65	9	2.82	2764.2	46	120	0.07795044
H-42	9	2.3565	2764.2	48	120	0.065138373
H-67	10	3.18975	2611	40	120	0.083284373

156

H-1	11	1.758	2501.6	40	100	0.043978128
H-58	11	3.084	2501.6	80	120	0.077149344
H-75	11	3.846	2501.6	47	120	0.096211536
H-40	11	3.846	2501.6	57	120	0.096211536
H-10	12	1.73325	2392.2	40	100	0.041462807
H-53	12	3.13725	2392.2	40	120	0.075049295
H-31	12	2.608925	2392.2	40	120	0.062410704
H-19	13	8	2282.8	42	120	0.182624
H-72	15	6.986	2064	46	120	0.14419104
H-25	15	3.4725	2064	40	120	0.0716724
H-37	15	6.986	2064	47	120	0.14419104
H-73	16	6.58725	1980.4	40	120	0.130453899
H-38	16	6.58725	1980.4	45	120	0.130453899
MEAN	8.55	2.758584375	2906.76	44.225	112.5	0.072528862
MEDIAN	8	2.27975	2917.4	40	120	0.065842134
MAX	16	8	4217	80	120	0.182624
MIN	2	0.73725	1980.4	40	80	0.029025533
Q. ¾	11	3.1239375	3338.7	46	120	0.077750166

157

APPENDIX K1

MEASURED MALE RISK MORTALITY PARAMETERS FOR HEAD

			RISK MORALITY MALE			
ID	AGE	Effective Dose	LAR	Tube Current	Tube Voltage	RISK %
	Y	mSv		mAs	KVP	
H-39	2	0.912	1000.2	40	80	0.009121824
H-3	3	1.172	950.8	40	100	0.011143376
H-63	3	1.172	950.8	50	100	0.011143376
H-71	3	0.73725	950.8	40	80	0.007009773
H-4	5	1.494	852	40	100	0.01272888
H-12	5	2.3385	852	41	120	0.01992402
H-64	5	1.494	852	40	100	0.01272888
H-68	5	1.8975	852	40	120	0.0161667
H-35	5	1.374	852	40	100	0.01170648
H-70	5	1.374	852	46	100	0.01170648
H-66	6	1.707	824	40	120	0.01406568
H-30	6	1.8675	824	40	120	0.0153882
H-51	6	2.13225	824	40	120	0.01756974
H-34	6	1.9147	824	41	120	0.015777128
H-9	7	2.2785	796	56	120	0.01813686
H-18	7	2.3565	796	40	120	0.01875774
H-59	7	1.4315	796	40	100	0.01139474
H-61	8	2.281	768	40	120	0.01751808
H-62	8	2.28825	768	40	120	0.01757376
H-28	8	1.98525	768	40	120	0.01524672
H-48	8	2.06225	768	40	120	0.01583808
H-56	8	2.13825	768	67	120	0.01642176
H-15	9	2.4675	740	50	120	0.0182595
H-23	9	2.469	740	40	120	0.0182706
H-65	9	2.82	740	46	120	0.020868
H-42	9	2.3565	740	48	120	0.0174381
H-67	10	3.18975	712	40	120	0.02271102
H-1	11	1.758	690.2	40	100	0.012133716

158

H-58	11	3.084	690.2	80	120	0.021285768
H-75	11	3.846	690.2	47	120	0.026545092
H-40	11	3.846	690.2	57	120	0.026545092
H-10	12	1.73325	668.4	40	100	0.011585043
H-53	12	3.13725	668.4	40	120	0.020969379
H-31	12	2.608925	668.4	40	120	0.017438055
H-19	13	8	646.6	42	120	0.051728
H-72	15	6.986	603	46	120	0.04212558
H-25	15	3.4725	603	40	120	0.020939175
H-37	15	6.986	603	47	120	0.04212558
H-73	16	6.58725	584.6	40	120	0.038509064
H-38	16	6.58725	584.6	45	120	0.038509064
MEAN	8.55	2.758584375	763.785	44.225	113.3	0.019626353
MEDIAN	8	2.27975	768	40	120	0.01747809
MAX	16	8	1000.2	80	120	0.051728
MIN	2	0.73725	584.6	40	80	0.007009773
Q. ¾	11	3.1239375	845	46	120	0.020961828

159

APPENDIX K2

MEASURED FEMALE RISK MORTALITY PARAMETERS FOR HEAD

			RISK MORALITY FEMALE			
ID	AGE	Effective Dose	LAR	Tube Current	Tube Voltage	RISK %
	Y	mSv		mAs	KVP	
H-39	2	0.912	1600.4	40	80	0.014595648
H-3	3	1.172	1515.8	40	100	0.017765176
H-63	3	1.172	1515.8	50	100	0.017765176
H-71	3	0.73725	1515.8	40	80	0.011175236
H-4	5	1.494	1347	40	100	0.02012418
H-12	5	2.3385	1347	41	120	0.031499595
H-64	5	1.494	1347	40	100	0.02012418
H-68	5	1.8975	1347	40	120	0.025559325
H-35	5	1.374	1347	40	100	0.01850778
H-70	5	1.374	1347	46	100	0.01850778
H-66	6	1.707	1298.4	40	120	0.022163688
H-30	6	1.8675	1298.4	40	120	0.02424762
H-51	6	2.13225	1298.4	40	120	0.027685134
H-34	6	1.9147	1298.4	41	120	0.024860465
H-9	7	2.2785	1249.8	56	120	0.028476693
H-18	7	2.3565	1249.8	40	120	0.029451537
H-59	7	1.4315	1249.8	40	100	0.017890887
H-61	8	2.281	1201.2	40	120	0.027399372
H-62	8	2.28825	1201.2	40	120	0.027486459
H-28	8	1.98525	1201.2	40	120	0.023846823
H-48	8	2.06225	1201.2	40	120	0.024771747
H-56	8	2.13825	1201.2	67	120	0.025684659
H-15	9	2.4675	1152.6	50	120	0.028440405
H-23	9	2.469	1152.6	40	120	0.028457694
H-65	9	2.82	1152.6	46	120	0.03250332
H-42	9	2.3565	1152.6	48	120	0.027161019
H-67	10	3.18975	1104	40	120	0.03521484

160

H-1	11	1.758	1066	40	100	0.01874028
H-58	11	3.084	1066	80	120	0.03287544
H-75	11	3.846	1066	47	120	0.04099836
H-40	11	3.846	1066	57	120	0.04099836
H-10	12	1.73325	1028	40	100	0.01781781
H-53	12	3.13725	1028	40	120	0.03225093
H-31	12	2.608925	1028	40	120	0.026819749
H-19	13	8	990	42	120	0.0792
H-72	15	6.986	914	46	120	0.06385204
H-25	15	3.4725	914	40	120	0.03173865
H-37	15	6.986	914	47	120	0.06385204
H-73	16	6.58725	883.6	40	120	0.058204941
H-38	16	6.58725	883.6	45	120	0.058204941
MEAN	8.55	2.758584375	1193.51	44.225	122.5	0.030422999
MEDIAN	8	2.27975	1201.2	40	120	0.027280196
MAX	16	8	1600.4	80	120	0.0792
MIN	2	0.73725	883.6	40	80	0.011175236
Q. ¾	11	3.1239375	1334.85	46	120	0.032440223

APPENDIX L

MEASURED MALE RISK INCIDENCE PARAMETERS FOR CHEST

RISK INCIDENCE MALE

ID	AGE Y	Effective Dose mSv	LAR	Tube Current mAs	Tube Voltage KVP	RISK %
CH-41	1	3.9848	2413.6	40	80	0.096177133
CH-74	2	6.2016	2264.2	40	100	0.140416627
CH-33	2	3.9848	2264.2	50	100	0.090223842
CH-29	2	3.315	2264.2	40	80	0.07505823
CH-71	3	3.4204	2114.8	40	100	0.072334619
CH-23	3	6.2084	211.8	41	120	0.013149391
CH-33	4	3.5921	1965.4	40	100	0.070599133
CH-34	4	3.4017	1965.5	40	120	0.066860414
CH22	5	12.903	1816	40	100	0.23431848
CH11	5	11.20113	1816	46	100	0.203412521
CH-32	6	13.4742	1741.8	40	120	0.234693616
CH-44	6	12.8316	1741.8	40	120	0.223500809
CH-47	6	13.4946	1741.8	40	120	0.235048943
CH-60	6	12.6684	1741.8	41	120	0.220658191
CH-81	7	9.7342	1667.6	56	120	0.162327519
CH-50	7	15.9392	1667.6	40	120	0.265802099
CH-43	8	12.8724	1593.4	40	100	0.205108822
CH-5	9	19.176	1519.2	40	120	0.291321792
CH-49	9	27.0453	1519.2	40	120	0.410872198
CH-78	9	16.0242	1519.2	40	120	0.243439646
CH-57	9	15.4836	1519.2	40	120	0.235226851
CH-46	10	21.8144	1445	67	120	0.31521808
CH-54	10	14.4534	1445	50	120	0.20885163
CH-52	10	17.4471	1445	40	120	0.252110595
CH-27	11	18.1152	1392.5	46	120	0.25225416
CH-20	11	20.9525	1392.5	48	120	0.291763563
CH-21	12	36.1624	1339.8	40	120	0.484503835
CH-8	12	20.6703	1339.8	40	100	0.276940679

162

CH-11	12	15.8185	1339.8	80	120	0.211936263
CH-14	12	22.5182	1339.8	47	120	0.301698844
CH-16	13	22.6287	1287.2	57	120	0.291276626
CH-2	13	50.5852	1287.2	40	100	0.651132694
CH-12	13	20.6278	1287.2	40	120	0.265521042
CH-23	14	24.0363	1234.6	40	120	0.29675216
CH-11	14	19.0944	1234.6	42	120	0.235739462
CH-08	15	35.95313	1182	46	120	0.424965997
CH-90	15	15.0552	1182	40	120	0.177952464
CH-45	16	22.2955	1141	47	120	0.254391655
CH-44	16	21.3588	1141	40	120	0.243703908
CH-32	16	19.0808	1141	45	120	0.217711928
MEAN	8.95	16.6406115	1541.6325	44.225	113.5	0.236124412
MEDIAN	9	15.87885	1482.1	40	120	0.235137897
MAX	16	50.5852	2413.6	80	120	0.651132694
MIN	1	3.315	211.8	40	80	0.013149391
Q. ¾	12.75	21.257225	1741.8	46	120	0.28769264

163

APPENDIX M

MEASURED FEMALE RISK INCIDENCE PARAMETERS FOR CHEST

RISK INCIDENCE FEMALE

ID	AGE Y	Effective Dose mSv	LAR	Tube Current mAs	Tube Voltage KVP	RISK %
CH-41	1	3.9848	4497	40	80	0.179196456
CH-74	2	6.2016	4217	40	100	0.261521472
CH-33	2	3.9848	4217	50	100	0.168039016
CH-29	2	3.315	4217	40	80	0.13979355
CH-71	3	3.4204	3937	40	100	0.134661148
CH-23	3	6.2084	3937	41	120	0.244424708
CH-33	4	3.5921	3657	40	100	0.131363097
CH-34	4	3.4017	3657	40	120	0.124400169
CH22	5	12.903	3377	40	100	0.43573431
CH11	5	11.20113	3377	46	100	0.37826216
CH-32	6	13.4742	3223.8	40	120	0.43438126
CH-44	6	12.8316	3223.8	40	120	0.413665121
CH-47	6	13.4946	3223.8	40	120	0.435038915
CH-60	6	12.6684	3223.8	41	120	0.408403879
CH-81	7	9.7342	3070.6	56	120	0.298898345
CH-50	7	15.9392	3070.6	40	120	0.489429075
CH-43	8	12.8724	2917.4	40	100	0.375539398
CH-5	9	19.176	2764.2	40	120	0.530062992
CH-49	9	27.0453	2764.2	40	120	0.747586183
CH-78	9	16.0242	2764.2	40	120	0.442940936
CH-57	9	15.4836	2764.2	40	120	0.427997671
CH-46	10	21.8144	2611	67	120	0.569573984
CH-54	10	14.4534	2611	50	120	0.377378274
CH-52	10	17.4471	2611	40	120	0.455543781
CH-27	11	18.1152	2501.6	46	120	0.453169843
CH-20	11	20.9525	2501.6	48	120	0.52414774
CH-21	12	36.1624	2392.2	40	120	0.865076933
CH-8	12	20.6703	2392.2	40	100	0.494474917
CH-11	12	15.8185	2392.2	80	120	0.378410157

164

CH-14	12	22.5182	2392.2	47	120	0.53868038
CH-16	13	22.6287	2282.8	57	120	0.516567964
CH-2	13	50.5852	2282.8	40	100	1.154758946
CH-12	13	20.6278	2282.8	40	120	0.470891418
CH-23	14	24.0363	2173.4	40	120	0.522404944
CH-11	14	19.0944	2173.4	42	120	0.41499769
CH-08	15	35.95313	2064	46	120	0.742072603
CH-90	15	15.0552	2064	40	120	0.310739328
CH-45	16	22.2955	1980.4	47	120	0.441540082
CH-44	16	21.3588	1980.4	40	120	0.422989675
CH-32	16	19.0808	1980.4	45	120	0.377876163
MEAN	8.95	16.6406115	2894.25	44.225	112.5	0.430815867
MEDIAN	9	15.87885	2764.2	40	120	0.431189465
MAX	16	50.5852	4497	80	120	1.154758946
MIN	1	3.315	1980.4	40	80	0.124400169
Q. ¾	12.75	21.257225	3338.7	46	120	0.511044702

165

APPENDIX N

MEASURED MALE RISK MORTALITY PARAMETERS FOR CHEST

			RISK MORALITY MALE			
ID	AGE	Effective Dose	LAR	Tube Current	Tube Voltage	RISK %
	Y	mSv		mAs	KVP	
CH-41	1	3.9848	1049.6	40	80	0.041824461
CH-74	2	6.2016	1000.2	40	100	0.062028403
CH-33	2	3.9848	1000.2	50	100	0.03985597
CH-29	2	3.315	1000.2	40	80	0.03315663
CH-71	3	3.4204	950.8	40	100	0.032521163
CH-23	3	6.2084	950.8	41	120	0.059029467
CH-33	4	3.5921	901.4	40	100	0.032379189
CH-34	4	3.4017	901.4	40	120	0.030662924
CH22	5	12.903	852	40	100	0.10993356
CH11	5	11.20113	852	46	100	0.095433628
CH-32	6	13.4742	824	40	120	0.111027408
CH-44	6	12.8316	824	40	120	0.105732384
CH-47	6	13.4946	824	40	120	0.111195504
CH-60	6	12.6684	824	41	120	0.104387616
CH-81	7	9.7342	796	56	120	0.077484232
CH-50	7	15.9392	796	40	120	0.126876032
CH-43	8	12.8724	768	40	100	0.098860032
CH-5	9	19.176	740	40	120	0.1419024
CH-49	9	27.0453	740	40	120	0.20013522
CH-78	9	16.0242	740	40	120	0.11857908
CH-57	9	15.4836	740	40	120	0.11457864
CH-46	10	21.8144	712	67	120	0.155318528
CH-54	10	14.4534	712	50	120	0.102908208
CH-52	10	17.4471	712	40	120	0.124223352
CH-27	11	18.1152	690.2	46	120	0.12503111
CH-20	11	20.9525	690.2	48	120	0.144614155
CH-21	12	36.1624	668.4	40	120	0.241709482
CH-8	12	20.6703	668.4	40	100	0.138160285

166

CH-11	12	15.8185	668.4	80	120	0.105730854
CH-14	12	22.5182	668.4	47	120	0.150511649
CH-16	13	22.6287	646.6	57	120	0.146317174
CH-2	13	50.5852	646.6	40	100	0.327083903
CH-12	13	20.6278	646.6	40	120	0.133379355
CH-23	14	24.0363	624.8	40	120	0.150178802
CH-11	14	19.0944	624.8	42	120	0.119301811
CH-08	15	35.95313	603	46	120	0.216797374
CH-90	15	15.0552	603	40	120	0.090782856
CH-45	16	22.2955	584.6	47	120	0.130339493
CH-44	16	21.3588	584.6	40	120	0.124863545
CH-32	16	19.0808	584.6	45	120	0.111546357
MEAN	8.95	16.6406115	760.345	44.225	113.5	0.117159556
MEDIAN	9	15.87885	740	40	120	0.113062498
MAX	16	50.5852	1049.6	80	120	0.327083903
MIN	1	3.315	584.6	40	80	0.030662924
Q. ¾	12.75	21.257225	845	46	120	0.140966871

167

APPENDIX O

MEASURED FEMALE RISK MORTALITY PARAMETERS FOR CHEST

|			RISK MORALITY FEMALE			
ID	AGE Y	Effective Dose mSv	LAR	Tube Current mAs	Tube Voltage KVP	RISK %
CH-41	1	3.9848	1685.4	40	80	0.067159819
CH-74	2	6.2016	1600.4	40	100	0.099250406
CH-33	2	3.9848	1600.4	50	100	0.063772739
CH-29	2	3.315	1600.4	40	80	0.05305326
CH-71	3	3.4204	1515.8	40	100	0.051846423
CH-23	3	6.2084	1515.8	41	120	0.094106927
CH-33	4	3.5921	1431.2	40	100	0.051410135
CH-34	4	3.4017	1431.2	40	120	0.04868513
CH22	5	12.903	1347	40	100	0.17380341
CH11	5	11.20113	1347	46	100	0.150879221
CH-32	6	13.4742	1298.4	40	120	0.174949013
CH-44	6	12.8316	1298.4	40	120	0.166605494
CH-47	6	13.4946	1298.4	40	120	0.175213886
CH-60	6	12.6684	1298.4	41	120	0.164486506
CH-81	7	9.7342	1249.8	56	120	0.121658032
CH-50	7	15.9392	1249.8	40	120	0.199208122
CH-43	8	12.8724	1201.2	40	100	0.154623269
CH-5	9	19.176	1152.6	40	120	0.221022576
CH-49	9	27.0453	1152.6	40	120	0.311724128
CH-78	9	16.0242	1152.6	40	120	0.184694929
CH-57	9	15.4836	1152.6	40	120	0.178463974
CH-46	10	21.8144	1104	67	120	0.240830976
CH-54	10	14.4534	1104	50	120	0.159565536
CH-52	10	17.4471	1104	40	120	0.192615984
CH-27	11	18.1152	1066	46	120	0.193108032
CH-20	11	20.9525	1066	48	120	0.22335365
CH-21	12	36.1624	1028	40	120	0.371749472
CH-8	12	20.6703	1028	40	100	0.212490684

168

CH-11	12	15.8185	1028	80	120	0.16261418
CH-14	12	22.5182	1028	47	120	0.231487096
CH-16	13	22.6287	990	57	120	0.22402413
CH-2	13	50.5852	990	40	100	0.50079348
CH-12	13	20.6278	990	40	120	0.20421522
CH-23	14	24.0363	952	40	120	0.228825576
CH-11	14	19.0944	952	42	120	0.181778688
CH-08	15	35.95313	914	46	120	0.328611608
CH-90	15	15.0552	914	40	120	0.137604528
CH-45	16	22.2955	883.6	47	120	0.197003038
CH-44	16	21.3588	883.6	40	120	0.188726357
CH-32	16	19.0808	883.6	45	120	0.168597949
MEAN	8.95	16.6406115	1187.205	44.225	112.5	0.18136534
MEDIAN	9	15.87885	1152.6	40	120	0.17683893
MAX	16	50.5852	1685.4	80	120	0.50079348
MIN	1	3.315	883.6	40	80	0.04868513
Q. ¾	12.75	21.257225	1334.85	46	120	0.218889603

169

APPENDIX P

MEASURED MALE RISK INCIDENCE PARAMETERS FOR ABDOMINAL-PELVIS

			RISK INCIDENCE MALE			
ID	AGE	Effective Dose	LAR	Tube Current	Tube Voltage	RISK %
	Y	mSv		mAs	KVP	
AP-76	1	3.516	2413.6	40	80	0.084862176
AP-36	3	4.4235	2114.8	40	100	0.093548178
AP-13	4	12.888	1965.4	50	100	0.253300752
AP-22	1	3.516	2413.6	40	80	0.084862176
AP-66	2	3.516	2264.2	40	100	0.079609272
AP-55	2	3.516	2264.2	41	120	0.079609272
AP-43	4	4.4235	1965.4	40	100	0.086939469
AP-23	5	3.516	1816	40	120	0.06385056
AP-41	5	3.516	1816	40	100	0.06385056
AP-32	4	4.4235	1965.4	46	100	0.086939469
AP-34	3	4.4235	2114.8	40	120	0.093548178
AP-23	3	4.698	2114.8	40	120	0.099353304
AP-33	3	3.516	2114.8	40	120	0.074356368
AP-44	5	12.888	1816	41	120	0.23404608
AP-40	1	3.516	2413.6	56	120	0.084862176
AP-11	4	4.4235	1965.4	40	120	0.086939469
AP-6	6	10.242	1741.8	40	100	0.178395156
AP-17	6	7.872	1741.8	40	120	0.137114496
AP-45	6	11.16	1741.8	40	120	0.19438488
AP-80	6	11.322	1741.8	40	120	0.197206596
AP-69	6	11.4882	1741.8	40	120	0.200101468
AP-26	7	12.1275	1667.6	67	120	0.20223819
AP-55	7	10.548	1667.6	50	120	0.175898448
AP-24	8	14.8335	1593.4	40	120	0.236356989
AP-79	8	11.358	1593.4	46	120	0.180978372
AP-7	10	19.1385	1445	48	120	0.276551325
AP-22	10	15.579	1445	40	120	0.22511655
AP-6	12	0.912	1339.8	40	100	0.012218976

170

AP-17	13	1.172	1287.2	80	120	0.015085984
AP-45	13	1.172	1287.2	47	120	0.015085984
AP-80	13	0.73725	1287.2	57	120	0.009489882
AP-69	15	1.494	1182	40	100	0.01765908
AP-26	15	2.3385	1182	40	120	0.02764107
AP-55	15	1.494	1182	40	120	0.01765908
AP-24	15	1.8975	1182	42	120	0.02242845
AP-79	15	1.374	1182	46	120	0.01624068
AP-7	15	1.374	1182	40	120	0.01624068
AP-55	16	2.281	1141	47	120	0.02602621
AP-24	16	2.28825	1141	40	120	0.026108933
AP-79	16	1.98525	1141	45	120	0.022651703
Mean	7.975	5.92269875	1684.385	44.225	113.5	0.102483916
Median	6	3.516	1741.8	40	120	0.084862176
Max	16	19.1385	2413.6	80	120	0.276551325
Min	1	0.73725	1141	40	80	0.009489882
¾ Q	13	11.007	1965.4	46	120	0.180332568
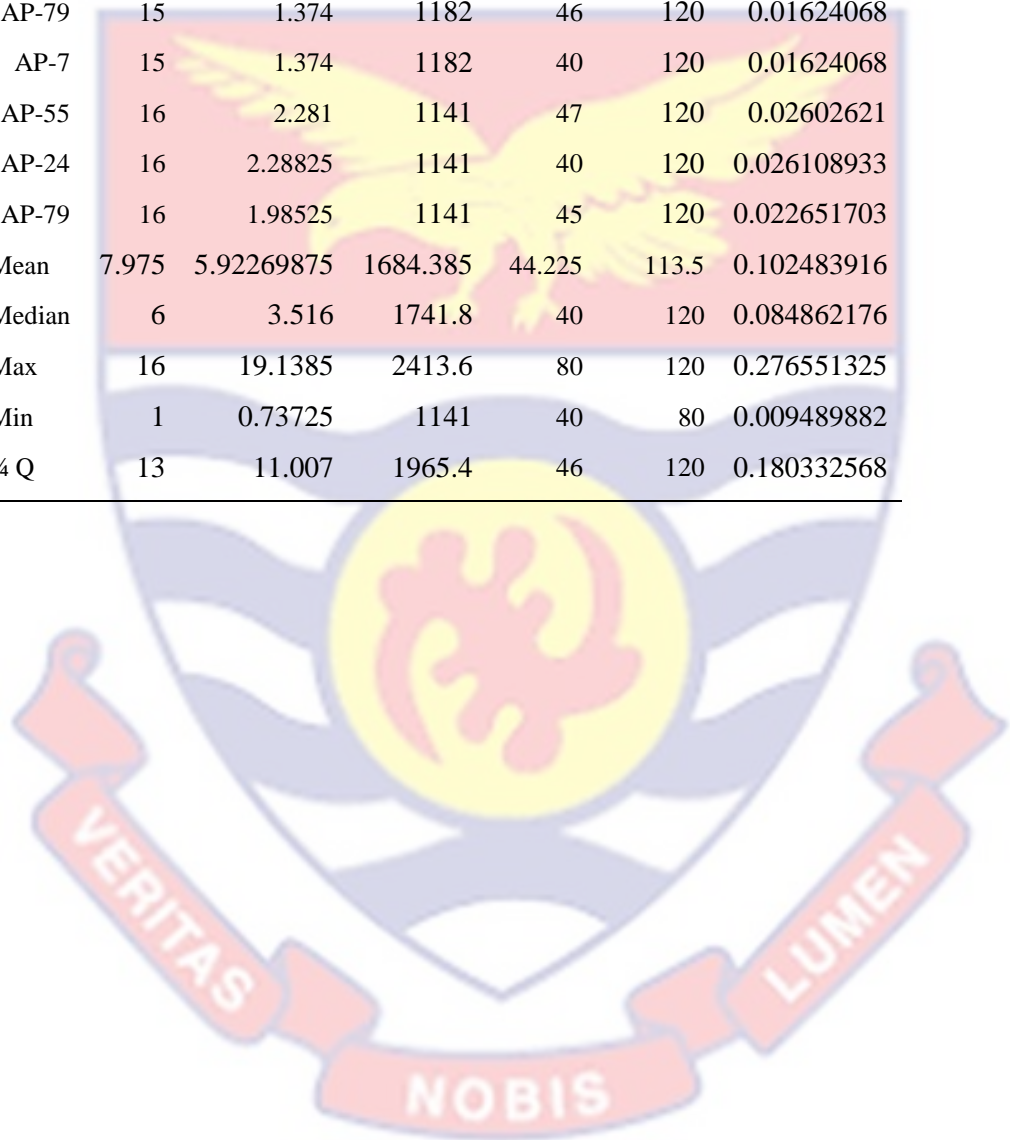
APPENDIX Q

MEASURED FEMALE RISK INCIDENCE PARAMETERS FOR ABDOMINAL-PELVIS

			RISK INCIDENDCE FEMALE			
ID	AGE	Effective Dose	LAR	Tube Current	Tube Voltage	RISK %
	Y	mSv		mAs	KVP	
AP-76	1	3.516	4497	40	80	0.15811452
AP-36	3	4.4235	3937	40	100	0.174153195
AP-13	4	12.888	3657	50	100	0.47131416
AP-22	1	3.516	4497	40	80	0.15811452
AP-66	2	3.516	4217	40	100	0.14826972
AP-55	2	3.516	4217	41	120	0.14826972
AP-43	4	4.4235	3657	40	100	0.161767395
AP-23	5	3.516	3377	40	120	0.11873532
AP-41	5	3.516	3377	40	100	0.11873532
AP-32	4	4.4235	3657	46	100	0.161767395
AP-34	3	4.4235	3937	40	120	0.174153195
AP-23	3	4.698	3937	40	120	0.18496026
AP-33	3	3.516	3937	40	120	0.13842492
AP-44	5	12.888	3377	41	120	0.43522776
AP-40	1	3.516	4497	56	120	0.15811452
AP-11	4	4.4235	3657	40	120	0.161767395
AP-6	6	10.242	3223.8	40	100	0.330181596
AP-17	6	7.872	3223.8	40	120	0.253777536
AP-45	6	11.16	3223.8	40	120	0.35977608
AP-80	6	11.322	3223.8	40	120	0.364998636
AP-69	6	11.4882	3223.8	40	120	0.370356592
AP-26	7	12.1275	3070.6	67	120	0.372387015
AP-55	7	10.548	3070.6	50	120	0.323886888
AP-24	8	14.8335	2917.4	40	120	0.432752529
AP-79	8	11.358	2917.4	46	120	0.331358292
AP-7	10	19.1385	2611	48	120	0.499706235
AP-22	10	15.579	2611	40	120	0.40676769
AP-6	12	0.912	2392.2	40	100	0.021816864

AP-17	13	1.172	2282.8	80	120	0.026754416
AP-45	13	1.172	2282.8	47	120	0.026754416
AP-80	13	0.73725	2282.8	57	120	0.016829943
AP-69	15	1.494	2064	40	100	0.03083616
AP-26	15	2.3385	2064	40	120	0.04826664
AP-55	15	1.494	2064	40	120	0.03083616
AP-24	15	1.8975	2064	42	120	0.0391644
AP-79	15	1.374	2064	46	120	0.02835936
AP-7	15	1.374	2064	40	120	0.02835936
AP-55	16	2.281	1980.4	47	120	0.045172924
AP-24	16	2.28825	1980.4	40	120	0.045316503
AP-79	16	1.98525	1980.4	45	120	0.039315891
Mean	7.975	5.92269875	3082.87	44.225	112.5	0.188640536
Median	6	3.516	3223.8	40	120	0.15811452
Max	16	19.1385	4497	80	120	0.499706235
Min	1	0.73725	1980.4	40	80	0.016829943
¾ Q	13	11.007	3657	46	120	0.331064118

APPENDIX R

MEASURED MALE RISK MORTALITY PARAMETERS FOR ABDOMINAL-PELVIS

|						
			RISK MORALITY MALE			
ID	AGE	Effective Dose	LAR	Tube Current	Tube Voltage	RISK %
	Y	mSv		mAs	KVP	
AP-76	1	3.516	1049.6	40	80	0.036903936
AP-36	3	4.4235	950.8	40	100	0.042058638
AP-13	4	12.888	901.4	50	100	0.116172432
AP-22	1	3.516	1049.6	40	80	0.036903936
AP-66	2	3.516	1000.2	40	100	0.035167032
AP-55	2	3.516	1000.2	41	120	0.035167032
AP-43	4	4.4235	901.4	40	100	0.039873429
AP-23	5	3.516	852	40	120	0.02995632
AP-41	5	3.516	852	40	100	0.02995632
AP-32	4	4.4235	901.4	46	100	0.039873429
AP-34	3	4.4235	950.8	40	120	0.042058638
AP-23	3	4.698	950.8	40	120	0.044668584
AP-33	3	3.516	950.8	40	120	0.033430128
AP-44	5	12.888	852	41	120	0.10980576
AP-40	1	3.516	109.6	56	120	0.003853536
AP-11	4	4.4235	901.4	40	120	0.039873429
AP-6	6	10.242	824	40	100	0.08439408
AP-17	6	7.872	824	40	120	0.06486528
AP-45	6	11.16	824	40	120	0.0919584
AP-80	6	11.322	824	40	120	0.09329328
AP-69	6	11.4882	824	40	120	0.094662768
AP-26	7	12.1275	796	67	120	0.0965349
AP-55	7	10.548	796	50	120	0.08396208
AP-24	8	14.8335	768	40	120	0.11392128
AP-79	8	11.358	768	46	120	0.08722944
AP-7	10	19.1385	712	48	120	0.13626612
AP-22	10	15.579	712	40	120	0.11092248
AP-6	12	0.912	668.4	40	100	0.006095808

174

AP-17	13	1.172	646.6	80	120	0.007578152
AP-45	13	1.172	646.6	47	120	0.007578152
AP-80	13	0.73725	646.6	57	120	0.004767059
AP-69	15	1.494	603	40	100	0.00900882
AP-26	15	2.3385	603	40	120	0.014101155
AP-55	15	1.494	603	40	120	0.00900882
AP-24	15	1.8975	603	42	120	0.011441925
AP-79	15	1.374	603	46	120	0.00828522
AP-7	15	1.374	603	40	120	0.00828522
AP-55	16	2.281	584.6	47	120	0.013334726
AP-24	16	2.28825	584.6	40	120	0.01337711
AP-79	16	1.98525	584.6	45	120	0.011605772
Mean	7.975	5.92269875	770.65	44.225	113.5	0.047455016
Median	6	3.516	810	40	120	0.036903936
Max	16	19.1385	1049.6	80	120	0.13626612
Min	1	0.73725	109.6	40	80	0.003853536
¾ Q	13	11.007	901.4	46	120	0.0865206

175

APPENDIX S

MEASURED MALE RISK MORTALITY PARAMETERS FOR ABDOMINAL-PELVIS

			RISK MORALITY FEMALE			
ID	AGE	Effective Dose	LAR	Tube Current	Tube Voltage	RISK %
	Y	mSv		mAs	KVP	
AP-76	1	3.516	1685.4	40	80	0.059258664
AP-36	3	4.4235	1515.8	40	100	0.067051413
AP-13	4	12.888	1431.2	50	100	0.184453056
AP-22	1	3.516	1685.4	40	80	0.059258664
AP-66	2	3.516	1600.4	40	100	0.056270064
AP-55	2	3.516	1600.4	41	120	0.056270064
AP-43	4	4.4235	1431.2	40	100	0.063309132
AP-23	5	3.516	1347	40	120	0.04736052
AP-41	5	3.516	1347	40	100	0.04736052
AP-32	4	4.4235	1431.2	46	100	0.063309132
AP-34	3	4.4235	1515.8	40	120	0.067051413
AP-23	3	4.698	1515.8	40	120	0.071212284
AP-33	3	3.516	1515.8	40	120	0.053295528
AP-44	5	12.888	1347	41	120	0.17360136
AP-40	1	3.516	1685.4	56	120	0.059258664
AP-11	4	4.4235	1431.2	40	120	0.063309132
AP-6	6	10.242	1298.4	40	100	0.132982128
AP-17	6	7.872	1298.4	40	120	0.102210048
AP-45	6	11.16	1298.4	40	120	0.14490144
AP-80	6	11.322	1298.4	40	120	0.147004848
AP-69	6	11.4882	1298.4	40	120	0.149162789
AP-26	7	12.1275	1249.8	67	120	0.151569495
AP-55	7	10.548	1249.8	50	120	0.131828904
AP-24	8	14.8335	1201.2	40	120	0.178180002
AP-79	8	11.358	1201.2	46	120	0.136432296
AP-7	10	19.1385	1104	48	120	0.21128904
AP-22	10	15.579	1104	40	120	0.17199216
AP-6	12	0.912	1028	40	100	0.00937536

176

AP-17	13	1.172	990	80	120	0.0116028
AP-45	13	1.172	990	47	120	0.0116028
AP-80	13	0.73725	990	57	120	0.007298775
AP-69	15	1.494	914	40	100	0.01365516
AP-26	15	2.3385	914	40	120	0.02137389
AP-55	15	1.494	914	40	120	0.01365516
AP-24	15	1.8975	914	42	120	0.01734315
AP-79	15	1.374	914	46	120	0.01255836
AP-7	15	1.374	914	40	120	0.01255836
AP-55	16	2.281	883.6	47	120	0.020154916
AP-24	16	2.28825	883.6	40	120	0.020218977
AP-79	16	1.98525	883.6	45	120	0.017541669
Mean	7.975	5.92269875	1245.52	44.225	112.5	0.075953053
Median	6	3.516	1298.4	40	120	0.059258664
Max	16	19.1385	1685.4	80	120	0.21128904
Min	1	0.73725	883.6	40	80	0.007298775
¾ Q	13	11.007	1431.2	46	120	0.135569754
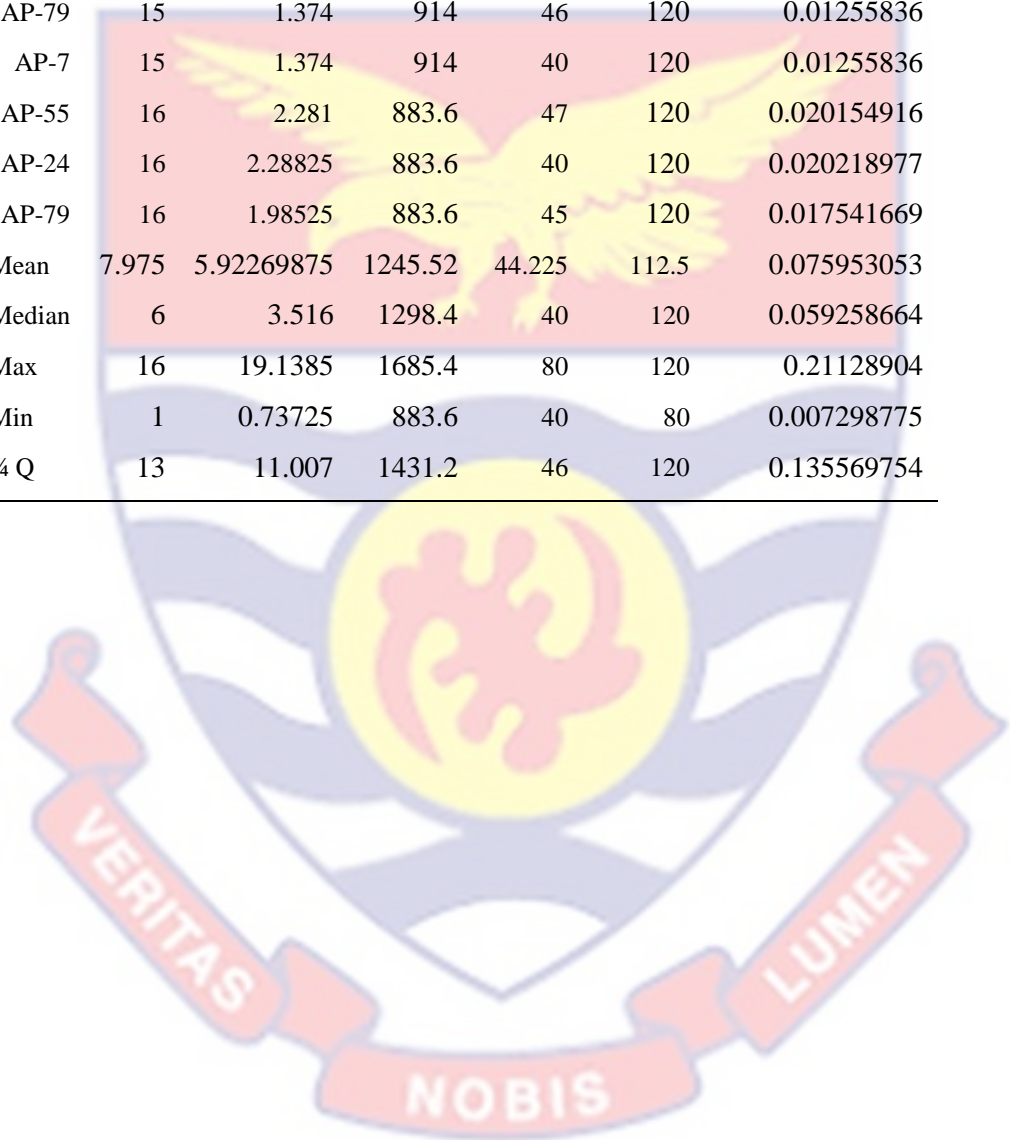
APPENDIX T

FORM A FOR PRE SCAN DATA

Patient ID	Scan Region	Age years	Sex M/F	W Kg	H cm	PATIENT COMMEN

178

APPENDIX U

FORM B FOR SCANOGRAM PROTOCOL

Projection	kV	mA	Typical Scan Length (mm)	Slice Width	Total mAs (just Scanogram)
Eg A.P	120	50	240	2x1	240

179

APPENDIX V

FORM C FOR SCAN PARAMETERS

Protocol Name/ID	Helical/ axial	FOV/filter setting	Pitch or increment	Rotation time	mA modulation setting used (noise index/ref mA)		kV or auto kV setting	Acquisition Slice Width	Reconstruction algorithm (FBP or level of iterative recon)
Eg Paed Head	axial	Small	32mm	1s	Ref mA	200	120	64x0.5mm	IR level 3

APPENDIX W

FORM D FOR PATIENTS DATA COLLECTION

FORM D

Hospital/Clinic: _____   Scanner Details: _____
Examination:
Paediatric Age Group: ▮▮▮▮

Paediatric Patient: Clinical CT Sheet

CTDI ref phantom size: 32cm/16cm (circle 1)
Reference of Study(ies) provided for detailed analysis (at least one for each protocol):
NB Enter details for each phase separately below – new number for each patient

	Exam /image reference	Age (yr/mo) or DOB (dd-mm-yy)	Height (cm)	Weight (kg)	Protocol Used	Effective mAs	Scan Length (Range) mm	Comments on phase Any parameters changed from protocol	Total DLP for phase (mGycm)	Mean CTDI for phase (mGy)	Image Quality Score 1. Non-diagnostic 2. Adequate 3. Excellent
Eg	123	6 mth	60	12	Paed Head	140	120	Non-contrast	405	3.2	2
1											
2											
3											
4											

180